Growth of Single-Wall Carbon Nanotubes by Chemical Vapor Deposition for Electrical Devices

INAUGURALDISSERTATION

zur
Erlangung der Würde eines Doktors der Philosophie
vorgelegt der
Philosophisch-Naturwissenschaftlichen Fakultät
der Universität Basel
von

Jürg Furer

aus Hemishofen (SH)

Basel, 2006

Genehmigt von der Philosophisch-Naturwissenschaftlichen Fakultät auf Antrag der Herren Professoren:

Prof. Dr. Christian Schönenberger
Prof. Dr. László Forró (Ecole Polytechnique Fédérale de Lausanne)
Prof. Dr. Hans-Werner Fink (Universität Zürich)

Basel, den 25. Oktober 2005

Prof. Dr. H.-J. Wirz, Dekan

Und über dem allen, mein Sohn, lass dich warnen;
denn des vielen Büchermachens ist kein Ende,
und viel Studieren macht den Leib müde.

Der Prediger Salomo 12, 12

Contents

Chapter 1

Introduction

Carbon emerges in different forms. Diamond and graphite have been well known materials for centuries. Moreover fullerenes and nanotubes were discovered only a few years ago. H. W. Kroto *et al.* depicted the fullerenes in 1985 [1]. A few years later, in 1991, S. Iijima described carbon nanotubes (CNTs) for the first time [2] (Figure 1.1).

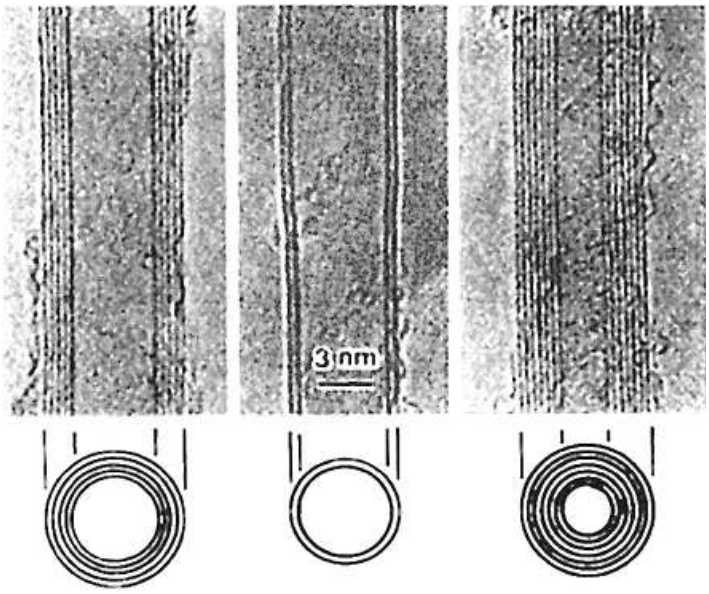

Figure 1.1: TEM pictures of multi-wall carbon nanotubes [2].

CNTs have a close relation to graphite, since a single-wall carbon nanotube is like a rolled-up graphite mono layer. However a nanotube has with its curved shape a higher chemical reactivity than a flat graphite layer. Both the side wall and the caps can be modified chemically [3]. Carbon nanotubes are regular carbon clusters with attractive mechanical and electronic properties [4]. Nanotubes have a high mechanical strength due to a very large Young's modulus [5]. They can be used for the storage of hydrogen [5,6], to store energy in electrochemical double layer capacitors [7] or to reinforce composite materials [3]. A single nanotube can be used as a sensor [8–12], a nanorelay [13], a vessel [14] or as a template [3, 15]. It is possible to produce light bulbs [16] and fibers [17] with carbon nanotubes. An array of CNTs can act as a flat panel display [3, 5] using their feature to act as field emitting devices [18–21].
CNTs are either metallic (1/3) or semiconducting (2/3). Nowadays it is not possible to select the desired characteristic of a nanotube in advance. It is only possible to separate metallic from semiconducting tubes by using an electrical field [22]. Metallic nanotubes with their

diameter of a few nm represent the ultimate conducting wire whereas the semiconducting ones can be used as transistors [23–25] even on a transparent and flexible substrate [26]. The transistors can be optimized by the chemical control of the nanotube-electrode interface [27]. Quantum dots [28, 29] and spin valves [30–32] can be built alike simple logic gates [33] and a Y-junction rectifier [34].

Carbon nanotubes have a very interesting property: they are "1-dimensional" molecules [35]. This has to be explained in a few words. In general, quantum confinement leads to a spacing of the allowed eigenenergies. Electrons cannot hop into a higher energy level if the thermal energy is much smaller than this energy difference. In a nanotube an electron is confined in the directions perpendicular to the tube axis. The nanotube becomes a 1-dimensional conductor. For several years members of our research group are exploring the electrical properties of this very special conductor. The behavior of carbon nanotubes is investigated with electrical transport measurements at low temperatures (down to 50 mK) and in high magnetic fields (up to 10 T).
The raw material for the first experiments [36–38] were multi-wall carbon nanotubes obtained from L. Forró (Ecole Polytechnique Fédérale de Lausanne) which were produced using laser ablation. The multi-wall carbon nanotubes were used to investigate the suppression of tunnelling [36, 39], multiple Andreev reflection [28, 37], electrical spin injection [30–32] and quantum dots [37, 40–43].
The next step was to grow single-wall carbon nanotubes using chemical vapor deposition (CVD) [8,44–46]. This procedure has the advantage to be faster than an external collaboration and in addition the growth of the tubes directly on the device makes the samples ready for use without an additional treatment.
It was verified that the CVD grown tubes are suitable of for electrical devices [47]. Vibrating nanotubes [48] and an ambipolar field-effect transistor [23] were studied. Kondo effect [49] and Fano-Resonances [50] were investigated as well.
The latter experiments reveal one common deficiency. The grown tubes are often not separated but bundled [47] (Figure 6.10). Moreover it is not clear if they are multi- or single-wall tubes. This means for electronic transport measurements that several tubes are measured simultaneously. Thus the tube with the best conductivity dominates the measurement, whereas the other tubes perturb the measured signal by there presence.

The main focus of this thesis is the development of a growth process of single-wall carbon nanotubes by using CVD. The aim is to overcome the problem of bundling. The grown nanotubes have to be free of lattice defects and they need to have good electrode-nanotube contacts in order to make them suitable for electronic transport measurements. They have to lay flat, well separated and optimally distributed on SiO_2 our standard substrate. On the one hand the tube density should not be too high since this would increase the probability of shortcuts between the electrodes due to nanotube-nanotube contacts. On the other hand it should not be too low since this would make the localization of an appropriate nanotube much more time consuming (Figure 1.2).
Two ways to achieve this goal were tried. The single-wall nanotubes can be bought, dissolved in a solvent and spread after cleaning and separation [51–57], as in the thesis [46]. The second possibility is to grow the tubes directly on the device as presented in this thesis.
Growing carbon nanotubes with CVD is very simple, at least in principle. There are only a few essential things needed: an oven, a substrate, a catalyst and a carbon feedstock. The main challenge is to acquire the right knowhow.
The first step was to build up the CVD system. Afterwards the proper growth conditions and a simple method to check the demanded properties of the grown tubes had to be found. Scanning electron microscopy (SEM) is the standard characterization tool used in this thesis.

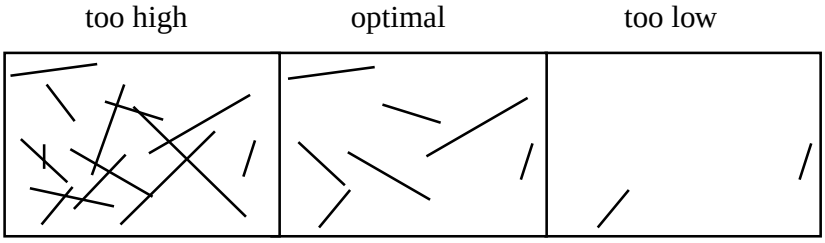

Figure 1.2: The tubes have to be well separated with the optimal density.

Transmission electron microscopy (TEM) is a helpful mean in order to show that the tubes are separated and single-wall, since it allows the investigation of the tubes' internal structure. Atomic force microscopy (AFM) and Raman spectroscopy are used in addition.

Outline of this thesis

- Chapter 2 gives a short overview with respect to the properties, the growth and the characterization of carbon nanotubes.
- The oven and the gas system are delineated in Chapter 3. Different carbon feedstocks were used: ethylene/hydrogen, methane, methane/ethylene and methane/hydrogen.
- The steps towards a suitable catalyst are presented in Chapter 4. Evaporated and liquid based catalysts were tested. An iron molybdenum alumina catalyst dissolved in 2-propanol provides the best results.
- Chapter 5 gives a comparison of the results obtained utilizing different growth processes, and describes the formation of amorphous carbon and the oxidation of nanotubes.
- Chapter 6 summarizes experiments on different TEM grids (Au, Cu, Mo, Ni, stainless steel, Ti, quantifoils) and silicon nitride windows.
- The results from collaborations with other group members are presented in Chapter 7. These experiments show the good quality of the grown tubes.

Chapter 2

Properties and growth of carbon nanotubes

This chapter gives an overview of the properties and the growth of carbon nanotubes (CNTs) in the first two sections. The last section presents different characterization methods.

2.1 Carbon Nanotubes

The amazingly different structures of diamond, graphite, fullerenes and carbon nanotubes are presented in Figure 2.1.

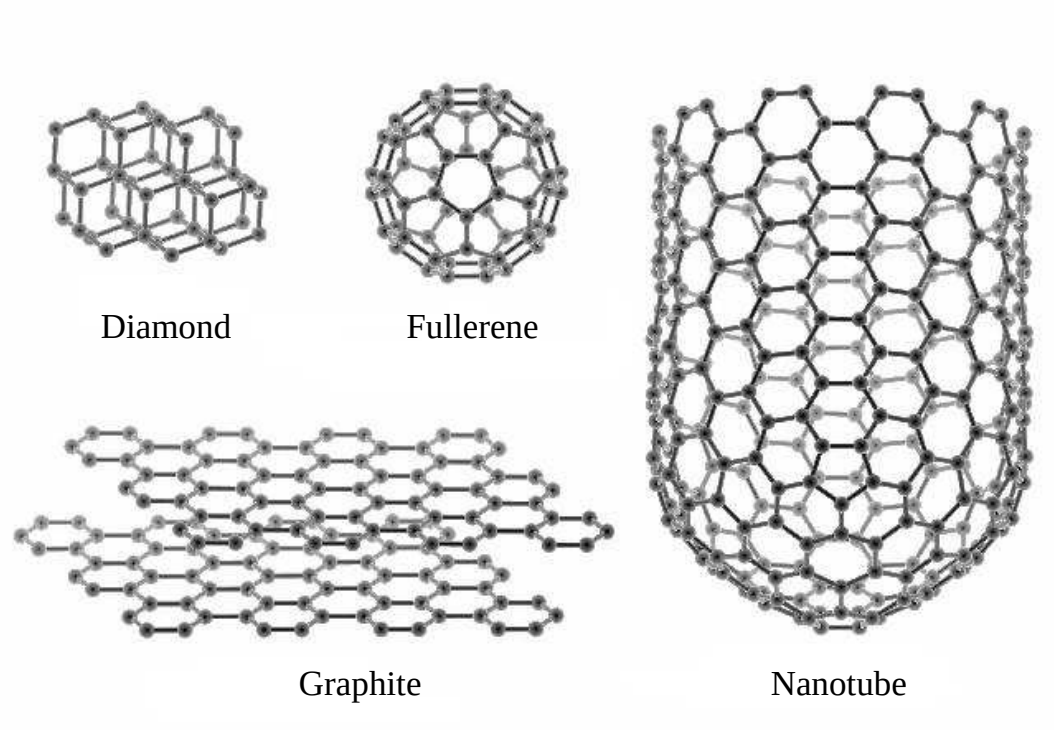

Figure 2.1: Different manifestations of carbon [58].

These structural differences can be explained by the fact that a carbon atom can bind to 2, 3 or 4 other atoms. The electronic ground state configuration of carbon is $1s^2 2s^2 2p^2$. The four electrons in the outer shell can combine to three types of hybrid orbitals. Carbon can

form 4 sp^3, 3 sp^2 or 2 sp^1 hybrid orbitals. The hybridization equalizes the energy differences between the participating atomic orbitals.
In a covalent bond of two atoms the first pair of overlapping hybrid orbitals forms a σ-bond, whereas the remaining pair(s) of atomic orbitals build one or two π-bonds [59, 60]. The sp^3 orbitals are tetragonal and 3-dimensional as for example in diamond and CH_4, the latter has four σ-bonds between the carbon and the hydrogen atoms. The sp^2 orbitals are trigonal and planar as for instance in graphite and $H_2C{=}CH_2$, the latter has two σ-bonds between the carbon and the hydrogen atoms and a σ-π-double-bond between the carbon atoms. The linear sp^1 orbitals in $HC{\equiv}CH$ form σ-bonds between the carbon and the hydrogen atoms and a σ-π-π-triple-bond between the carbon atoms.
Figure 2.1 shows that graphite consists of separated layers with a honeycomb pattern. The individual carbon atoms are sp^2 hybridized. The left over electrons (one per carbon atom) form a mesomery stabilized π-electron system. A simple example for such a system is the benzene ring. The π-electrons are not assigned to a specific carbon atom, but build up a charge cloud around the benzene ring. A graphite layer is enclosed by a similar cloud on both sides. There are no chemical bonds between two adjacent layers, therefore they can be displaced very easily, which makes graphite useful as lubricant [61].
Carbon nanotubes share these properties, since a graphite layer is like a single-wall carbon nanotube (SWNT) (Figure 2.2) with infinite diameter. Multi-wall carbon nanotubes (MWNTs) are built up by several of these SWNTs with different diameters in a concentrical arrangement (Figures 1.1 and 2.2). The inter-tube spacing is 0.34 nm, which corresponds to the inter-layer distance of 0.35 nm in graphite [5]. While the diameter of a CNT is in the range of a few nm down to 0.4 nm [62, 63], the length can be up to some mm [64]. As in graphite the shells of a MWNT can be displaced against each other due to the absence of chemical bonds between the shells.

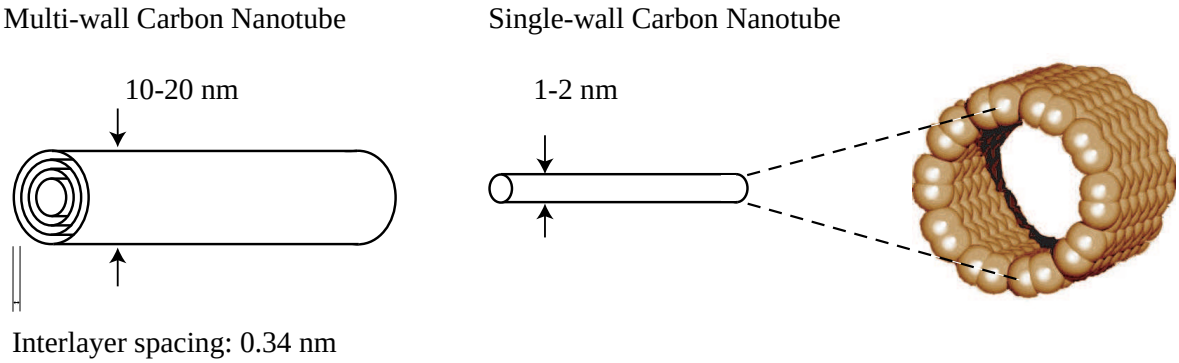

Figure 2.2: Schematics of a single- and a multi-wall carbon nanotube.

A SWNT is usually characterized by its chiral vector C_h which is defined by two integers (n, m) as well as two base vectors a_1 and a_2 (Figure 2.3) [5, 62, 65]. The graphite layer is bent in such a way that both ends of the vector lie on top of each other.

$$C_h = na_1 + ma_2 \equiv (n, m) \tag{2.1}$$

These two integers (n, m) determine unambiguously the diameter d and the chiral angle θ of the tube. θ represents the angle between the chiral vector and the direction $(n, 0)$.

$$d = \frac{a}{\pi}\sqrt{n^2 + m^2 + nm} \tag{2.2}$$

$$\sin\theta = \frac{\sqrt{3}m}{2\sqrt{n^2+m^2+nm}} \tag{2.3}$$

There are two special types of SWNTs: armchair-tubes (n,n) and zig-zag-tubes (n,0). All other tubes are called chiral-tubes (Figure 2.3).

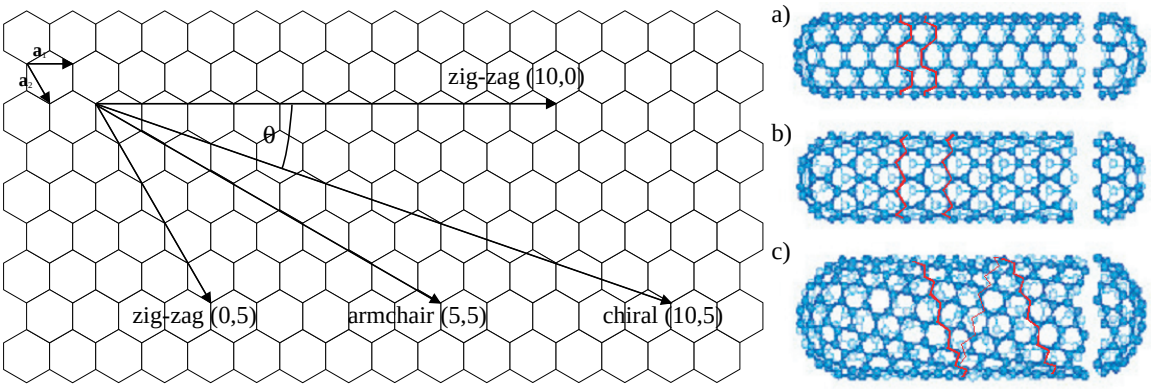

Figure 2.3: Left: Different chiral vectors and chiral angle θ. Right: a) $(5,5)$ arm-chair-tube, b) $(9,0)$ zig-zag-tube and c) $(10,5)$ chiral-tube with matching fullerenes [5].

Nanotubes are either metallic (1/3) or semiconducting (2/3). This characteristic depends from m and n. A tube is metallic when $\frac{m-n}{3}$ is an integer. All other CNTs are semiconducting (Figure 2.4). This means that m and n determine the diameter, the chirality and the physical properties of a SWNT [66].

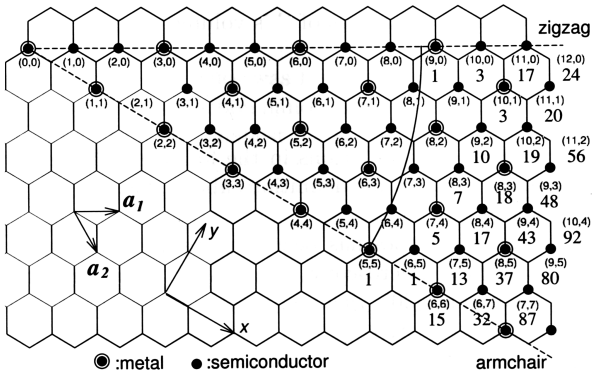

Figure 2.4: The characteristic (metallic/semiconductiong) depends on the chiral vector [5].

2.2 Growth of carbon nanotubes

Carbon nanotubes can be prepared by various methods such as arc-discharge and laser ablation [5,67] schematically depicted in Figure 2.5.
Here we focus on chemical vapor deposition. For the growth of CNTs by CVD [3,5,7,62,65,68] different gasses can be used as carbon feedstock (methane, ethylene, acetylene, CO, ...) [69,70].

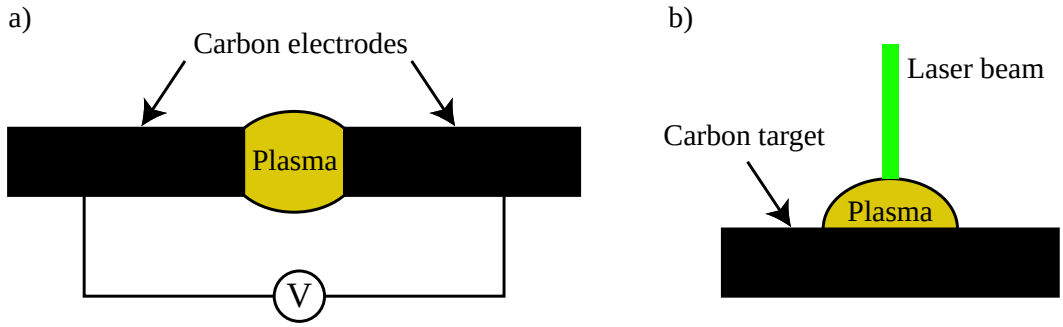

Figure 2.5: The CNTs grow within a plasma. a) Arc-discharge: A plasma is formed due to a voltage which is applied between two carbon electrodes. b) Laser ablation: A plasma is formed with a laser which heats a carbon target.

It is possible to grow carbon nanotubes in a plasma without using a catalyst [5], whereas for growing SWNTs with CVD a transition metal catalyst (e.g. Fe, Ni, Co, ...) is required. An exception is the growth of CNTs on SiGe islands on a Si substrate without a metal catalyst using methane and hydrogen [71]. Nevertheless it is common to use either an evaporated catalyst (e.g. Al/Fe/Mo layers [72]), a liquid based catalyst (e.g. Fe/Mo/alumina [73]) or a combination as a liquid Fe/Mo catalyst coalesced with an evaporated Al layer [74].
Quality and shape of the grown tubes depend on the growth temperature [75]. Typical growth temperatures are 550-750 °C for MWNTs and 850-1'000 °C for SWNTs [70, 76, 77].
Figure 2.6 shows the setup of a typical CVD system. A sample covered with catalyst is placed within the oven and heated in a constant flow of a protective gas (Ar in our case). When the desired growth temperature is reached, the carbon feedstock is added (methane or ethylene).

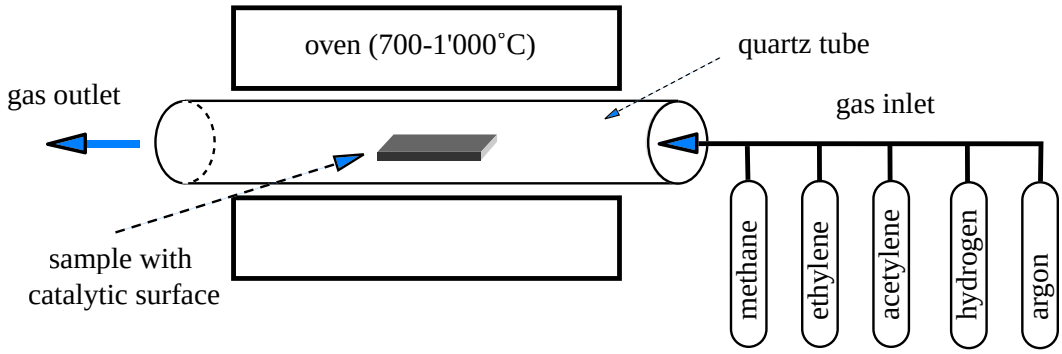

Figure 2.6: Setup of a typical CVD system.

The principle of growth is shown on Figure 2.7. The hydrocarbons (benzene) in the gas phase bind to the catalyst (spheres), the hydrogen is split off and the remaining carbon forms the growing tubes. These reactions can be enhanced by heating the sample. (For more details about the used setup see Chapter 3.)
Branching [79] and orientation of the grown tubes can be controlled on different ways, as with alumina patterns [74], an electrical [80–82] or a magnetic field [83], a gas flow cell [84] or growing the tubes from pillar to pillar [85, 86]. Diameter and location can be controlled using lithographically patterned samples [87].

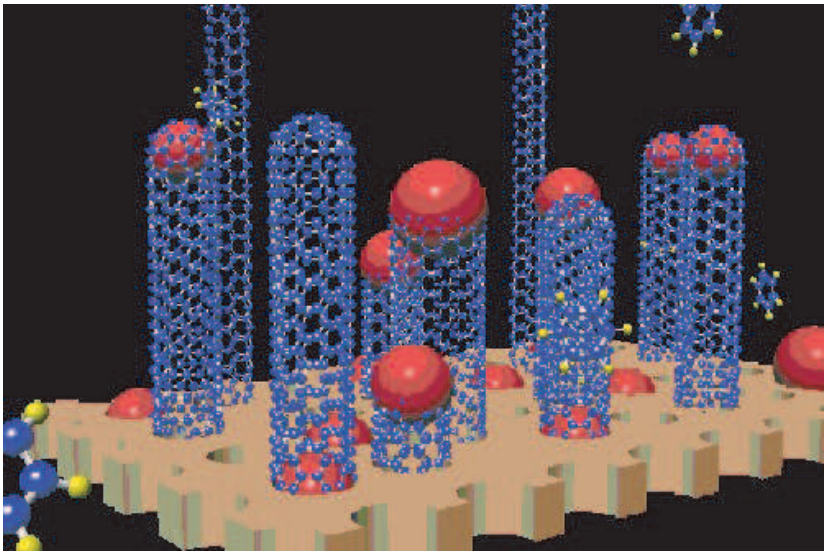

Figure 2.7: Growth of carbon nanotubes using CVD [78].

2.2.1 Pyrolysis

Organic materials decompose when heated in the absence of oxygen. This process is called pyrolysis, with pure carbon as the end product. The other elements present in the carbon feedstock form gaseous products and diffuse away. Besides carbon nanotubes also highly oriented pyrolytic graphite (HOPG), graphite whiskers, carbon fibers, glassy and amorphous carbon form due to pyrolysis [68].
Amorphous carbon is a highly disordered network of carbon atoms. It is a permanent and unwanted companion of CVD. It has no long-range order but some short-range order (1 nm) which depends on the carbon bond type (sp^2/sp^3) and the hydrogen content.
The growth of carbon nanotubes by CVD is a controlled pyrolysis of the carbon feedstock. Hydrocarbon molecules decompose when they are heated and become thereby activated. A mathematical model for the mechanism of the decomposition of methane in the gas phase can be found in [88].
The activated molecules are either taken up by the catalyst and form nanotubes or they precipitate on the whole sample surface forming amorphous carbon. The quantity of the formed amorphous carbon has to be kept as small as possible since the catalyst becomes inactivated when covered with a layer of amorphous carbon. Moreover the quality of the tubes suffers due to the deposition of amorphous carbon on the grown tubes leading to a reduced electrical contact to the electrodes.

2.2.2 Radicals

The activation of a molecule by heating can be explained by the formation of radicals [89]. The most simple definition for a radical is a molecule which contains unpaired electrons. A single unpaired electron is represented by a dot, the other electrons in the outer shell are not shown. Simple examples are $H^{\bullet}$ and $Cl^{\bullet}$. These unpaired electrons make the radicals usually highly reactive. So radicals are likely to take part in chemical reactions. This high reactivity is due to the unpaired electrons which would like to "pair" with another electron to form a filled outer shell [90]. Radicals can react in different ways. The most important reactions in radical chemistry are [91]:

Formation:	$H_3C\text{-}H$	$\longrightarrow$	$H_3C^{\bullet} + {}^{\bullet}H$
	$H_2C{=}CH_2$	$\longrightarrow$	${}^{\bullet}H_2C\text{-}CH_2^{\bullet}$
Propagation:	$H_3C^{\bullet} + H\text{-}CH_3$	$\longrightarrow$	$CH_3\text{-}CH_2^{\bullet} + H_2$
Termination:	$CH_3\text{-}CH_2^{\bullet} + {}^{\bullet}CH_3$	$\longrightarrow$	$CH_3\text{-}CH_2\text{-}CH_3$

The formation of radicals needs energy which can be provided by impact processes [92, 93]. The kinetic energy of a heated gas increases, which implies: the higher the temperature is, the more radicals are formed.
The number of radicals is not only dependent on temperature. The type of chemical bond is even more important. In order to break a chemical bond a characteristic bond dissociation energy needs to be provided. This energy depends on the atoms which build the bond, the chemical environment of the bond (Table 2.1) and the temperature (Figure 2.8). Methane is for example more stable than ethane, since a C-H bond is more stable than a C-C bond [91].

$HC{\equiv}CH$	962 kJ/mol
$H_2C{=}CH_2$	682 kJ/mol
$H_3C\text{-}CH_3$	386 kJ/mol
$(H_3C)(H_2C)\text{-}H$	410 kJ/mol
$H_3C\text{-}H$	435 kJ/mol
$H\text{-}H$	436 kJ/mol

Table 2.1: Mean binding enthalpies of different hydrocarbon bonds [59].

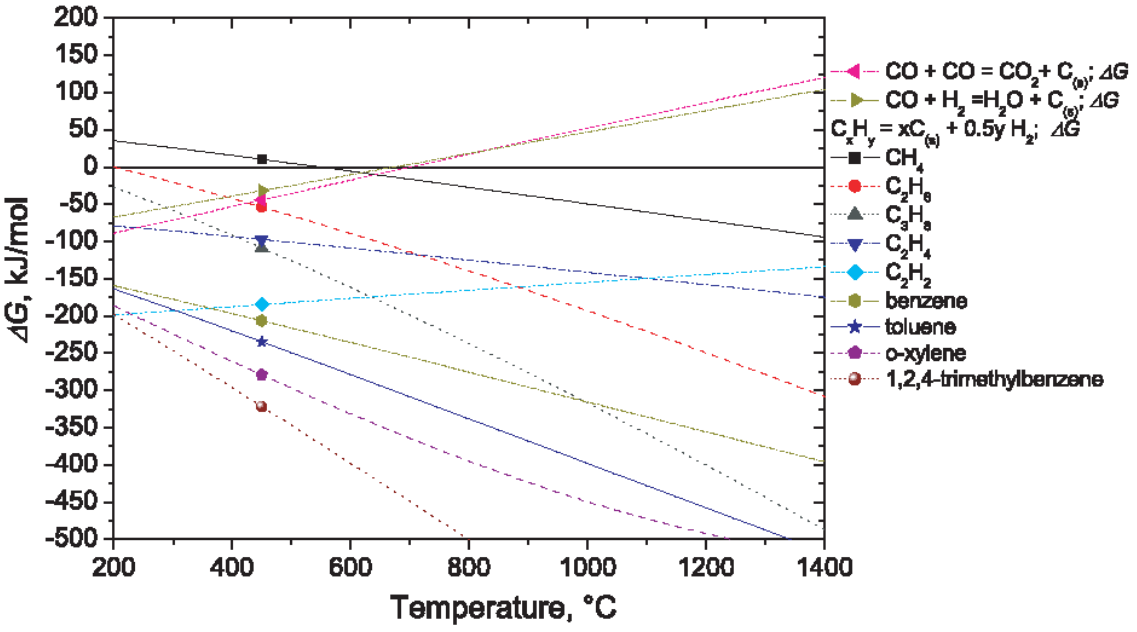

Figure 2.8: Gibbs energy of different hydrocarbons [70]

The selectivity of the propagation reactions is very low [94], since a radical can react with any molecule it collides with. Which results in a whole series of different hydrocarbons [95]. As a consequence, the carbon accumulates in growing molecules, which can become huge if they are not removed.
The process can be controlled not only by changing the temperature. During the process of carbon accumulation the excessive hydrogen is released. The equilibrium of this reaction

can be influenced by changing the relative concentrations of the reactants (methane) and products (CNTs, intermediate products and hydrogen). A big surplus of hydrogen slows down the reaction velocity [96, 97].
The formation of radicals is restricted since the necessary reaction temperature is reached only in a very small area. In order to avoid the formation of carbon clusters, the CVD process is performed in a constant flow of the reaction gas, which removes the unwanted products.
These reactions can be calculated, at least principally, using the principles of chemical kinetics [98–103].

2.2.3 The catalyst

The catalysts used for the presented experiments consist of either evaporated Fe, Ni or Al layers or a mixture of iron nitrate ($Fe(NO_3)_3$-$9H_2O$), molybdenum dioxide dichloride (MoO_2Cl_2) and alumina (Al_2O_3) nanopowder (with two different diameters of 4 and 40 nm) solved in 2-propanol [73]. (For more details about the catalyst preparation see Chapter 4.)
The substrate is usually silicon dioxide (SiO_2). The process gasses are methane (CH_4), ethylene (C_2H_4), hydrogen (H_2) and argon (Ar). The environmental gasses are oxygen (O_2), water (H_2O) and nitrogen (N_2). The active components of the catalyst are Fe and Ni, since CNTs do not grow when Mo or Al are used alone (see Section 4.2 for more details). Therefore Fe is surely the most important catalyst component, since Ni was used only for a few experiments. O, Mo, Al and Si (from the substrate) are known to interact with Fe, whereas H, N, Ar and Cl are neglected for the following considerations.
The Fe-C-phase diagram in Figure 2.9 is very complex, since Fe and C can appear in different pure and mixed phases, depending on the temperature and the C content. For pure Fe the body centered cubic (bcc) α-Fe transforms into face centered cubic (fcc) γ-Fe at 911 °C. At 1'392 °C the γ-Fe transforms back to the bcc phase (δ-Fe) [105].
At a (growth) temperature of 1'050 °C either a γ-Fe-C phase (with up to 9 atom % C [106]) is found or a mixture of a saturated γ-Fe-C phase in addition with graphite inclusions or iron carbide (Fe_3C, cementite). This can be explained by the fact that the γ-Fe-C phase can take up only a limited C fraction, when this is exceeded the C segregates into either graphite inclusions or iron carbide. At 850 °C an α-Fe-C phase (with up to 0.1 atom % C) and a mixed α- and γ-Fe-C phase can be found in addition.
The fact that nanotubes grow means that the carbon fraction is surely high enough to allow the formation of graphite inclusions or iron carbide. Fe_3C is crystalline compared with this a carbon nanotube can be seen as a special graphite inclusion. Therefore it can be assumed that iron carbide is a bad precursor for the growth of CNTs. The formation of either graphite inclusions or iron carbide depends on the iron alloy. Graphite inclusions are stable in C, Si, Al, Ti, Ni or Cu rich alloys [107]. Iron carbide is metastable in Mn, Cr, Mo or V rich alloys. The setup with C, Al and Si favors the formation of graphite inclusions. Only Mo counteracts, therefore its use has to be justified. The presence of Mo in the catalyst lowers the necessary growth temperature [108]. Mo can substitute Fe atoms [106], and it is known to catalyze the formation of $CH_3^{\bullet}$ radicals from methane [109, 110].
There are other factors which might influence the growth of carbon nanotubes. Si binds oxygen [111], and Al reduces iron oxide to iron in a strongly exothermic reaction (Fe_2O_3 + 2 Al $\longrightarrow$ 2 Fe + Al_2O_3 ΔH_R = -852 kJ/mol [112]). This reaction is technically used e.g. for welding rails. Therefore Al and Si act as oxygen absorbers and protect Fe from oxidation.
Fe and Al can form an intermetallic phase [113], therefore pure Al can dissolve a small amount of Fe. The combination of Al and Si is even more unfavorable, since a 20 nm Al layer below a 2 nm Fe layer on a Si(100) substrate depletes the Fe completely [114]. This is explained due to the formation of an Al-Si alloy with an eutectic point at 577 °C which getters a typical metal very efficiently. When an alumina layer is used instead of Al the growth of nanotubes

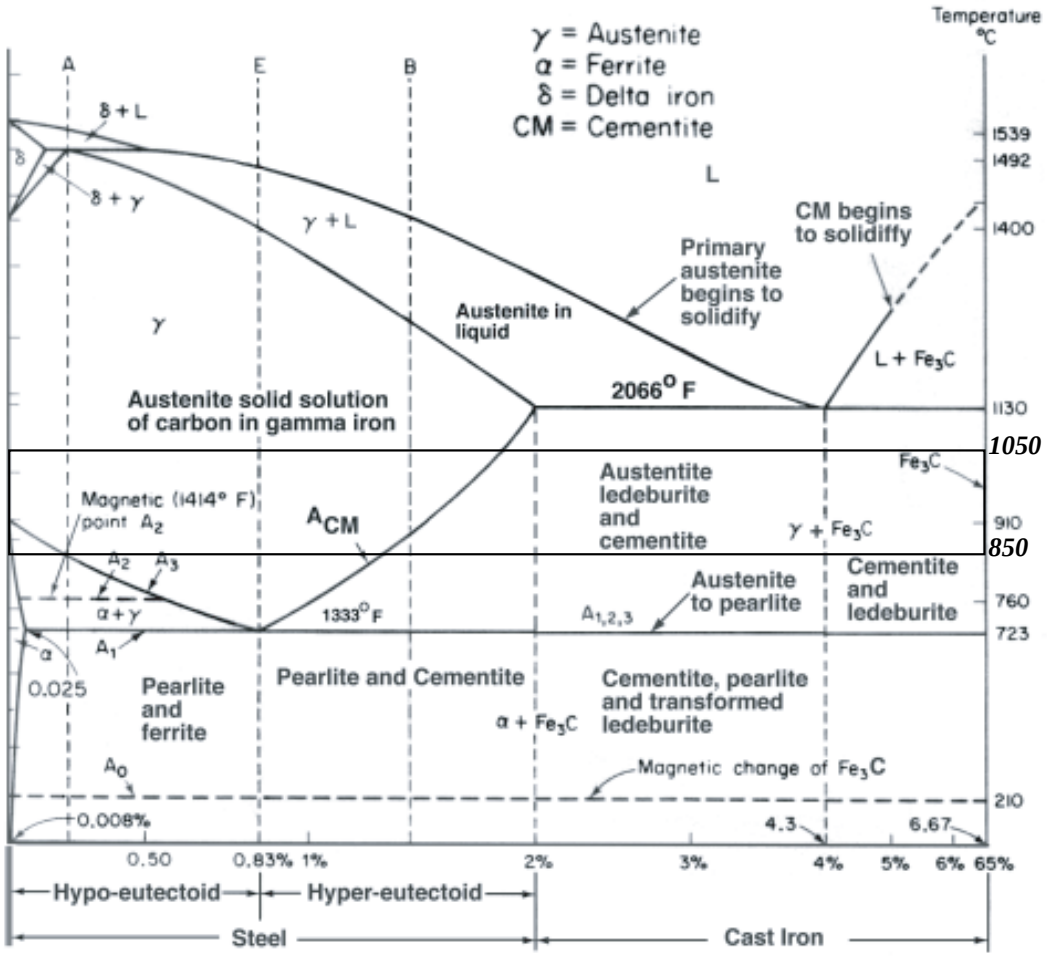

Figure 2.9: The Fe-C-phase diagram shows the weight % of C in Fe against the temperature [104].

is very efficient on the contrary [115]. Therefore the direct contact of Fe with pure Al has to be suppressed which makes the presence of oxygen indispensable, for a thin alumina layer between Al and Fe prevents the formation of an intermetallic phase which would hinder the growth of CNTs.

2.2.4 Growth mechanism

The growth mechanism for carbon nanotubes with CVD is still unclear. It surely can not be explained with a homogeneous gas-phase reaction [116]. The following section gives an overview of the current hypothesis.

The growth of CNTs happens very fast, since almost all growth occurs within the first minute [117]. Growth rates of up to 60 μm/min have been reported [118]. The diameter of the grown tubes depends on the temperature [119].

CNTs grow from catalyst particles, as shown on the schematics in Figure 2.10. Depending on the strength of the interaction between the catalyst particle and the substrate the catalyst can maintain its contact to the substrate (base-growth) or loses it (tip-growth) [5,65,68]. The growing nanotube can have a catalyst particle on one or on both sides.

CNTs do not grow on every available catalyst particle. It is not clear which qualities the catalyst surface must provide to allow the nucleation necessary for the growth of a CNT.

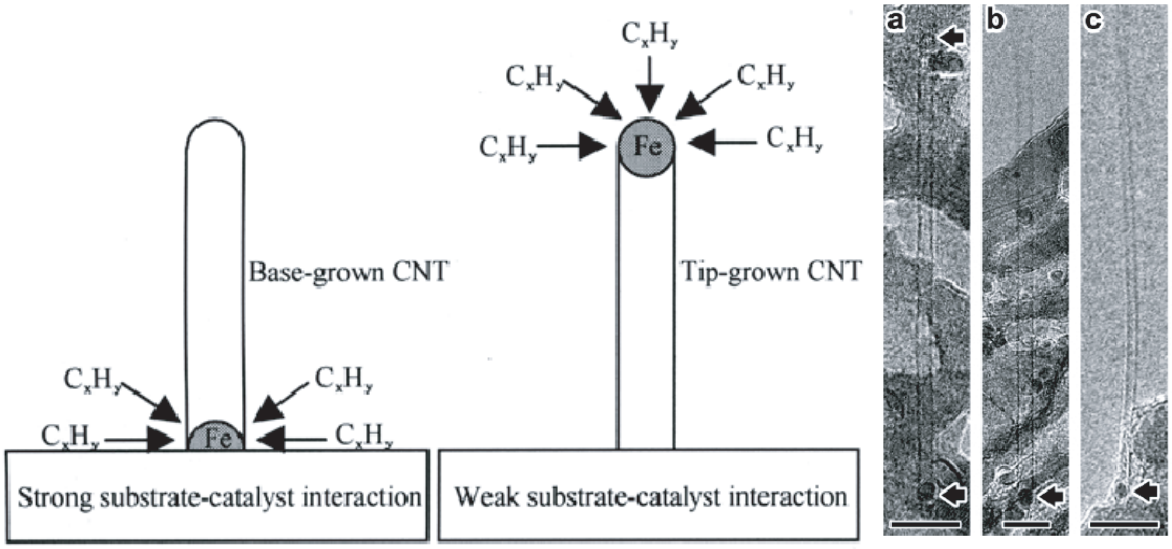

Figure 2.10: Left: Schematics of base and tip growth [120]. Right: TEM pictures of carbon nanotubes with catalyst particles on both sides a) and only at the base end b) and c) [121].

Figure 2.11 shows a possible mechanism of the growth of carbon nanotubes. The methane molecules disintegrate at the catalyst surface, the carbon atoms diffuse away and form the nanotube at a different location.

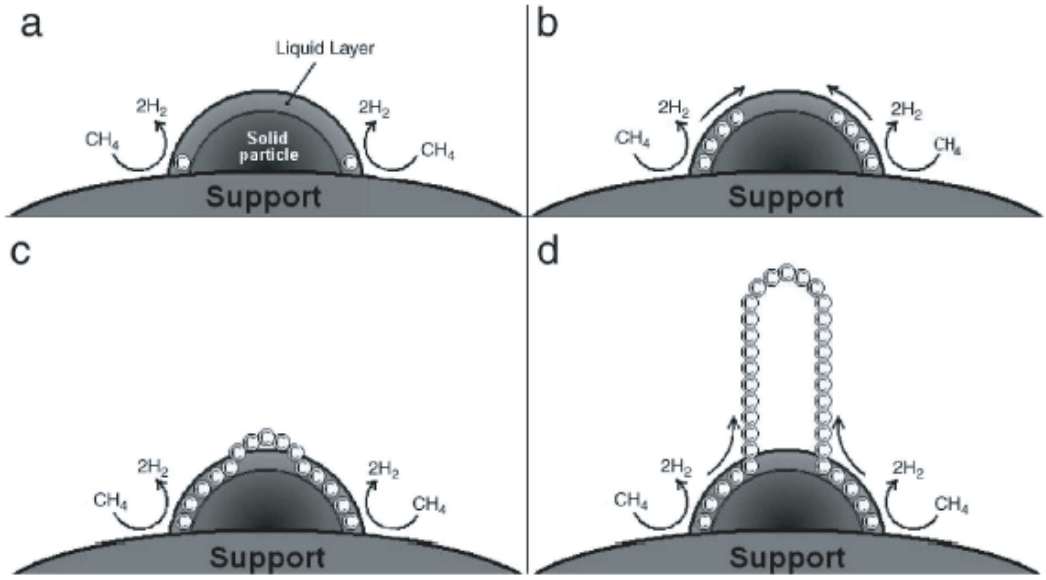

Figure 2.11: Schematic view of the mechanism for the formation of SWNTs. a) Adsorption and decomposition of the hydrocarbon. b) Diffusion in the liquid surface layer of the particle. c) Supersaturation of the surface and formation of the cap. d) Growth of the SWNT. [77]

This diffusion can be explained with the fact that the dissociation of methane into carbon and hydrogen is a highly exothermic reaction causing a local heating of the catalyst particle. The hydrogen reduces the catalyst locally and the carbon diffuses to a colder spot [122] resulting in a carbon and a temperature gradient within the catalyst particle [123]. A simulation of this process is presented in [122].

A carbon atom which is set free on the surface of the catalyst diffuses through the particle. The time t until it has reached the other side of the catalyst particle depends on the particle diameter, which corresponds to the diffusion way Δx. It can be estimated with:

$$\Delta x = \sqrt{Dt} \Rightarrow t = \Delta x^2 / D \tag{2.4}$$

where D is the diffusion coefficient [124]. The diffusion constant of C in γ-Fe at 800 °C is 10^{-8} cm^2/s [111]. The typical size of a catalyst particle is 100 nm, which corresponds to a diffusion time $t = (10010^{-9}m)^2/(10^{-8}(0.01m)^2 s) = 1ms$. This is very short compared to the growth time. Hence it can be assumed that the equilibrium of C dissolved in Fe is reached nearly instantaneously.

2.2.5 Conclusions

The growth mechanism can be summarized as follows: Heating the carbon feedstock causes the formation of radicals in the gas phase. The released (or added) hydrogen reduces the catalyst and slows down a too fast radical formation in the gas phase, reducing thereby the formation of amorphous carbon on the sample surface. The catalyst components serve different purposes (Figure 2.12): Fe is the base for the growth of carbon nanotubes. Mo catalyzes the decomposition of CH_4 directly at the catalyst surface. The released C diffuses to Fe rich areas. Al is the support of the other components and traps O_2 to protect Fe from oxidation.

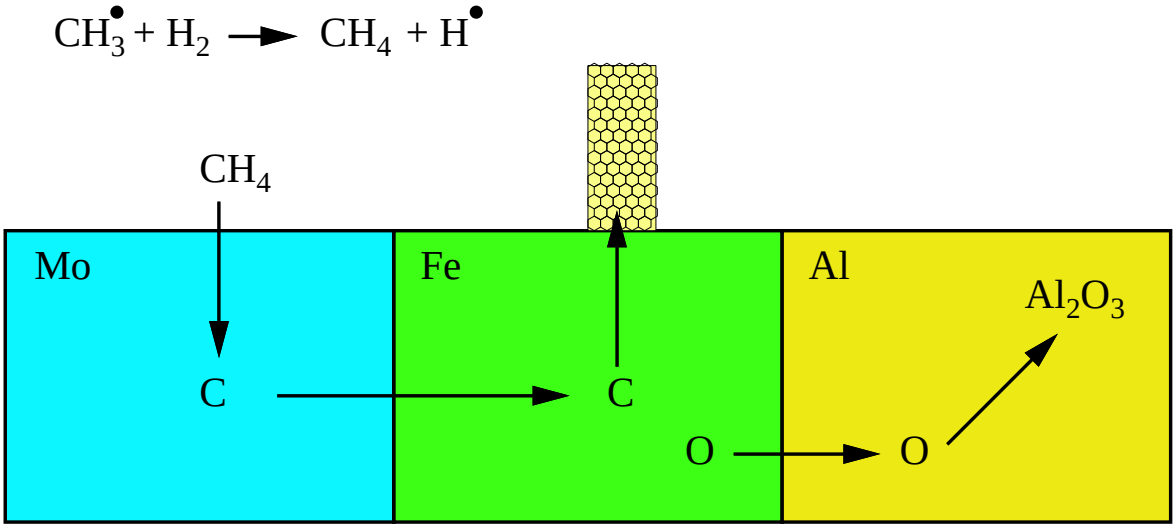

Figure 2.12: A possible growth mechanism.

2.3 Characterization methods

Quality, structure and physical properties of carbon nanotubes depend strongly on the growth conditions e.g. temperature, catalyst, gas type and flow rates. All this makes a proper characterization of the grown nanotubes indispensable. The growth of CNTs can be influenced by the substrate. Since SiO_2 on Si is our standard substrate it must be proven that the results of a measurement are applicable if another substrate is used instead.
The following listing gives a brief description of the methods used for the characterization of carbon nanotubes.

Scanning Electron Microscopy

SEM is the standard characterization method used in this thesis. It is very fast and user-friendly. It provides information about the density, the shape and the rough diameter of the grown tubes. It is not suitable as a measure for the quality of the grown tubes, since it is limited in resolution and does not deliver detailed information about the internal structure of the CNTs. For this purpose other characterization methods have to be used.
Functional principle: Emitted electrons (either from a cathode filament or via field emission) are accelerated to an energy ranging from a few 100 eV to 50 keV and focused by condenser lenses into a beam with a very fine spot size of 1 to 5 nm. The beam is deflected by two pairs of scanning coils in a raster fashion. The primary electrons are inelastically scattered by atoms in the sample which leads to the emission of secondary electrons which are detected.

Atomic Force Microscopy

The resolution of AFM is around one nanometer. It provides structural information of the surface of the CNTs. The handling of an AFM is more time consuming and less simple than that of a SEM, since it is very sensitive to a bumpy sample surface (Figure 2.13).

Figure 2.13: Catalyst clusters disturb AFM measurements (obstacles cause shadowing).

Functional principle: A cantilever with a sharp tip at its end is brought into close proximity to the sample surface. The force between the tip and the sample leads to a deflection of the cantilever which is measured using a laser spot reflected from the top of the cantilever into an array of photodiodes [125, 126].

Transmission Electron Microscopy

Observation by TEM promises a resolution in the nm-range and gives an insight into the internal structure of the nanotubes. The drawback of TEM is the really extensive and time consuming sample preparation, since the sample has to be partially transparent for electrons in order to allow imaging. Furthermore the CNTs can be damaged during imaging (Figure 6.11b)) [125, 127]). (Experiments leading to the preparation of samples which can be investigated with TEM are presented in Chapter 6.)
Functional principle: Accelerated electrons are focused onto a specimen. A part of the electrons is blocked or deflected away by the sample. The enlarged image of the transmitted electrons can be detected on a fluorescent screen, a photographic film or by a CCD camera.

Raman spectroscopy

Raman spectroscopy allows to check wether the grown CNTs are really single-wall and not bundled.
Functional principle: Raman spectroscopy is used to study vibrational, rotational and other low-frequency modes in a system. Incoming photons from a laser scatter inelastically with phonons or other excitations in the system. The energy of the scattered photons can be shifted up or down. This shift in energy gives information about the phonon modes in the system [128, 129].
There are several peaks which are interesting for the analysis of carbon nanotubes: the "G-band" at 1'582 cm^{-1} (whereas G means graphite) and the "D-band" around 1'350 cm^{-1} (disorder) [7, 130]. The latter mode is forbidden in perfectly ordered graphite and becomes only active in presence of disorder. The ratio of the integrated D- and G-band is inversely proportional to the crystallite size of graphite. This allows the distinction of SWNTs and MWNTs. Another important mode is the radial breathing mode which is only active in unbundled SWNTs (see [131] for an animation). It is distorted in bundles and MWNTs by Van der Waals interactions. This is a simple mean to distinguish between bundles and separated SWNTs. There is an additional interesting feature of this mode. The frequency depends on the tube diameter [62, 65].

Scanning tunnelling microscopy

STM is another possible measurement technique, it has atomic resolution and allows to distinguish bundles from separated carbon nanotubes. STM needs a conducting sample surface whereas SiO_2 is insulating. This makes a special sample preparation necessary. (Some preliminary experiments are shown in Section 5.3.)
Functional principle: A sharp tip is moved over the electrically conducting surface of the investigated sample, while a voltage is applied between tip and surface in order to measure the tunnelling current, which depends on the distance between tip and surface. A feedback loop keeps the tunnelling current constant by adjusting the distance between the tip and the surface by using piezoelectric elements. The height is related to the voltage applied to the piezo elements and can be used to reconstruct the surface structure [132, 133].

Electrical transport measurements

To perform an electrical transport measurements is the most direct check of the quality of the grown tubes. The drawback of this method is the really extensive sample preparation.
Functional principle: The common setup for such experiments consists of a nanotube contacted with several electrodes. Figure 2.14 shows a schematics of a very simple setup.

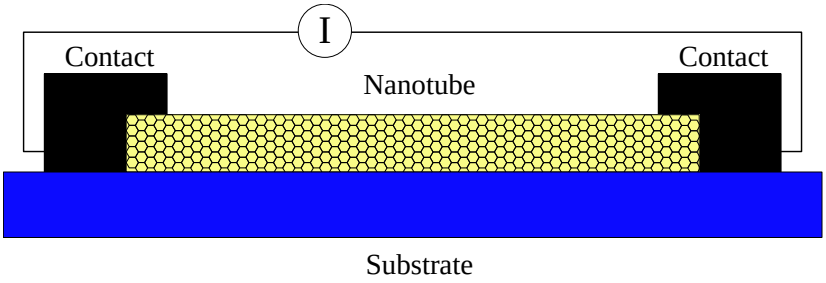

Figure 2.14: Schematics of the setup of a simple electrical transport measurement.

Fluorescence microscopy

Another method for the observation of CNTs is fluorescence microscopy [134, 135].

Mechanical properties

A nanotube is comparable to a thin rope or rod. Therefore it is possible to measure and simulate values as its Youngs modulus [136], oscillatory behavior [48, 137–139], superplasticity [140] or torsion constant [141]. CNTs break under tension [142] and deflect in response to external atomic collisions [143]. CNT cantilevers can be used for zeptogram-level mass detection [144], nanorelays [145] or as rotational bearings [146, 147]. They can bundle through Wigner defects [148] and form T-junctions [149] and zippers [150].

Chapter 3

The CVD system

Base for the growth of carbon nanotubes by chemical vapor deposition (CVD) is an oven in combination with a gas system (Figure 3.1). This chapter gives an overview of the utilized setups. The presented system is the supplement to a still useable older CVD oven which will not be described in detail. The old oven has its own gas system which was used for some experiments.
The setup of a CVD system consists of two main parts the oven and the gas system. The most important element is surely the oven. Furthermore several other components are needed, as gas bottles, different types of valves, flowmeters, manometers, tubes and connecting pieces which build the gas system.

Figure 3.1: The CVD oven and the actually used gas system.

The main focus of this chapter are two sections with descriptions of the different setups of the oven and the gas systems. The subsequent section gives a deeper insight into the function and the reliability of the used flowmeters, and the last section presents the different protocols which were used to grow carbon nanotubes.

3.1 CVD Oven

The oven used for CVD is a MTF 12/38/250 tube furnace from Carbolite [151]. The oven chassis provides the power supply for the cylindrical oven which contains a 300 mm long ceramic work tube with an inner diameter of 38 mm. The oven is heated with a resistance

wire wound around the work tube. The heated length is 250 mm long. The maximal reachable temperature is 1'200 °C. A quartz tube with a length of 1 m and a diameter of 30 mm is placed within the boring of the work tube and closed on both sides with stainless steel plates (Figure 3.2). Ring clips are mounted on the tube on both sides and three screws with wing nuts are used to fix the plates. This mounting is very delicate, since the tube breaks when the ring clips are tightened to much, and the system leaks when they are not tightened enough. A heat shield inside of the quartz tube reduces the heat flow out of the oven.

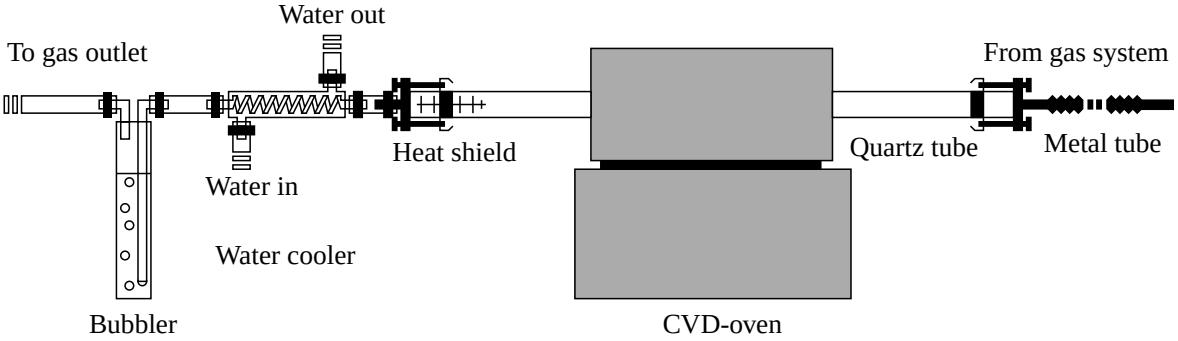

Figure 3.2: Schematics of the CVD oven. The samples are mounted from the right side.

The uniformity of temperature within the tube was tested by the manufacturer. When the tube is closed on both sides then the temperature fluctuates by ± 10 °C expect for the last 10 cm at both ends. The fluctuation within the middle zone of 95 mm is only ± 5 °C. The samples are placed in the middle of the oven on a quartz sample holder with a length of 70 mm. This means that it might be assumed that the temperature is approximately equal for all samples grown in one run.
The inlet of the oven is connected to the gas system with a flexible metal tubing. The outlet of the oven and a water cooler are joined with a short piece of teflon tube, since a plastic tube would be destroyed by the hot and aggressive exhaust gas. The cooler is connected with a piece of plastic tube to a bubbler and this again to the outside. The cooler is used to reduce the temperature of the exhaust gas to prevent the damage of the plastic tube. It is only necessary when methane with a flow of 5 l/min is used, and when the growth temperature is higher than 1'050 °C. The cooler is not used for lower growth temperatures and flows.
The presence of bubbles within the bubbler indicates that there is no major leak in the system. However there is a more important effect of the bubbler, since it serves as a diffusion barrier. There is always some unwanted gas diffusion into the oven since the system is open to the outside. This flow is reduced since it has to pass the water inside the bubbler. This means there is surely some water vapor inside the reaction tube however the amount is limited to the vapor pressure of water. Other gasses can pass the bubbler but they have to overcome two water gas boundary layers with areas of only 1 cm^2 and 5 cm^2, the surface of the bubble and the water air boundary of the bubbler, respectively. The reaction tube is flushed with argon during heating (around 30 minutes) which reduces the content of environmental gasses which are present due to the fact that the tube has to be opened to mount the sample. However there is always a small quantity of water vapor, nitrogen, oxygen and the other trace gasses of the environment present in the oven during growth in addition to the used reaction gasses. The reaction tube is flushed with argon (and in the actually used process with hydrogen too) during cooling-down to prevent the oxidation of the grown nanotubes.

3.2 The gas systems

The gas system provides the oven with the desired reaction gasses (a list with the gas purities can be found in Appendix A.3). Each of the presented gas systems contains at least one flowmeter which allows the correct setting of the desired gas flow. All gas systems consist of several gas lines for different gasses which join before the oven. The origin of each gas line is a gas bottle equipped with a reduction valve which allows the setting of the desired gas pressure. The next part is a one-way valve which protects the connected gas bottle in the case of an explosion within the gas line. It opens only when the pressure from the side of the gas bottle is higher then the pressure from the other side. The pressure stroke of an explosion would close the one-way valve and prevent the hot explosion gasses from penetrating the gas bottle. A following two way valve permits the fast opening and closing of the gas line without changing the settings of the dedicated reduction valve and flowmeter. Manometers before and after the flowmeter allow the setting of a desired pressure drop over the flowmeter (see Section 3.3 for more information about the functionality of the flowmeters). The different parts are connected with stiff stainless steel tubes with an outer diameter of 6 mm. With one exception: more flexible tubes with an outer diameter of 3 mm are used to connect the reduction valves with the one way valves to guarantee the necessary flexibility which is needed when the gas bottles have to be changed.

Dead volume and pressure drop

One possible source of measuring errors is the dead volume of the gas system. The reaction on the closing or opening of a valve is not instantaneous, since the 'old' gas in the gas line has to be replaced by the 'new' gas. The exchange time t is equal the dead volume V divided by the volume flow Φ_v. The tubes with an outer diameter of 3 mm (6 mm) have an inner diameter of 1.6 mm (4 mm). This corresponds to volumes per meter tube length of 2 ml and 50 ml, respectively. The total length of the 6 mm tubes of the gas systems is approximatively 3 m this results in a total dead volume of 3x50 ml = 150 ml. The 12 m long tube with an outer diameter of 3 mm has a volume of 24 ml. This corresponds to an exchange time of around 10 s for a gas flow of 1'500 ml. This is short compared with the usual growth time of 10 minutes. Therefore this effect can be neglected.
The pressure drop (Δp) within a tube is another aspect to be considered. It can be calculated as follows [152]:

$$\Delta p = \lambda \frac{L}{2r} \frac{\varrho_M}{2} v^2 \tag{3.1}$$

Where λ is the coefficient of friction (depending on v and the pipe roughness), L the pipe length and r the inside radius of the pipe, ϱ_M the density and v the velocity of the medium. The inner radii of the utilized tubes are 0.8 mm and 2 mm this has a big influence on the pressure drop. The proportion $\Delta p_1(0.8\text{ mm})/\Delta p_2(2\text{ mm})$ can be calculated exploiting the fact that the volume flow $\Phi_V = Av$ is constant for a constant density ϱ_M. Where $A = \pi r^2$ is the tube area. This means:

$$\frac{\Delta p_1(0.8)}{\Delta p_2(2)} = \frac{\lambda \frac{L}{2r_1} \frac{\varrho_M}{2} {v_1}^2}{\lambda \frac{L}{2r_2} \frac{\varrho_M}{2} {v_2}^2} = \frac{r_2 {v_1}^2}{r_1 {v_2}^2} = \frac{r_2 (\frac{\Phi_V}{\pi {r_1}^2})^2}{r_1 (\frac{\Phi_V}{\pi {r_2}^2})^2} = \frac{{r_2}^5}{{r_1}^5} = \frac{2^5}{0.8^5} = 97.7 \tag{3.2}$$

The 12 m long tube with an outer diameter of 3 mm used in gas system II causes a very high pressure drop compared with the remaining gas system. It is surely wise to hold it as small as possible by making the gas lines as short as possible and by avoiding small tube diameters.

3.2.1 Overview of the gas systems

Gas system I (with one variable area flowmeter, see Section 3.2.2) served for the first experiments which proved the possibility to grow carbon nanotubes with the new oven. It was very simple and did not allow the simultaneous use of two or more gasses.
Gas system II (with three thermal profile flowmeters and a variable area flowmeter, see Section 3.2.3) belongs to the old CVD system and was connected to the oven with a 12 m long tube of a diameter of 3 mm.
Gas system III (with two variable area flowmeters, a needle valve and a switch, see Section 3.2.4) was less sophisticated than gas system II but it allowed the simultaneous use of methane and argon.
Gas system IV (with three variable area flowmeters, see Section 3.2.5) allows the accurate setting of the flows of methane, hydrogen and argon.

3.2.2 Gas system I, with one variable area flowmeter

This is the most simple setup which was used (Figure 3.3). The gas lines for all used gasses (argon, methane and ethylene) were connected to the same variable area flowmeter from Kobold (KDG1137, 50 - 500 l/h, gauged to air). The gas flow was controlled by closing and opening the valves. The gas lines had an overall length from the gas bottles to the oven of approximately 3 m.

Used gasses: argon 60, methane 55 and ethylene 35.

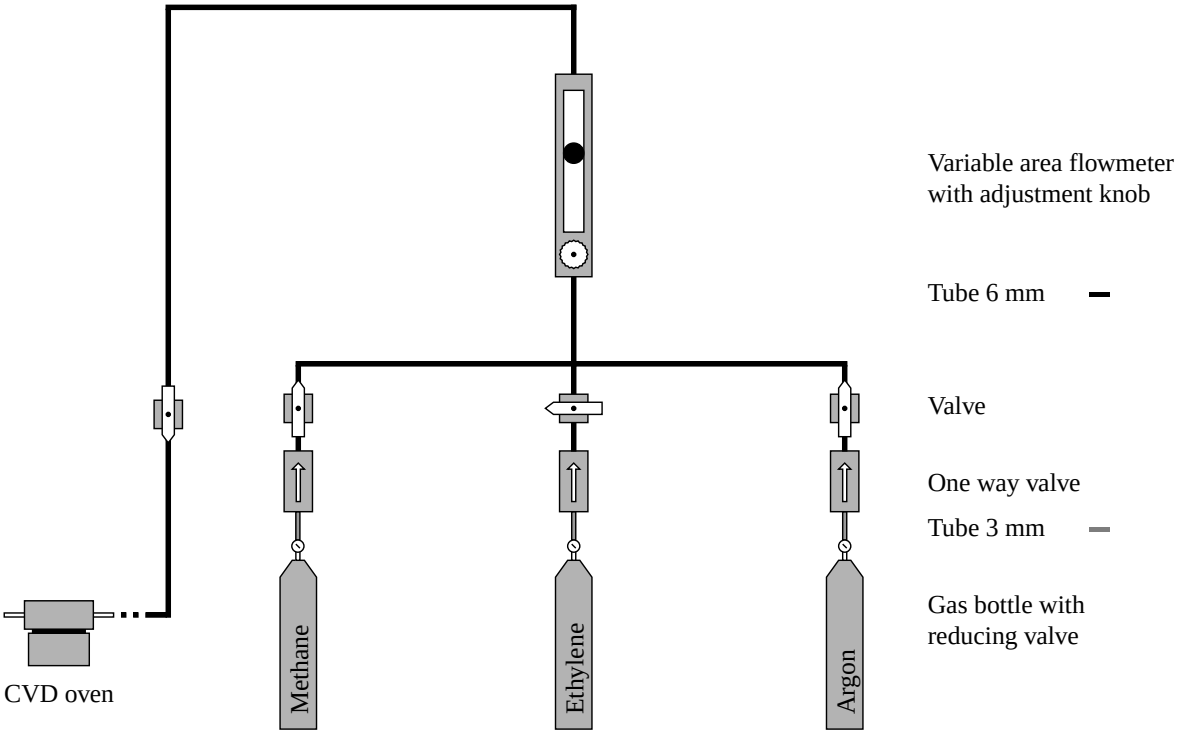

Figure 3.3: Schematics of gas system I, with one variable area flowmeter.

3.2.3 Gas system II, with three thermal profile flowmeters and a variable area flowmeter

This setup (Figure 3.4) belongs to the old CVD oven mentioned above. A Brooks instrument controller 0154 controls three Brooks instrument thermal profile flowmeters gauged to Ar (5850E, full scale flow: 1'000 ml/min), H_2 (5850E, full scale flow: 1'000 ml/min) and N_2 (5850S, full scale flow: 100 ml/min, used for the carbon feedstock: ethylene, methane or acetylene). An additional variable area flowmeter from Kobold (KDG1137, 50 - 500 l/h, gauged to air) can be used for high flows of methane. The gas system was connected to the oven with a 12 m long tube of a diameter of 3 mm. The gas lines had an overall length from the gas bottles to the oven of approximately 15 m.

Used gasses: argon 48, hydrogen 60, methane 55, ethylene 35 and acetylene 92.

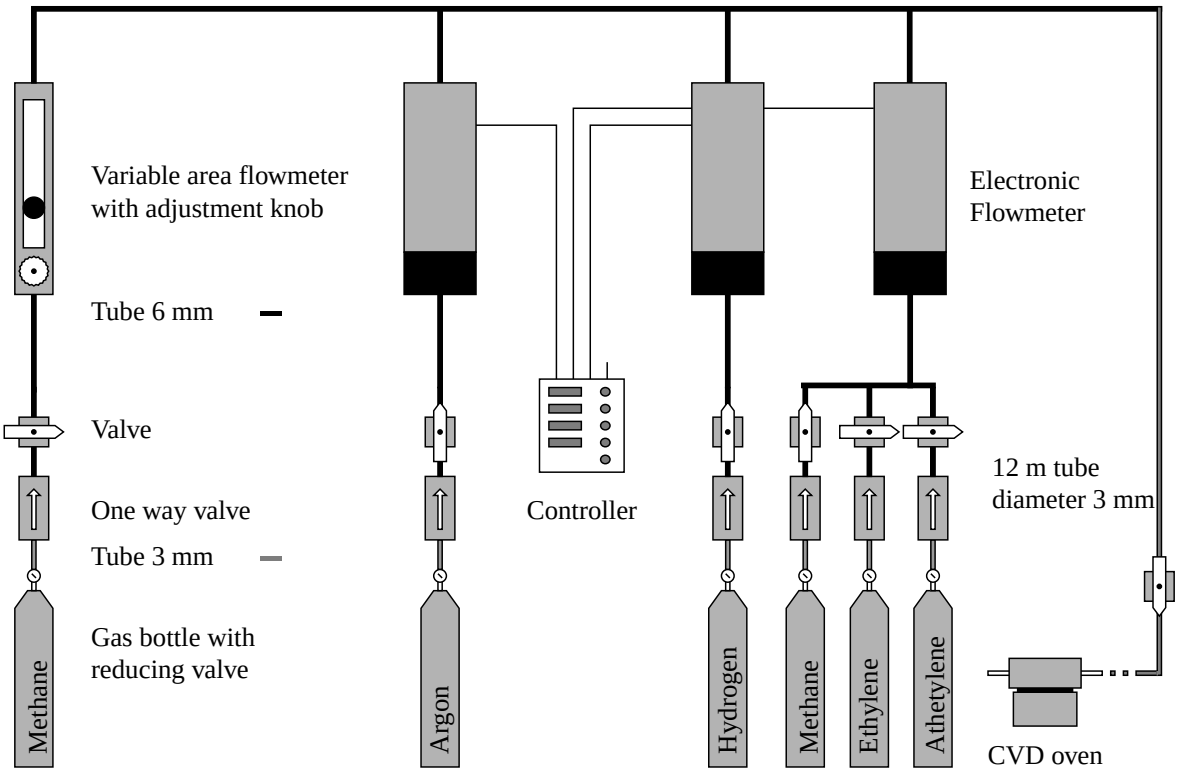

Figure 3.4: Schematics of gas system II, with three thermal profile flowmeters and a variable area flowmeter.

3.2.4 Gas system III, with two variable area flowmeters, a needle valve and a switch

The distinctiveness of this setup (Figure 3.5) was a switch which was used to toggle between argon and the carbon feedstock, which was usually methane. For some experiments a small amount of ethylene was added to the methane flow with a needle valve. The argon and the methane gas lines were equipped with variable area flowmeters from Kobold (KDG1228, 10 - 100 l/h, gauged to air). The gas flow was controlled by using the switch. It has two inlets (for argon and methane) and two outlets (to the oven and outward). The switch has two positions. In position 1 the methane line was connected to the oven and the argon line was connected outward. In position 2 the argon line was connected to the oven and the methane line was connected outward. The pressure after the switch was ≈0.1 bar ±10% relative (due to the fluctuations of the air pressure from day to day) and the pressure before the flowmeters was set to 0.2 bar relative using the manometers (this corresponds to a pressure drop of ≈0.1 bar over the flowmeters). A special feature of this system was a needle valve which was used to add a small quota of ethylene to the methane flow. The gas lines had an overall length from the gas bottles to the oven of approximately 3 m.

Used gasses: argon 60, methane 55 and ethylene 35.

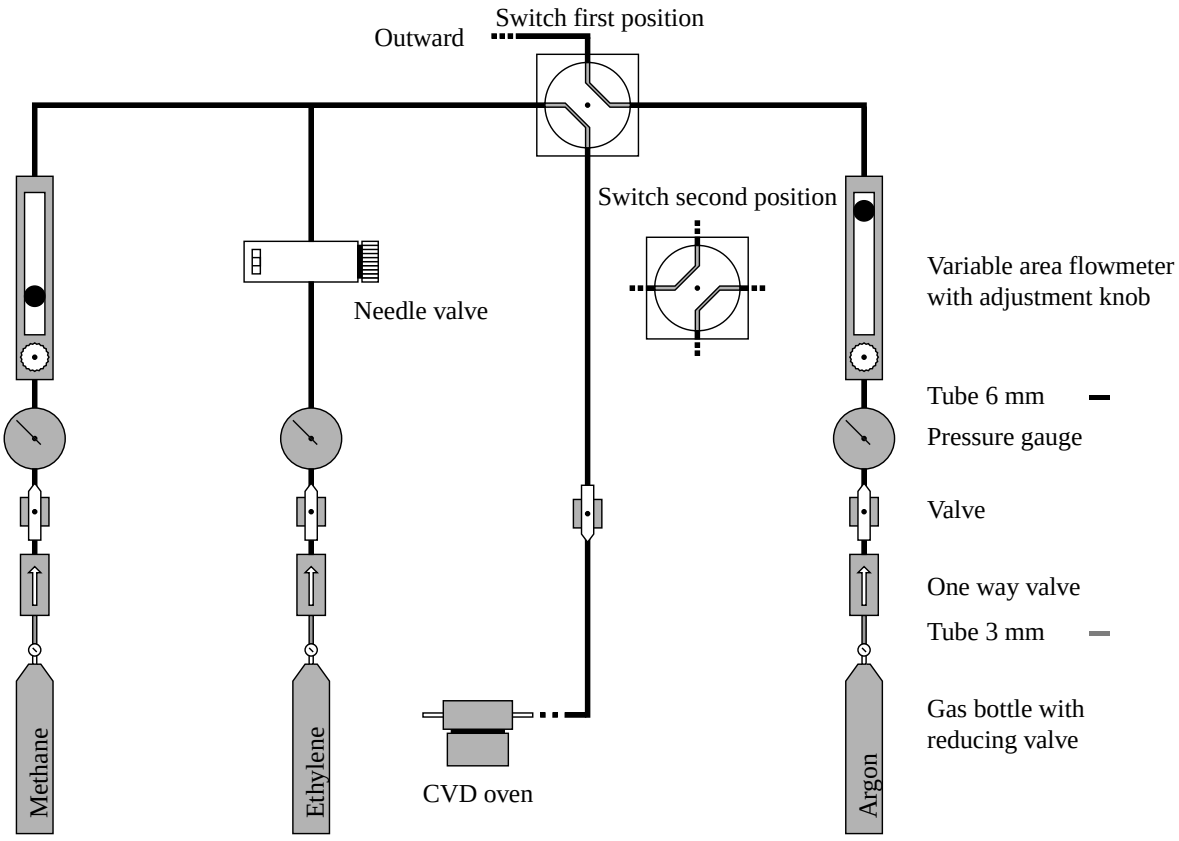

Figure 3.5: Schematics of gas system III, with two variable area flowmeters, a needle valve and a switch.

3.2.5 Gas system IV, with three variable area flowmeters

This is the currently used gas system (Figure 3.6). It allows the simultaneous use of argon, methane and hydrogen. All gas lines are equipped with variable area flowmeters from Kobold (KDG1228, 10 - 100 l/h, gauged to air for methane and argon; KDG1213, 1.6 - 16 l/h, gauged to air for hydrogen). Manometers before and after the flowmeters allow the exact setting of the pressure drop over the flowmeters (the pressure after the flowmeter depends from the actual air pressure and fluctuates by maximally ±10% from day to day). Since the flowmeters are gauged to 0.2 bar the pressure drop over the flowmeters is set to 0.2 bar, using the reduction valves of the gas bottles considering the readout of the manometers in front of each flowmeter. This makes a pressure correction unnecessary. A correction for the used gas is necessary since the flowmeters are gauged to air. (A correction table can be found in Appendix B.2.) The gas lines have an overall length from the gas bottles to the oven of approximately 3 m.

Used gasses: argon 60, hydrogen 60 and methane 55.

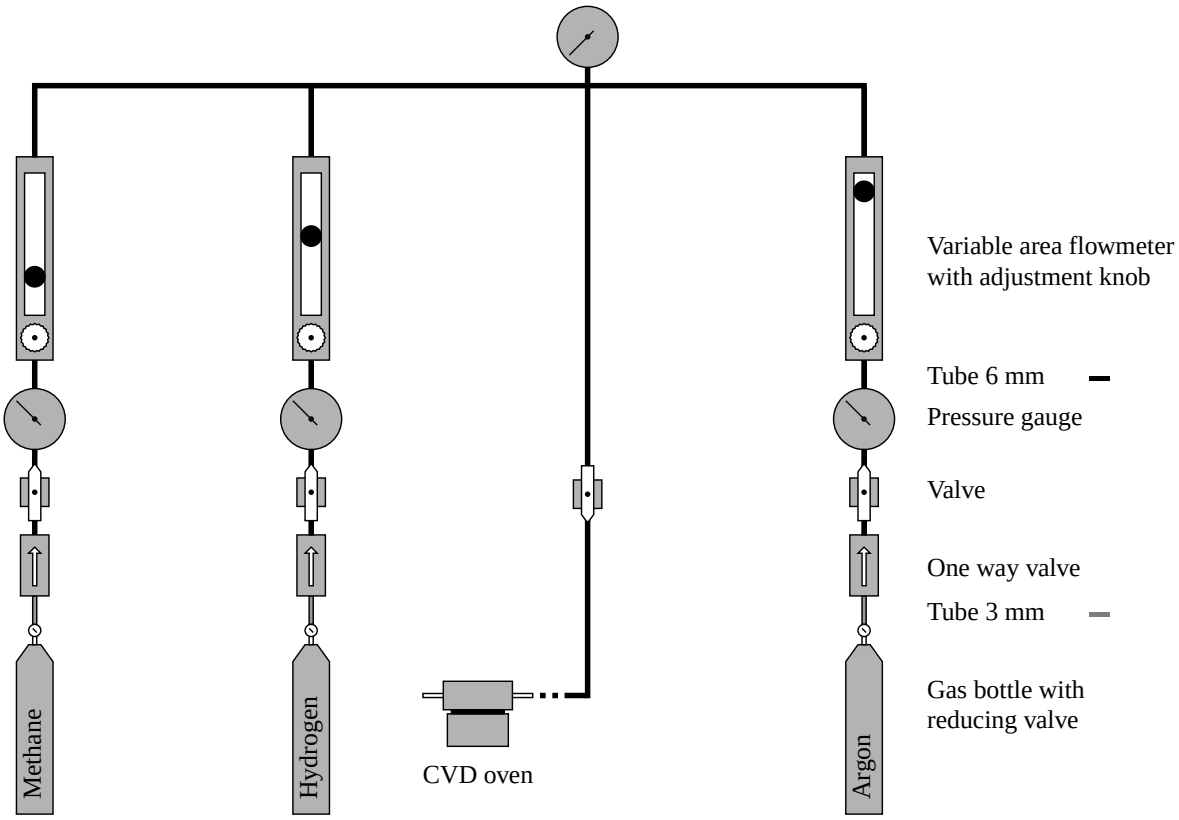

Figure 3.6: Schematics of gas system IV, with three variable area flowmeters.

3.3 Flowmeters

Flowmeters are used to measure the flow of gasses and liquids. There are several types of flowmeters available: differential pressure flowmeters, positive displacement flowmeters, turbine flowmeters, vortex flowmeters, ultrasonic flowmeters, ... [152]. Two types of flowmeters were used for the gas systems presented in the last section: variable area flowmeters from Kobold [153] and thermal profile flowmeters from Brooks Instruments [154, 155]. The functionality of these two flowmeter types will be explained below, and a valuation of there accuracy and reliability will follow.

3.3.1 Variable area flowmeters

Variable area flowmeters are very simple and cost-efficient instruments. A spherical float (other forms are common too) hovers in a conical tube which is installed vertically (Figure 3.7). The float is lifted up by the medium flowing upwards. The higher the flow rate is the higher the float is raised. Under a constant flow rate the position stabilizes. A calibrated scale on the tube allows the reading of the actual flow. The geometry of the float and the tube as well as the floating medium have an influence on the actual position of the float. This means that the scale is only correct for a specific gas at defined temperature and pressure. Any deviation from these default values makes a correction necessary. The way how this correction has to be done is described subsequently [152, 156, 157].

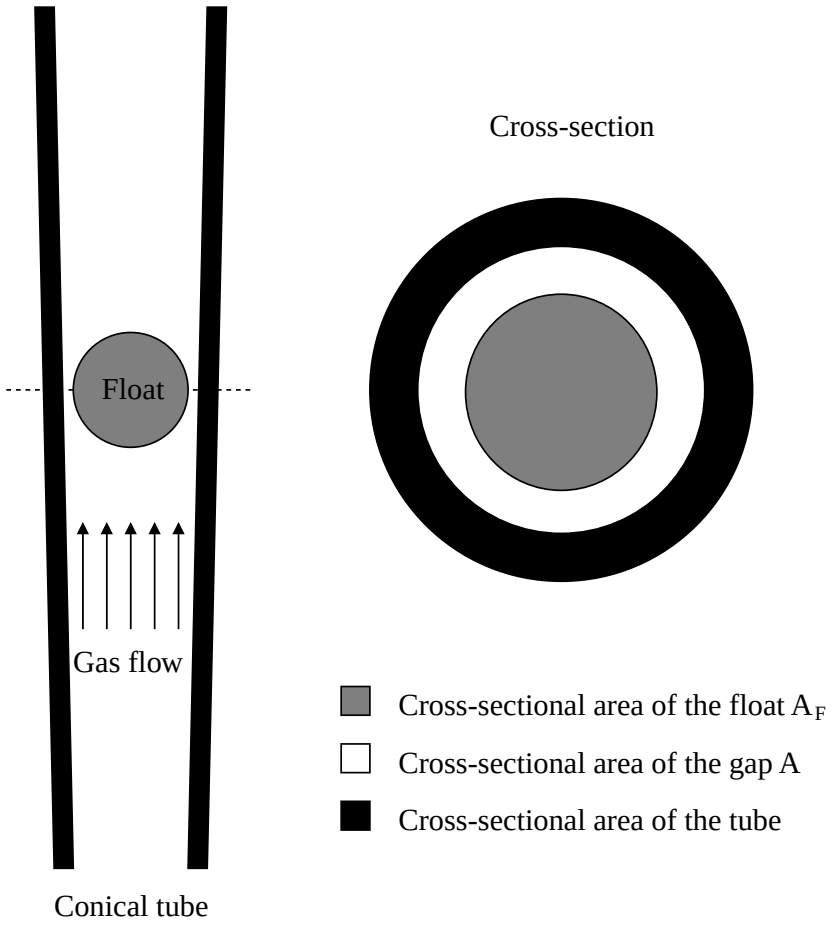

Figure 3.7: Setup of the variable area flowmeter.

The physical description of an area flowmeter is very simple: the weight of the float (F_W) is

balanced by its buoyancy (F_B) and drag (F_D), $F_W = F_B + F_D$ with:

$$F_W = V_F \varrho_F g = m_F g \tag{3.3}$$
$$F_B = V_F \varrho_M g = m_F g \frac{\varrho_M}{\varrho_F} \tag{3.4}$$
$$F_D = \frac{1}{2} c_D A_F \varrho_M v^2 \tag{3.5}$$

Where V_F is the volume of the float, g the gravitational acceleration (9.81 m/s^2), ϱ_F and ϱ_M, the density of the float and the medium, respectively, c_D the coefficient of drag, A_F the cross-sectional surface of the float and v the velocity of the medium. It follows:

$$v^2 = \frac{m_F g (1 - \frac{\varrho_M}{\varrho_F})}{\frac{1}{2} c_D A_F \varrho_M} \tag{3.6}$$

Since fraction ϱ_M / ϱ_F is negligible for gasses with small density, the last equation can be simplified to:

$$v^2 = \frac{m_F g}{\frac{1}{2} c_D A_F \varrho_M} \tag{3.7}$$

The velocity depends likewise on the size of the cross-sectional area A of the gap between float and tube wall. This area changes dependent on the position of the float, due to the conical shape of the tube (Figure 3.7). It is smaller (bigger) when the float is at the bottom (top) of the flowmeter. The mass flow (Φ_m) links velocity, cross-sectional area and density. The conservation of mass determines the constance of the mass flow. The volume flow (Φ_V) is constant too but only for a medium with constant density.

$$\Phi_m = \frac{dm}{dt} = \varrho v A \qquad [kg/s] \tag{3.8}$$
$$\Phi_V = \frac{dV}{dt} = vA = \frac{\Phi_m}{\varrho} \qquad [m^3/s] \tag{3.9}$$
$$\tag{3.10}$$

The aim of the following calculations is to find a possibility to make a correction if the calibrated scale can not be used, which means that the flowing gas (1) deviates in kind of gas, pressure or temperature from the calibration gas (0). This corresponds to the use of two flowmeters with two different gasses, where the float is in the same position for both flowmeters, which means that the cross-sectional area of the gap is the same in both flowmeters ($A_1 = A_0$).

$$\Phi_{V0} = v_0 A_0 \tag{3.11}$$
$$\Phi_{V1} = v_1 A_1 \tag{3.12}$$
$$\Rightarrow \frac{\Phi_{V1}}{v_1} = A_1 = A_0 = \frac{\Phi_{V0}}{v_0} \tag{3.13}$$
$$\Rightarrow \Phi_{V1} = \Phi_{V0} \frac{v_1}{v_0} \tag{3.14}$$

The velocities in the last equation can be replaced with $v_0 = \sqrt{\frac{m_F g}{\frac{1}{2} c_D A_F \varrho_0}}$ and $v_1 = \sqrt{\frac{m_F g}{\frac{1}{2} c_D A_F \varrho_1}}$:

$$\Rightarrow \Phi_{V1} = \Phi_{V0}\frac{v_1}{v_0} = \Phi_{V0}\frac{\sqrt{\frac{m_F g}{\frac{1}{2}c_D A_F \varrho_1}}}{\sqrt{\frac{m_F g}{\frac{1}{2}c_D A_F \varrho_0}}} \tag{3.15}$$

$$\Rightarrow \Phi_{V1} = \Phi_{V0}\sqrt{\frac{\varrho_0}{\varrho_1}} \tag{3.16}$$

The last equation can be used directly if only the kind of gas was changed and pressure and temperature fit to the conditions used for the calibration of the scale. If pressure or temperature are different another effort has to be done.
It may be assumed that a gas with small density behaves like an ideal gas, and that the equation of state of the ideal gas may be used:

$$\frac{PV}{T} = nR = \text{constant} \tag{3.17}$$

$$\frac{P_0 V_0}{T_0} = \frac{P_1 V_1}{T_1} \tag{3.18}$$

where P is the pressure, V the volume, T the temperature, n the quantity of gas expressed in moles and R the gas constant.
Due to the conservation of mass it follows that $\varrho_0 V_0 = \varrho_1 V_1$

$$\Rightarrow \sqrt{\frac{\varrho_0}{\varrho_1}} = \sqrt{\frac{P_0}{P_1}}\sqrt{\frac{T_1}{T_0}} \tag{3.19}$$

where ϱ_0 and ϱ_1 are different densities of the same gas at different pressure or temperature. It follows that:

$$\Phi_{V1} = \Phi_{V0}\sqrt{\frac{\varrho_0}{\varrho_1}} = \Phi_{V0}\sqrt{\frac{P_0}{P_1}}\sqrt{\frac{T_1}{T_0}} \tag{3.20}$$

These corrections for another kind of gas and a different pressure or temperature can be combined to a general expression for the correction of the actual gas flow in an area flow meter:

$$\Phi_{V1} = \Phi_{V0}\sqrt{\frac{\varrho_0}{\varrho_1}}\sqrt{\frac{P_0}{P_1}}\sqrt{\frac{T_1}{T_0}} \tag{3.21}$$

Note that ϱ_0 and ϱ_1 are the densities of two different gasses at normal conditions.

3.3.2 Thermal profile flowmeters

This flowmeter type exploits the dissipation of heat [154,155]. The gas flow is divided in such a way that a constant fraction of the flow passes through a heating element. Two temperature sensors are mounted equidistantly upstream and downstream of the heat input (Figure 3.8). Without any flow both sensors measure the same temperature. However a streaming gas causes a convective heat transport within the bypass which cools the sensor upstream and heats the sensor downstream the heat source. An increasing temperature difference develops with an increasing flow. This temperature difference is proportional to the amount of gas flowing and the mass flow, respectively. It is measured with the two temperature sensors. A bridge circuit interprets the temperature (voltage) difference and an amplifier provides the output to the control circuitry, which compares the command set point to the flow signal and positions the control valve.

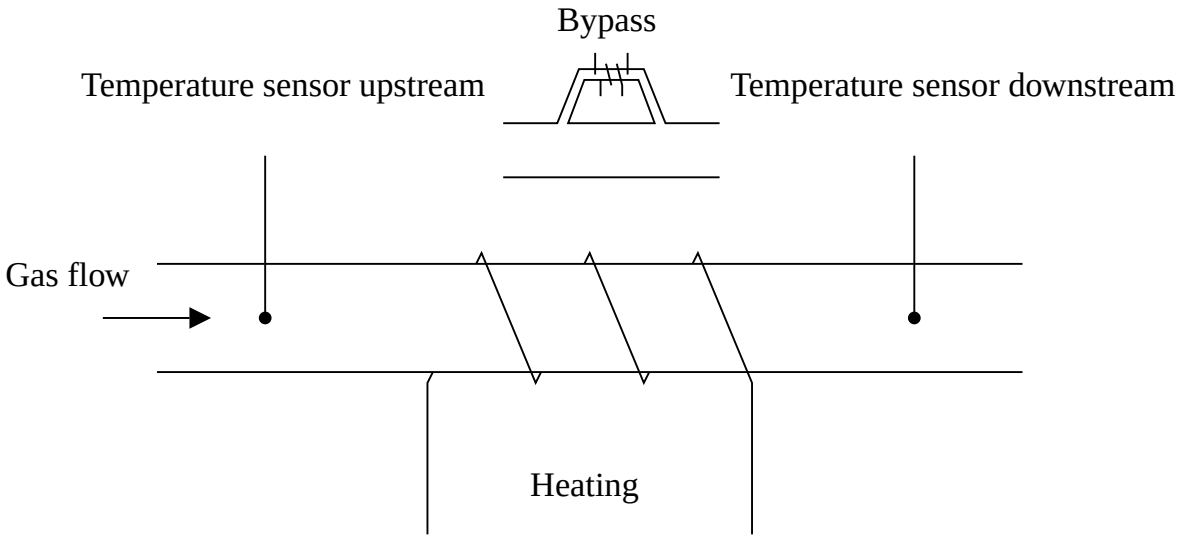

Figure 3.8: The measuring setup of a thermal profile flowmeter: the heat input with two adjacent resistance temperature measuring elements which are mounted equidistantly upstream and downstream.

This type of flowmeter can be characterized as follows [152]:

$$\Phi_m = \frac{H}{Ac_p\Delta T} \tag{3.22}$$

Where Φ_m is the mass flow rate, H the heat input, A a constant, c_p the specific heat at constant temperature and ΔT the measured temperature difference. The constant A respects the viscosity of the used gas and the effects of the measuring setup.
A correction for deviations in pressure or temperature from the calibration conditions is not necessary due to the functionality of this flowmeter. However if another gas is utilized than the gas the flowmeter was calibrated with, a correction has to be done:

$$\text{Actual gas flow rate} = \text{Output reading x } \frac{\text{gas factor of the new gas}}{\text{gas factor of the calibration gas}} \tag{3.23}$$

Only the flow of the carbon feedstock has to be corrected since the corresponding flowmeter was calibrated with nitrogen. The flowmeters used for argon and hydrogen were calibrated with the corresponding gasses and need no correction. Table 3.1 shows the gas factors and densities of different gasses.

Gas	Formula	Gas factor	Density (kg/m^3)
Nitrogen	N_2	1.000	1.251
Acetylene	C_2H_2	0.615	1.173
Ethylene	C_2H_4	0.619	1.261
Methane	CH_4	0.763	0.717
Air		0.998	1.293
Argon	Ar	1.395	1.784
Hydrogen	H_2	1.008	0.090

Table 3.1: Gas factor and density of different gasses [158].

3.3.3 Accuracy and reliability of the flowmeters

The kind of gas and its temperature and pressure can have an influence on the readout of a flowmeter, as shown in the last sections. The related issues are the accuracy and the reliability of the flowmeters.
The approach to check the accuracy of the flowmeters is shown in Figure 3.9: a measuring cylinder is filled with water, turned upside down and fixed in a bowl filled with water. The gas flows into the measuring cylinder and displaces the water. So the total flow can be measured very easily. The flow rate can be calculated by dividing the total volume by the duration of the flow. The water column inside the measuring cylinder has an influence on the pressure of the gas but it is negligible compared with the one bar environment pressure corresponding to a water column of 10 m. So a pressure correction was not done.
The flow measured with this method is compared with the reading of the flowmeter to estimate the accuracy of the flowmeter.

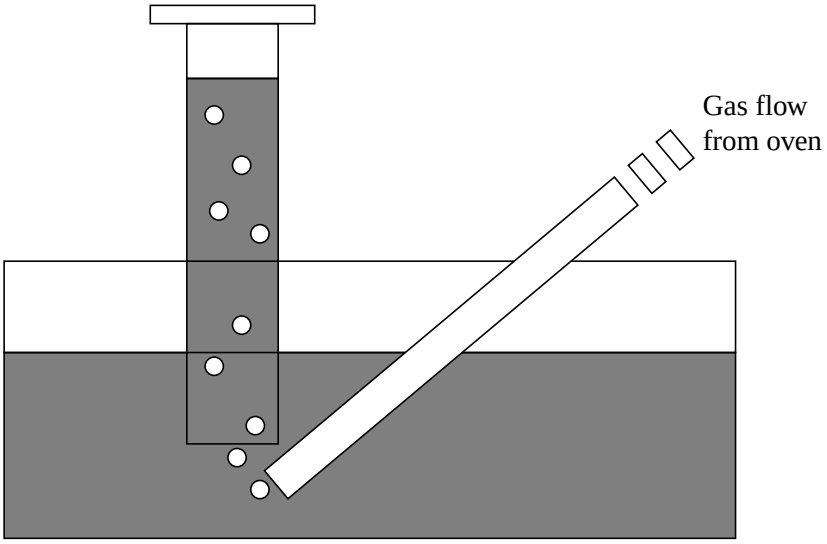

Figure 3.9: Setup for measuring the effective flow. The gas bubbles out off the tube and fills the measuring cylinder.

Accuracy of the variable area flowmeters

The mean argon flow in the variable area flowmeter is 513 ml/min using the above mentioned measuring setup (Table 3.2). The reading at the variable area flowmeter was 35 l/h and the pressure drop 0.2 bar (0.28-0.08 bar) this corresponds to a corrected flow of 496 ml/min ($\Phi_{V1} = \Phi_{V0}\sqrt{\frac{\varrho_0}{\varrho_1}} = \frac{35000ml}{60min}\sqrt{\frac{1.293}{1.784}} = 496ml/min$). The error is 513/496 = 1.03 and the inaccuracy of the reading is surely bigger than 2.5%. This check was not done with the explosive gases hydrogen and methane, however it may be assumed that their accuracy has the same order of 3%.
The room temperature (and therewith the temperature of the gasses) fluctuates over the year between 13 and 31 °C this corresponds to correction factors between $\sqrt{\frac{273+13}{273+20}} = 0.99$ and $\sqrt{\frac{273+31}{273+20}} = 1.02$. This effect is neglected.

Start vol (ml)	End vol (ml)	Total vol (ml)	Time (s)	Flow (ml/min)
25	500	475	55	518
35	500	465	55	507
Average flow				513

Table 3.2: The mean argon flow in the variable area flowmeter from two measurements is 513 ml/min.

Accuracy of the thermal profile flowmeters

The mean argon flow (Table 3.3) in the thermal profile flowmeter is 467 ml/min using the measuring setup described above. The flow was set to 400 ml/min on the controller which corresponds to an error of nearly $467/400 = 1.17$. This means the thermal profile flowmeters can not be called accurate, at least not in this setup with the 12 m long 3 mm tube. A setup without this long gas line was not tested. This check was not done with the explosive gasses hydrogen and ethylene, however it may be assumed that their accuracy has the same order of 20%.

Start vol (ml)	End vol (ml)	Total vol (ml)	Time (s)	Flow (ml/min)
25	500	475	61	467
20	500	480	60	480
25	500	475	61	467
Average flow				471

Table 3.3: The mean argon flow in the thermal profile flowmeter from three measurements is 471 ml/min.

Reliability of the thermal profile flowmeters

The gas system with the thermal profile flowmeters was not coupled directly to the oven for this test. The 12 m tube was connected with the argon line of the gas system with the variable area flowmeters. So it was possible to make an independent flow measurement. The flow through the thermal profile flowmeters depends from the pressure (Table 3.4). However the measurement error is constant for all pressures and the flow is constant above a certain threshold. This means that it is possible to operate the thermal profile flowmeters in such a way that they are pressure independent when the pressure is high enough.

Conclusions

The accuracy of the variable area flowmeters of 3% is surely higher than the accuracy of 20% of the thermal profile flowmeters. However the supplier promises an accuracy of 1% for the thermal profile flowmeters which is better than that of the variable area flowmeters. If this higher accuracy should be needed it would be surely worth the effort to test the thermal profile flowmeters without the 12 m long gas line and to work out a correction table for different flows.
A further improvement is the reduction of the dead volume of the gas system by displacing the point where the gas lines meet closer to the oven (Figure 3.10). However this signifies

Pressure bottle (bar)	Thermal (ml/min)	Area (l/h)	Pressure in (bar)	Pressure out (bar)	Corrected flow (ml/min)	Deviation
0.50	440	35	0.13	0.08	519	1.18
0.75	704	55	0.16	0.09	815	1.16
1.00	985	75	0.22	0.10	1111	1.13
1.25	1000	78	0.23	0.11	1156	1.16
1.50	1000	78	0.23	0.11	1156	1.16
1.75	1000	78	0.23	0.11	1156	1.16
2.00	1000	78	0.23	0.11	1156	1.16
2.25	1000	78	0.23	0.11	1156	1.16
2.50	1000	78	0.23	0.11	1156	1.16

Table 3.4: Pressure dependence of the thermal profile flowmeter. The flow is pressure independent when the pressure has exceeded a certain threshold. (*Thermal* means: the setting of the thermal profile flowmeter; *Area*: the reading of the variable area flowmeter; *Pressure in (out)*: the pressure before (after) the variable area flowmeter; *Corrected*: the corrected flow of the variable area flowmeter; *Deviation*: the corrected flow of the variable area flowmeter divided by the setting of the thermal profile flowmeter.)

that additional manometers have to be mounted to guarantee a precise setting of the pressure drop over the flowmeters.

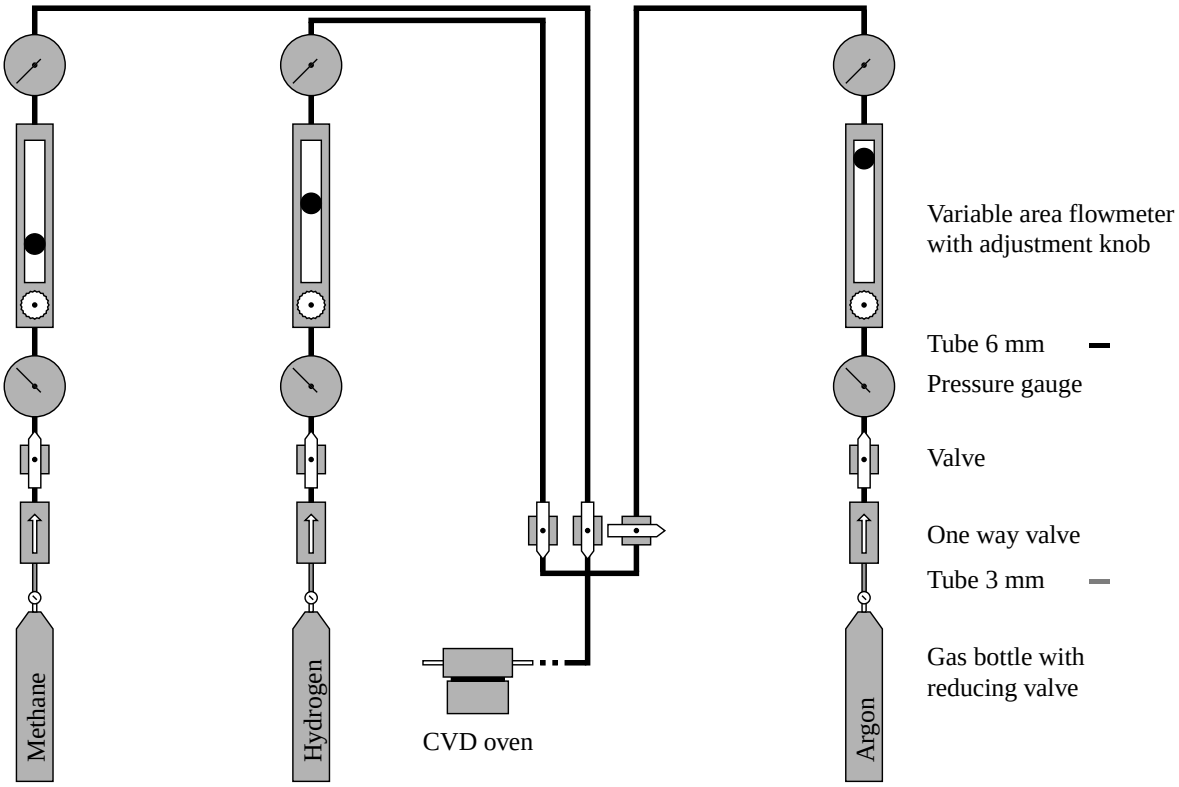

Figure 3.10: Proposal for a gas system with smaller dead volume.

3.4 Growth protocols

This section gives an overview of the utilized protocols. The step by step protocols can be found in Appendix B.1. For more details about the setup of the gas systems see Section 3.2. More information about how corrections have to be done can be found in Section 3.3. The effect of a room temperature deviating from the calibration temperature 20 °C is negligible ($< 2\%$).

All protocols have some common features

The samples are placed in the sample holder and the latter is positioned in the middle of the quartz tube of the oven. The heating of the oven is switched on. The argon line is opened contemporaneously to remove the environment gasses during the heating to the desired temperature. The gas lines of the reaction gasses (carbon feedstock and hydrogen) are opened when the growth temperature is reached. For some protocols the argon line is closed during growth and reopened afterwards, however it is important to maintain a permanent gas flow through the quartz tube, since a stop of the gas flow might implicate the formation of amorphous carbon (see Section 5.2 for more details.) The reaction gas lines are closed to stop the growth. The heating of the oven is switched off to allow the cooling down of the oven. Argon is used as a protective gas to avoid the oxidation of the grown nanotubes. The sample holder is taken out of the oven when the temperature is below 350 °C. To avoid the oxidation of the grown carbon nanotubes the samples are taken away from the still very hot sample holder as fast as possible and placed on a piece of metal to cool them down to room temperature as fast as possible.

3.4.1 Gas system I - Methane protocol

The gas system was operated with two gas lines for argon and methane, respectively. The pressure at the reducing valve of the gas bottles was set to 2 bar and the pressure after the flowmeter was 0.1 bar.
The carbon feedstock was methane with a flow of either 700 or 4'180 ml/min±3% with a growth time of 10 minutes. (The reading at the variable area flowmeter was either 50 or 300 l/h, this corresponds to a corrected flow of: $\frac{50'000ml}{60min}\sqrt{\frac{1.293}{0.717}}\sqrt{\frac{0.2+1}{2.0-0.1+1}} = 696ml/min.$)
Argon (at a flow of 880 ml/min±3%) was used as protecting gas during heating and cooling down, but not during growth. (The reading at the variable area flow meter was 100 l/h, this corresponds to a corrected flow of: $\frac{100'000ml}{60min}\sqrt{\frac{1.293}{1.784}}\sqrt{\frac{0.2+1}{2.0-0.1+1}} = 882ml/min.$)

3.4.2 Gas system II - Ethylene/hydrogen protocol

The gas system was operated with three gas lines for argon, hydrogen and ethylene, respectively. Ethylene was replaced by either methane or acetylene for some experiments.
The usual carbon feedstock was ethylene with a flow of either 1.2 or 12.4 ml/min±20% with a growth time of 10 minutes. (The reading at the controller was 2 or 20 ml/min, the flowmeter is calibrated with nitrogen, this corresponds to a correction for the other kind of gas of: $2ml/min\frac{0.619}{1.000} = 1.24ml/min.$)
For a few experiments the carbon feedstock was either methane (or acetylene) with a flow of either 1.5 (or 1.2) ml/min±20% or 15.3 (or 12.3) ml/min±20%. (The reading at the controller was 2 or 20 ml/min, the flowmeter is calibrated with nitrogen, this corresponds to a correction for the other kind of gas of: $2ml/min\frac{0.619}{1.000} = 1.24ml/min.$)
A hydrogen flow of 600 - 688 ml/min±20% was used simultaneous with the carbon feedstock. Argon (at a flow of 1'058 ml/min±20%) was used as protecting gas during the whole process.

3.4.3 Gas system II - Methane/ethylene protocol

The gas system was operated with three gas lines for argon, methane and ethylene, respectively.
The carbon feedstock was methane with a flow of 530 ml/min±20% in combination with an ethylene flow of 0.6 (or 1.9 or 5.6) ml/min±20% with a growth time of 10 minutes. This corresponds to about 1000 (or 3000 or 9000) ppm ethylene in the methane flow. (The reading at the controller was 700 ml/min methane, the flowmeter is calibrated with hydrogen, this corresponds to a correction for the other kind of gas of: $700ml/min\frac{0.763}{1.008} = 530ml/min$. The reading at the controller was 1, 3 or 9 ml/min ethylene, the flowmeter is calibrated with nitrogen, this corresponds to a correction for the other kind of gas of: $1ml/min\frac{0.619}{1.000} = 0.62ml/min$.)
Argon (at a flow of 1'058 ml/min±20%) was used as protecting gas during heating and cooling down, but not during growth.

3.4.4 Gas system III - Methane protocol

The gas system was operated with two gas lines for argon and methane as well as a switch with two inlets (argon and methane) and two outlets (oven and out). The pressure at the manometers before the flowmeters was set to 0.2 bar for both gasses using the reduction valves of the gas bottles, the downstream pressure was 0.1 bar with an accuracy of 10%. This corresponds to a pressure drop of 0.1 bar over the flowmeters. The switch has two positions: In position 1 methane is connected to the oven and argon to out. In position 2 argon is connected to the oven and methane to out.
The carbon feedstock was methane with a flow of 1'400 ml/min±3% with a growth time of 10 minutes. (The reading at the variable area flowmeter was 60 l/h, this corresponds to a corrected flow of: $\frac{60'000ml}{60min}\sqrt{\frac{1.293}{0.717}}\sqrt{\frac{1.2}{1.1}} = 1'402ml/min$.)
Argon (at a flow of 890 ml/min±3%) was used as protecting gas during heating and cooling down, but not during growth. (The reading at the variable area flow meter was 60 l/h, this corresponds to a corrected flow of: $\frac{60'000ml}{60min}\sqrt{\frac{1.293}{1.784}}\sqrt{\frac{1.2}{1.1}} = 888ml/min$.)

3.4.5 Gas system IV - Methane/hydrogen protocol

The gas system is operated with three gas lines for argon, hydrogen and methane, respectively. The pressure drop over the flowmeters is set to 0.2 bar, using the reduction valves of the gas bottles. This setting makes a pressure correction unnecessary.
The carbon feedstock is methane with a flow of 1'000 ml/min±3% with a growth time of 10 minutes. (The reading at the variable area flowmeter is 45 l/h, this corresponds to a corrected flow of: $\frac{45'000ml}{60min}\sqrt{\frac{1.293}{0.717}} = 1'007ml/min$.)
A hydrogen flow of 500 ml/min±3% is used simultaneously with the carbon feedstock. (The reading at the variable area flowmeter is 8 l/h, this corresponds to a corrected flow of: $\frac{8'000ml}{60min}\sqrt{\frac{1.293}{0.090}} = 505ml/min$.)
Argon (at a flow of 1'500 ml/min±3%) is used as protecting gas during heating and cooling down, but not during growth. (The reading at the variable area flow meter is 105 l/h, this corresponds to a corrected flow of: $\frac{105'000ml}{60min}\sqrt{\frac{1.293}{1.784}} = 1'489ml/min$.)

Chapter 4

Catalyst and sample preparation

The main focus of this chapter is the development of an appropriate catalyst for the growth of single-wall carbon nanotubes by chemical vapor deposition (CVD). Such a catalyst can be obtained in different ways (Figure 4.1). The catalyst can be evaporated directly on the sample. This is easy, but the catalyst has to be annealed. A liquid based catalyst can be spread on the sample by means of a spin coater. This allows more complex catalysts, but the control is more difficult.

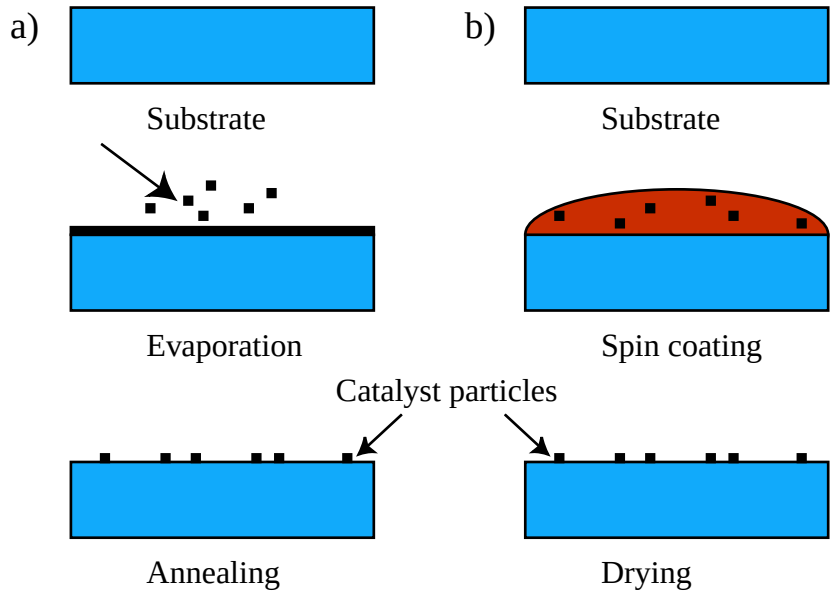

Figure 4.1: a) Catalyst evaporation. b) Spinning of a liquid based catalyst.

Since the grown single-wall carbon nanotubes will be used for electrical transport measurements the common setup for such experiments has to be taken into account (Figure 2.14). It consists of a nanotube contacted with several electrodes. This means the density of the tubes should not be too high to avoid shorts between the electrodes induced by a series of nanotubes in direct contact. On the other hand the density should be high enough to facilitate the fast search for an appropriate nanotube.
The catalyst can be spread evenly distributed over the whole sample or only in specific areas. Latter can be achieved by adapting the process shown in Figure 6.7. A pattern of equidistant squares is written using e-beam lithography and the plasma etching step is replaced by evaporating a metal layer or spreading a liquid catalyst. After this step some catalyst is on top of the PMMA and other directly on the substrate. The catalyst on the PMMA can

be removed together with the PMMA, leaving behind only the patterned catalyst on the substrate. The first approach is simpler however the probability of shorts due to nanotube nanotube contacts is higher. Both approaches were tested however the simple method resulted in a better outcome.

The next sections give an overview about how the evaporated and liquid catalysts were made. For results see the following Chapters. Details about the gas systems are described in Chapter 3.

4.1 Catalyst evaporation

Evaporating the catalyst is surely the most direct way to coat a sample with catalyst. It has the additional advantage that the amount of catalyst per area can be controlled very easily by changing the thickness of the evaporated metal layers. An e-gun in a PLS 500 Labor System from Balzers-Pfeiffer was used to evaporate Fe, Ni and Al layers [159, 160].
The principle of evaporation with an e-gun is very simple. Electrons are emitted from the hot filament of the e-gun and deflected by a tunable magnetic field. The e-beam is centered on the target material in a crucible which melts and evaporates. A shutter which covers the sample mounted on a sample holder is opened until the desired layer thickness is reached. The thickness is measured with an oscillating quartz crystal whose frequency changes depending on the layer thickness and the evaporated material. The electronic of the system calculates the effective thickness of the evaporated layer.
Fe and Ni are known to catalyze the growth of carbon nanotubes (see Section 2.2 for more details). Al is a component of the iron molybdenum alumina catalyst, therefore its suitability as a co-catalyst of Fe was tested. Although it does not show any catalytical activity when it is used unassisted it enhances the activity of Fe when it is evaporated prior to the Fe layer (Figure 4.2). This supports the proposal about a nanotube growth mechanism in Section 2.2.4. This seems to be in contradiction with the observation that a 20 nm Al layer below a 2 nm Fe layer on a Si(100) substrate depletes the Fe completely [114]. However when an Al_2O_3 layer is used instead of Al the growth of nanotubes is very efficient [115]. Since samples with a thick Fe layer have a rusty appearance after growth and the oxidation of Al is much easier than that of Fe, it might be assumed that the Al layer is oxidized during heating, at least partially.

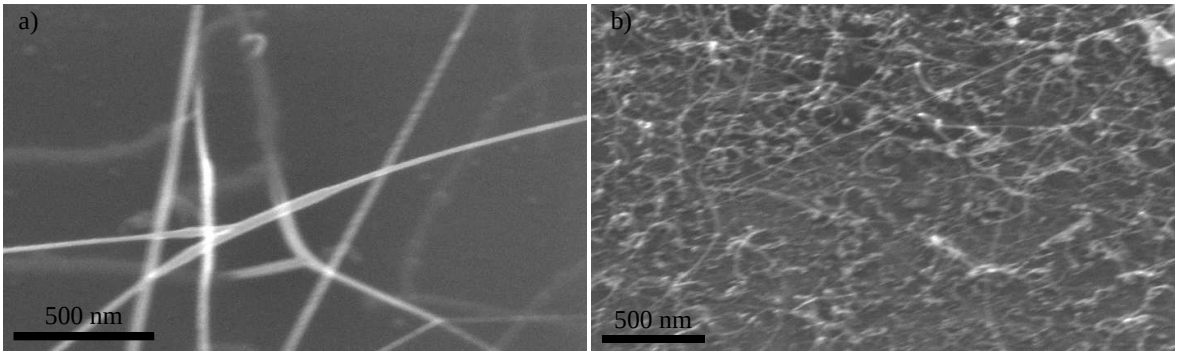

Figure 4.2: The presence of Al has a great influence on the number of grown tubes: a) a 0.4 nm thick Fe layer with only a few tubes and b) a 0.4 nm thick Fe layer on 10 nm Al with much more tubes. (The tubes were grown on SiO_2 at 950 °C with ethylene at 12 ml/min±20% and hydrogen at 680 ml/min±20%, the argon flow was 1'058 ml/min±20% during the whole process, using gas system II.)

A crucial point is the formation of clusters which act as origin for the growth of the nanotubes. They are formed during the heating of the samples. Figures 4.3, 4.4 and 4.5 show the dependency of the cluster size from the thickness of the evaporated Fe layer. The samples were heated to 900 °C in an argon flow of 1'058 ml/min±20%, using gas system II. The clusters have a size of 300 - 500 nm for a 20 nm thick Fe layer, and there are smaller clusters (50 nm) in the background. For a 5 nm layer the clusters have a diameter of roughly 50 nm. For a 2 nm thick Fe layer the clusters are almost invisible. On a 0.5 nm thick Fe layer there are no clusters visible. This shows a clear dependency of the cluster diameter from the layer thickness.

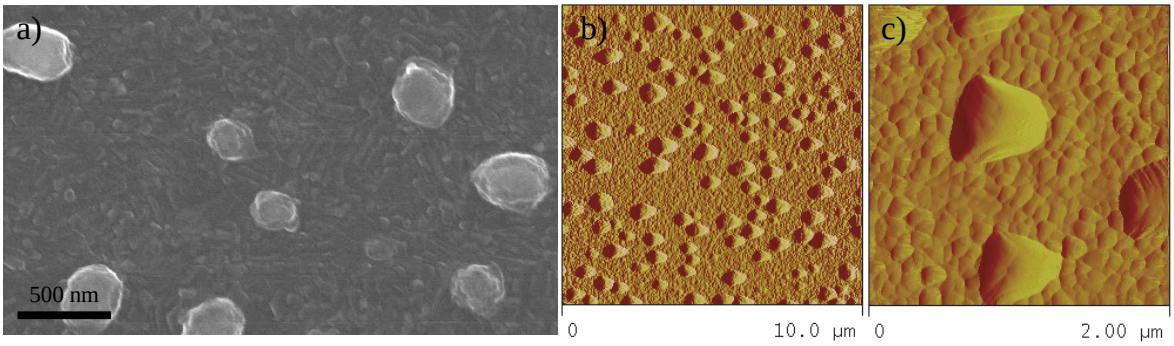

Figure 4.3: SEM and AFM pictures from Fe clusters formed from a 20 nm thick evaporated Fe layer on SiO_2.

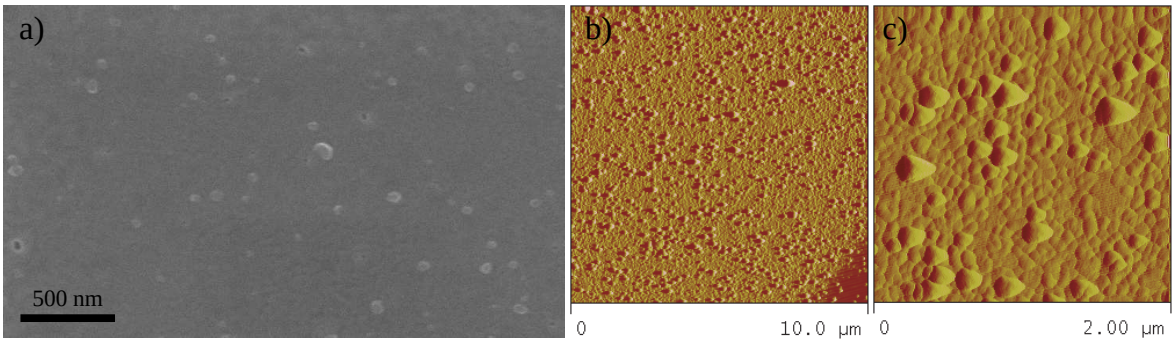

Figure 4.4: SEM and AFM pictures from Fe clusters formed from a 5 nm thick evaporated Fe layer on SiO_2.

Conclusions

It could be shown that evaporated Al enhances the catalytical effect of Fe, and that the size of the clusters formed during heating the sample depends from the thickness of the evaporated metal layer.

4.2 Liquid based catalysts

The following sections present the results of the liquid based catalyst consisting of iron nitrate ($Fe(NO_3)_3$-$9H_2O$), molybdenum dioxide dichloride (MoO_2Cl_2) and alumina (Al_2O_3) in different combinations. The alumina nanopowder is used with two different particle sizes with diameters of 4 and 40 nm.

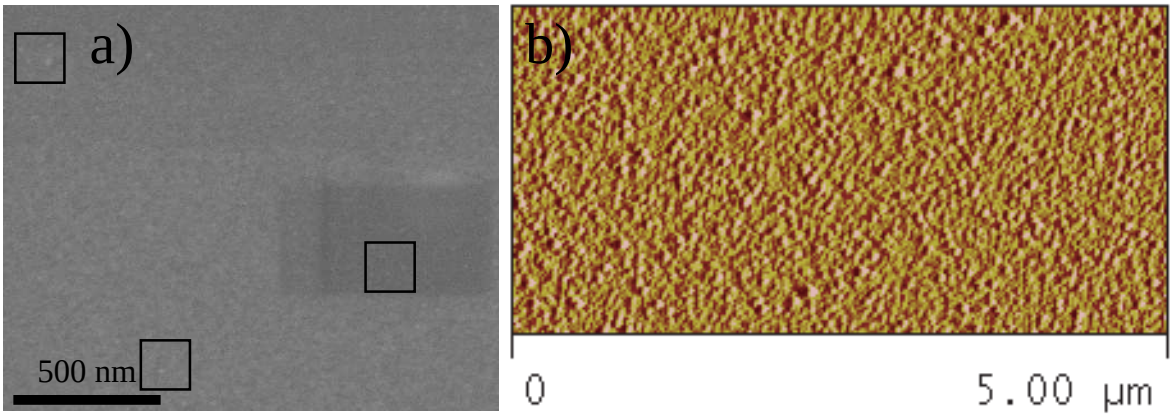

Figure 4.5: SEM and AFM pictures from Fe clusters formed from a 2 nm thick evaporated Fe layer on SiO_2.

The solvents are water, methanol, ethanol and 2-propanol (isopropylic alcohol). The solubility of the catalyst components depends on the solvent (Table 4.1). The solvent has to fulfill a very important requirement, it must not interact with other components on a sample, e.g. PMMA (polymethyl methacrylate). It will be shown that only 2-propanol is suitable for the production of samples for transport measurements.
The composition is similar to that of the catalyst used by J. Kong *et al.* [73]. However there is a difference in the recipe, MoO_2Cl_2 is used instead of MoO_2(acac) which was not available. Liquid based catalysts are more sophisticated than evaporated ones since there are more parameters to be controlled, since the catalyst can undergo chemical reactions and physical changes as recrystallization after it is mixed, which might influence the final composition and size of the catalyst particles.

Compound	MW	Soluble in
Al_2O_3	101.96	very slightly in acids, bases
$Fe(NO_3)_3$-$9H_2O$	404.00	water, alcohol, acetone; slightly in HNO_3
MoO_2Cl_2	198.84	water, alcohol, ether

Table 4.1: Molecular weight and solubility of alumina, iron nitrate and molybdenum dioxide dichloride [161].

Tests of the catalytical activity did show that nanotubes grow with iron nitrate alone and a combination of iron nitrate and molybdenum dioxide dichloride. Alumina and molybdenum dioxide dichloride show no growth when they are used alone (at 950 °C with a methane flow of 1'400 ml/min±3% for 10 minutes, the argon flow was 890 ml/min±3% during heating and cooling down, using gas system III).

Solution #30

The results of the experiments with iron nitrate dissolved in ethanol and water are not worth mentioning with one exception: Solution #30, a solution of 10 mM $Fe(NO_3)_3$-$9H_2O$ in water which was kept for 1 day at 85 °C (prepared by C. Schönenberger). Some results can be found in the following chapters.

Sample preparation

These steps are common for all liquid based catalysts. The SiO_2 samples are sonicated in acetone for 5 minutes and in 2-propanol for 2 minutes. To spread the catalyst the samples are placed on a spinning table and covered with catalyst. The excess solution is removed by the fast revolving of the spinning table (for 40 seconds). The amount of the deposited catalyst depends on the number of revolutions per minute (rpm) of the spinning table.

4.2.1 The iron molybdenum alumina catalyst dissolved in methanol

Methanol is the solvent used by J. Kong *et al.* [73] so this solvent was tested first. In fact it was possible to grow nanotubes with the catalyst dissolved in methanol.
First experiments did show growth between 850 and 1'050 °C. (The methane flow was 1'400 ml/min±3% for 10 minutes, and the argon flow was 890 ml/min±3% during heating and cooling down, using gas system III.)

- At 800 °C there was no visible growth.
- At 850 °C only a few tubes grew.
- At 900 °C a little more tubes grew.
- At 950 °C the grown tubes were nice and long.
- At 1'000 °C the tubes were less good visible, which might mean that they were thinner. They were strait and long and grew even from small particles.
- At 1'050 °C the tubes looked comparable to them grown at 1'000 °C, however there was some amorphous carbon visible.
- At 1'100 °C the sample was covered with amorphous carbon and no tubes could be found. Imaging was very hard due to charging effects.

These experiments were done with a solution of 200 mg $Fe(NO_3)_3$-$9H_2O$, 50 mg MoO_2Cl_2 and 150 mg Al_2O_3 4 nm nanopowder dissolved in 15 ml methanol. This stock solution was stirred overnight and sonicated for 1 hour prior to use. 1 ml of the sonicated solution was thinned with 9 ml methanol, sonicated for 4 hours and stirred over night. The SiO_2 samples were covered with the catalyst and a spinning table at 2'000 rpm was used the remove the excess solution.
This solution was tested with samples covered with PMMA, the resist used for e-beam-lithography. The PMMA film was attacked by the catalyst solution.

Conclusions

The catalyst is suitable for the growth of carbon nanotubes, however the solvent methanol is to aggressive to be used with PMMA. Water promises to be a less aggressive solvent.

4.2.2 The iron molybdenum alumina catalyst dissolved in water

A test did show that water has no negative interactions with PMMA. However this catalyst has the very unpleasant property to dry very slowly, in addition the catalyst tends to form huge clusters when it is spread using the spinning table. The biggest clusters are even clearly visible by eye. The cluster formation might be due to the fact that compared with methanol the boiling point and the surface tension of water are much higher (Table 4.2). Another possible explanation is the different solubility of the used components in water and methanol.

Solvent	Formula	Boiling point	Surface tension
		°C	mN/m at 25 °C
Ethanol	CH_3-CH_2(OH)	78.2	21.97
Methanol	CH_3(OH)	64.6	22.07
2-Propanol	CH_3-CH(OH)-CH_3	82.3	20.97
Water	H_2O	100.0	71.99

Table 4.2: Boiling point and surface tension of different solvents [161].

Alumina is soluble in acids and bases so it was tried to change the pH of the solution by adding acidic and basic solutions with the goal to overcome this problem. Another approach was to try to enhance the adhesion of the sample surface by cleaning the sample surface with a plasma etcher or spreading hexamethyldisilazane (HMDS is used as adhesion layer for the UV resist).
The subsequent stock solutions were used for the following experiments: 30 mg alumina nanoparticles (either 4 or 40 nm diameter) dissolved in 20 ml water, and 112 mg $Fe(NO_3)_3$-$9H_2O$ plus 15 mg MoO_2Cl_2 dissolved in water (iron molybdenum solution).
Diluted HCl affects the alumina nanoparticles they become smaller and the density per area sinks, as shown in Figure 4.6 a) with alumina nanoparticles of 4 nm diameter (spinning at 1'000 rpm) and b) with 4 nm alumina nanoparticles in $0.5x10^{-4}$ M HCl (1 ml of 4 nm alumina solution mixed with 1 ml 10^{-4} M HCl). Figure 4.7 compares the effect of the size of the alumina nanoparticles: in $0.5x10^{-2}$ M HCl the 4 nm particles a) are almost vanished, whereas a lot of the 40 nm particles b) are still present.

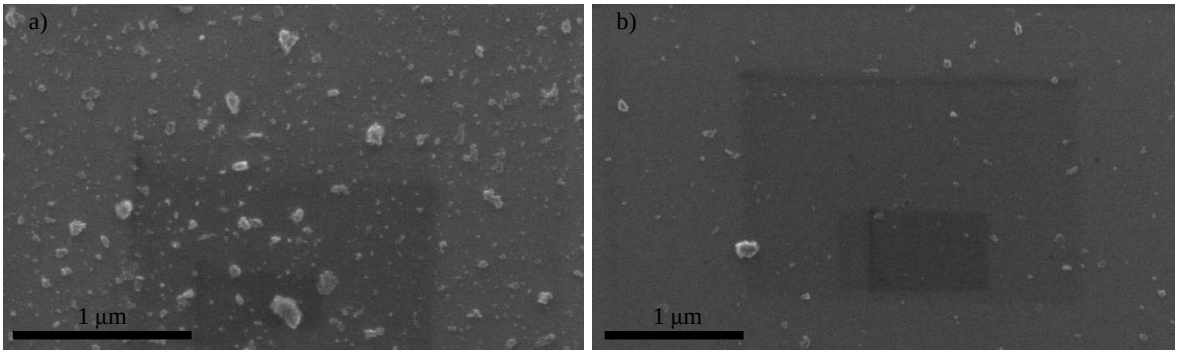

Figure 4.6: Alumina nanoparticles of 4 nm diameter dissolved in a) water and b) $0.5x10^{-4}$ M HCl.

Figure 4.8 a) shows that it is in fact possible to grow nanotubes with the acidic iron molybdenum alumina catalyst dissolved in water (a mixture of 0.5 ml iron molybdenum solution and 0.5 ml 4 nm alumina solution with 0.5 ml of 10^{-2} M HCl, spinning at 1'000 rpm) but the yield is very poor and the sample surface is very impure. Much better results could be achieved with a basic solution (a mixture of 0.5 ml iron molybdenum solution and 0.5 ml 4 nm alumina solution with 0.5 ml of 10^{-2} M NaOH, the sample was covered with this solution for 5 minutes and dipped into water and ethanol). The sample surface is cleaner and the nanotube density is comparable (Figure 4.8b)).
An additional cleaning step with the plasma etcher (5 seconds 16% O_2, 100 W, 0.025 Torr; 5 minutes 34% CHF_3, 4% O_2, 70 W, 0.025 Torr; 10 seconds 16% O_2, 100 W, 0.025 Torr) improved the adhesion of the catalyst, however it brought no additional benefit, compared with the result with the basic solution. This cleaning was to harsh, and the surface became

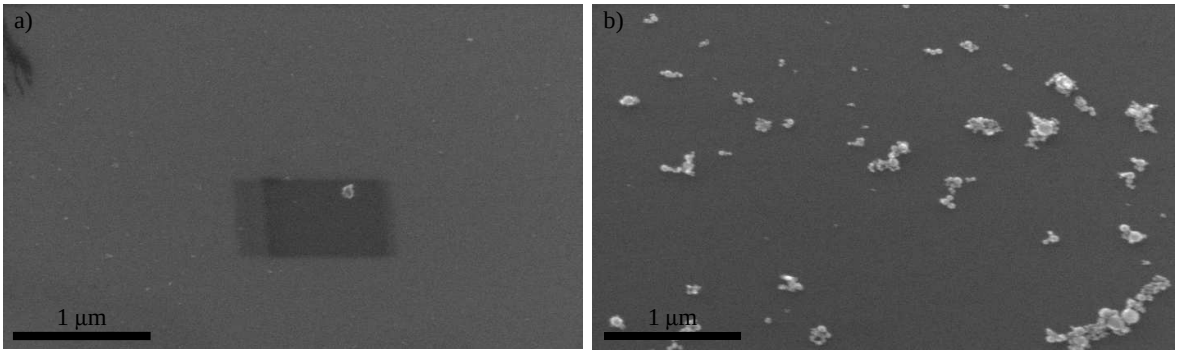

Figure 4.7: Alumina nanoparticles of a) 4 and b) 40 nm diameter dissolved in 0.5x10^{-2} M HCl.

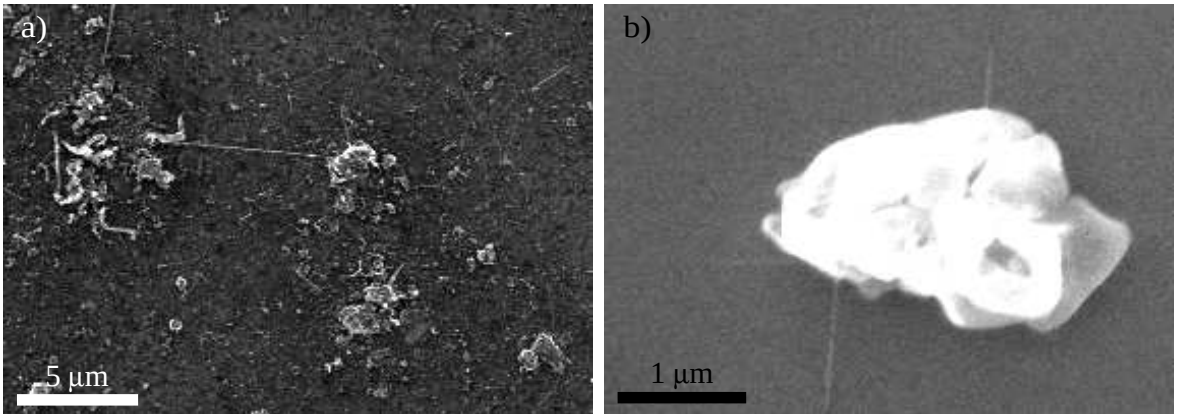

Figure 4.8: Nanotubes grown on SiO_2 with a) acidic and b) basic iron molybdenum alumina catalyst dissolved in water. (The tubes were grown at 950 °C with a methane flow of 1'400 ml/min±3% for 10 minutes, the argon flow was 890 ml/min±3% during heating and cooling down, using gas system III.)

bumpy. HMDS was another candidate for improving the adhesion of the catalyst to the sample surface. However it did not fulfill the expectations, since the adhesion was even worse than without HMDS.

Conclusions

These results (together with not presented ones) can be summarized as follows: Water is not the optimal solvent for spreading the catalyst with a spinner, since the adhesion of the catalyst particles to the sample surface is to weak. The use of a basic solution gave a slight improvement of the adhesion of the catalyst compared with the neutral and the acidic solutions. A surface cleaning with the plasma etcher resulted in a little additional improvement.

4.2.3 The iron molybdenum alumina catalyst dissolved in 2-propanol

As shown in the last sections methanol and water are not appropriate solvents for the iron molybdenum alumina catalyst. 2-propanol was chosen since it is an organic solvent like methanol with comparable boiling point and surface tension (Table 4.2). In addition 2-propanol is compatible with PMMA and less toxic than methanol.
Figure 4.9 b) shows that it is possible to grow nanotubes with this catalyst, however with

a very low yield. The catalyst has a very big tendency to accumulate in distinct clusters, as shown in a). (The tubes were grown at 950 °C with a methane flow of 1'400 ml/min±3% for 10 minutes, the argon flow was 890 ml/min±3% during heating and cooling down, using gas system III.) These are the common growth conditions used in this section.

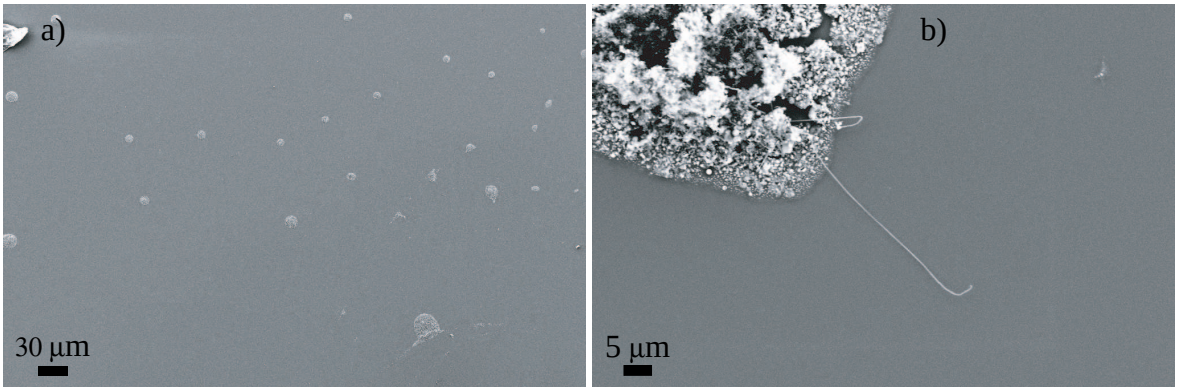

Figure 4.9: a) The catalyst has a very strong tendency to accumulate. b) Nanotubes grown on SiO_2 with the iron molybdenum alumina (40 nm) catalyst dissolved in water.

It was tried to use acidic and basic solutions to overcome this problem, however with little success. The solution was an additional cleaning step of the substrate. Figure 4.10 a) shows the results using the plasma etcher (1 minute 16% O_2, 200 W, 0.025 Torr) and b) the UV-ozone cleaner, respectively. Both results are acceptable however the operation of the UV-ozone cleaner is much simpler than that of the plasma etcher.

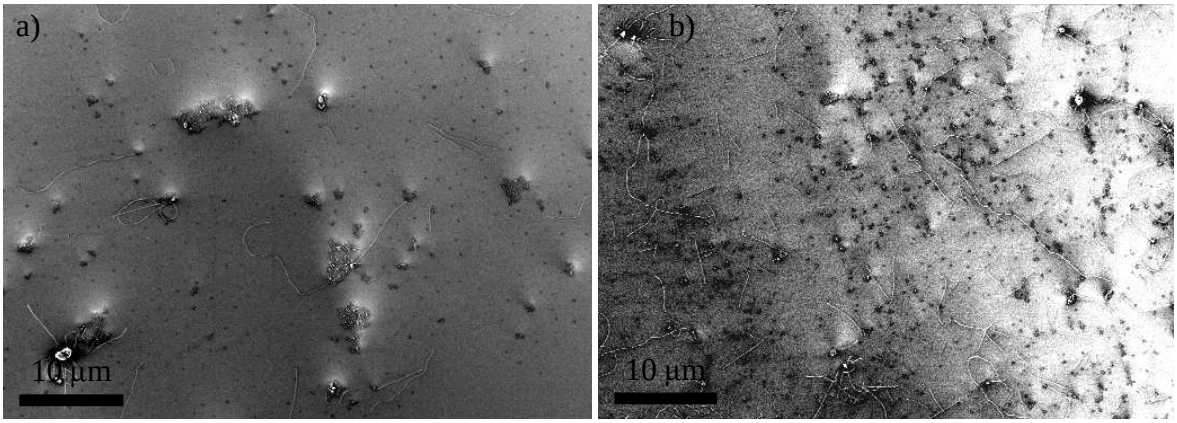

Figure 4.10: Nanotubes grown with the iron molybdenum alumina (4 nm) catalyst on SiO_2 cleaned with a) the plasma etcher or b) the UV-ozone cleaner. The catalyst is spread "homogenously" compared with Figure 4.9.

Also the catalyst can be spread "homogenously" over the whole sample by an additional cleaning step, the catalyst clusters are still huge and this is a big problem for AFM measurements with high resolution (Figure 2.13). This problem can be reduced by exploiting a special property of the catalyst, it sediments when it is left for a longer period of time. This can be utilized to remove the biggest clusters by a sedimentation step. Experiments with different sedimentation times did show that 10 to 30 minutes is the optimal period to get rid of the biggest clusters and to have still enough catalyst spread on the sample.

Catalyst preparation

The catalyst is prepared with stock solutions which guarantee a constant composition over time. 30 mg Al_2O_3 (either 4 or 40 nm nanopowder) is dissolved in 20 ml 2-propanol, 93 mg $Fe(NO_3)_3$-$9H_2O$ is dissolved in 20 ml 2-propanol and 27 mg MoO_2Cl_2 is dissolved in 20 ml 2-propanol. These stock solutions are sonicated over night with an Ultrasonic300, power and degas in middle position.
The stock solutions are sonicated overnight before they are mixed to the effective catalyst consisting of 0.5 ml alumina solution (either 4 or 40 nm), 0.5 ml iron nitrate solution and 0.5 ml molybdenum dioxide dichloride solution diluted with 18.5 ml 2-propanol to a final volume of 20 ml. The catalyst is sonicated overnight after mixing and for 2 hours prior to use. (This corresponds to final concentrations of 0.37 mM Al_2O_3, 0.29 mM $Fe(NO_3)_3$-$9H_2O$ and 0.17 mM MoO_2Cl_2.)

Sample preparation

The catalyst is sonicated 2 hours prior to use. The samples are sonicated in acetone for 5 minutes and in 2-propanol for 2 minutes as well as placed in the UV cleaner for 10 minutes. Simultaneously the biggest clusters are removed by a sedimentation step which lasts between 10 to 30 minutes. The sample is placed on a spinning table (2'000 rpm for 40 seconds), 1 droplet of catalyst is added when the maximal speed is reached.

Conclusions

2-propanol is an appropriate solvent for the iron molybdenum alumina catalyst, when the sample is cleaned with the UV-ozone cleaner.

4.2.4 Conclusions

It could be shown that it is possible to grow carbon nanotubes from evaporated catalyst as well as from a liquid based catalyst which is spread on the sample by means of a spin coater. An Al layer can be used as a co-catalyst which enhances growth.
An iron molybdenum alumina catalyst dissolved in 2-propanol yields very good homogeneity if the samples are cleaned with an UV-ozone cleaner.
Until now the composition of the iron molybdenum alumina catalyst was not changed. It might be improved by changing the relative proportion of the constituents. The approach of heating the catalyst (solution #30) for some period of time is very promising as well.
Time is a crucial factor for the catalyst preparation, since the iron molybdenum alumina catalyst is not yet active (no growth of nanotubes) directly after mixing. The components have to be sonicated for several hours. Therefore its chemical composition should be checked at different times, e.g. by a chemical analysis, ESCA (Electron spectrometry for chemical analysis), mass or X-ray spectroscopy.
There is no growth of nanotubes from most of the small catalyst particles, therefor it would be interesting to know which properties a catalyst particle must have to act as a precursor for the growth of nanotubes.
The evaporated catalyst is currently not utilized for growing nanotubes, if this should be changed in future the dependency of the cluster size from the metal layer thickness should be explored with AFM. It might be possible to get a regular pattern of clusters when PMMA structured with e-beam lithography is used as a mask for the evaporated metal layers. The patterned metal film which remains after removing the PMMA can be expected to form clusters. It should be possible to get only one cluster per square when the area of the squares and the layer thickness have the optimal size.

It should be tried to combine evaporated and liquid based catalysts. An evaporated Al layer might replace the alumina nanopowder to avoid the formation of clusters, and the MoO_2Cl_2 solution might improve the effect of the evaporated Fe layer. Instead of MoO_2Cl_2 another Mo salt (such as molybdenum-hexacarbonyl $Mo(CO)_6$) might be used to avoid Cl to be part of the catalyst. Instead of alumina nanoparticles alumina aerogel can be used as base for the catalyst [162]. It allows an excellent access of the carbon feedstock to the catalyst particles since it has a highly porous structure.
The use of methanol as a solvent was rejected since it solves PMMA. The currently utilized process does not use PMMA, therefore it should be checked if there is any advantage when 2-propanol is replaced by methanol.
If it should become necessary to use water as solvent the basic solution should be used together with a plasma etching step in a pure oxygen plasma (experiments with 2-propanol did show that this does not affect the sample surface).

Chapter 5

Growth on silicon dioxide

SiO_2 or more precise a 100 or 400 nm thick thermal oxide layer on Si (100) is our standard substrate for electronic transport measurements. This chapter gives an overview of the results using this substrate. In the first section the results obtained using different growth processes are compared. The next section describes the formation of amorphous carbon and the oxidation of nanotubes. The last section presents preliminary experiments for the characterization of carbon nanotubes (CNTs) with STM.

Details about the gas systems and the catalysts are described in Chapters 3 and 4, respectively.

5.1 Growth of carbon nanotubes with different processes

This section gives a short overview of the results of growth with different processes (ethylene/hydrogen, methane, methane/ethylene and methane/hydrogen). Only the methane plus hydrogen process allows the growth of unbundled single-wall carbon nanotubes.
Figures 5.1a) and b) show pictures of the first grown nanotubes. An analysis of the first results did show that the quality of the tubes is better when the methane flow is set high (4'120 instead of 700 ml/min±3%) and evaporated catalyst is used.

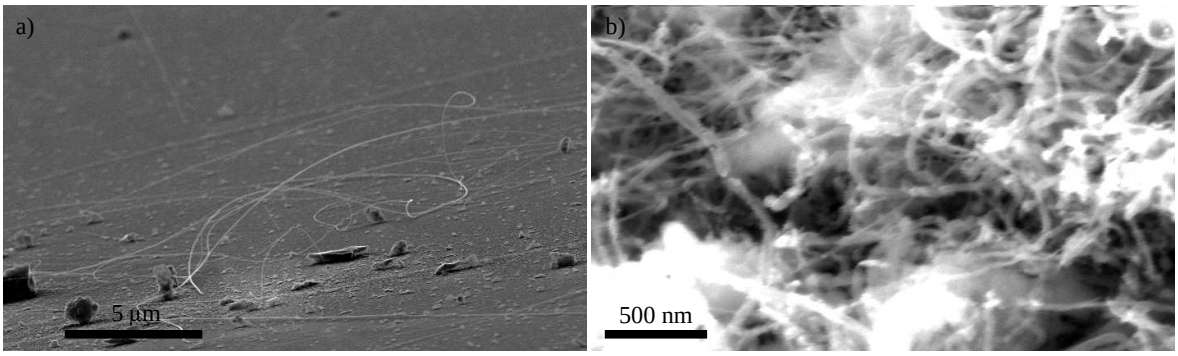

Figure 5.1: The first nanotubes. The catalyst was a) a 1 nm thick evaporated Fe layer (prepared by Z. Liu) (1'080 °C) and b) a solution of 30 mg alumina, 40 mg iron nitrate and 10 mg molybdenum dioxide dichloride in 15 ml methanol (sonicated for 1 hour and stirred over night) (1'060 °C). (Growth for 10 minutes with methane at 700 ml/min±3%, the argon flow was 880 ml/min±3% during heating and cooling down, but not during growth, using gas system I.)

Ethylene plus hydrogen process

Figure 5.2 shows a comparison of a) an evaporated 1 nm thick Fe layer and b) a 1 nm thick Fe layer on top of a 5 nm Al layer. The tube density of both samples is comparable. However the tubes on the sample without Al have some strange knots. The circles on Figure 5.2b) are artifacts of the investigation with SEM. The surface of the sample (probably the Al layer) starts to bubble when the resolution is higher than 200 nm. The circles are the consequence of the bubbling. (The tubes were grown at 900 °C for 10 minutes with ethylene at 1.2 ml/min±20% and hydrogen at 688 ml/min±20%, the argon flow was 1'058 ml/min±20% during the whole process, using gas system II.)

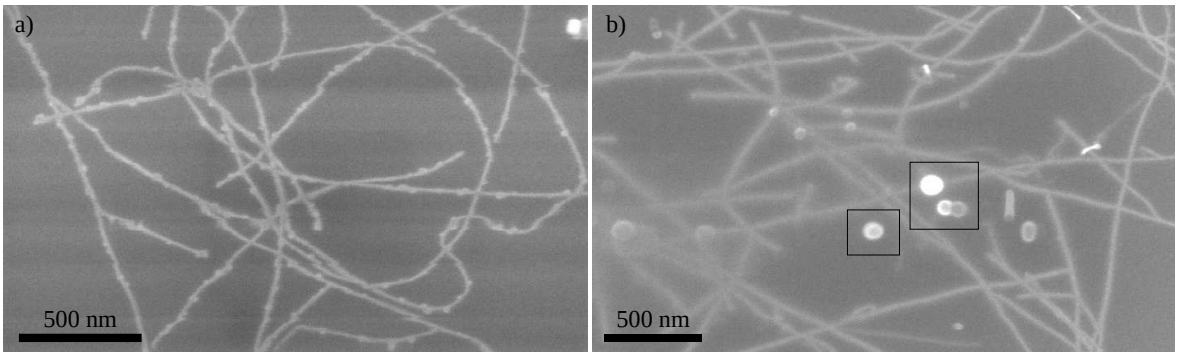

Figure 5.2: Nanotubes grown on a) an evaporated 1 nm thick Fe layer and b) a 1 nm thick Fe layer on top of a 5 nm Al layer.

For further experiments a 10 nm thick Ti layer was evaporated as a base for the catalyst, a 0.3 nm thick Fe layer in Figure 5.3a) and a 0.3 nm thick Ni layer in b). This has an unwanted effect, the nanotubes became huge, which means a Ti layer is not an appropriate base for the growth of carbon nanotubes. (The tubes were grown at 950 °C for 10 minutes, as above. The ethylene flow was 12.4 ml/min±20%.)

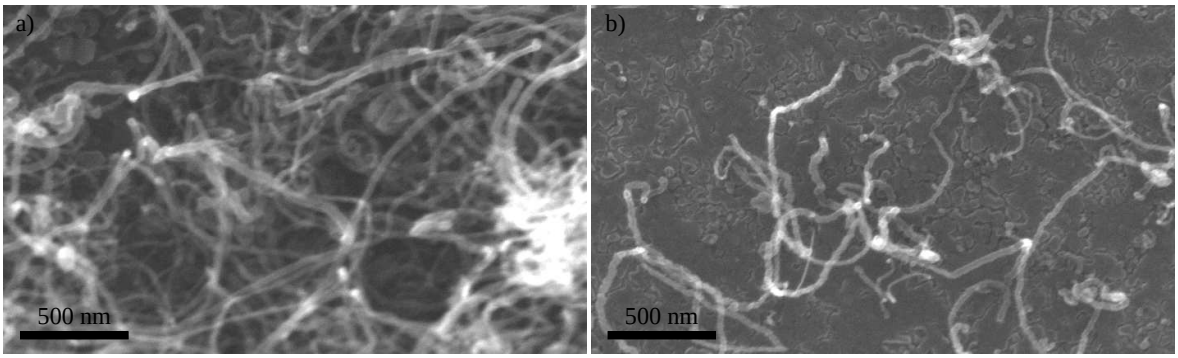

Figure 5.3: Nanotubes grown on an evaporated 10 nm thick Ti layer. The catalyst is a) a 0.3 nm thick Fe layer and b) 0.3 nm thick Ni layer.

More experiments which were done with this process with TEM grids and silicon nitride windows as substrate are presented in Chapter 6.

Methane process

Figure 5.4 shows typical tubes grown with the iron molybdenum alumina catalyst dissolved in 2-propanol (with 40 nm alumina nanoparticles) at 950 °C with a methane flow

of 1'400 ml/min±3% for 10 minutes, the argon flow was 890 ml/min±3% during heating and cooling down, using gas system III. Raman measurements by A. Hartschuh did show that the grown tubes are bundled.
More experiments which were done with this process are presented in Section 4.2.

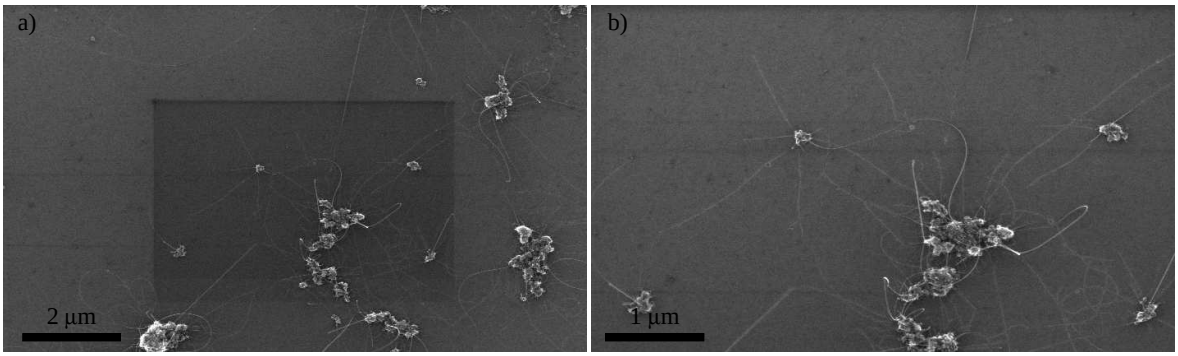

Figure 5.4: Nanotubes grown with the iron molybdenum alumina catalyst dissolved in 2-propanol.

Methane plus ethylene process

The used methane is very pure ($C_2H_6 < 0.1$ ppm and $C_nH_m < 0.05$ ppm, see Appendix A.3). The quota of trace gasses might have an influence on the growth. So it was tried to "pollute" methane with ethylene which is due to the presence of a double bond much more reactive than methane.
The carbon feedstock was methane with a flow of 530 ml/min±20% in combination with an ethylene flow of 0.6 (or 1.9 or 5.6) ml/min±20% and a growth time of 10 minutes. This corresponds to about 1'000 (or 3'000 or 9'000) ppm ethylene in the methane flow. (The argon flow was 1'058 ml/min±20% during heating and cooling down, but not during growth, using gas system II. The iron molybdenum alumina catalyst solved in 2-propanol was used.)
The results of mixing methane and ethylene are very interesting. With no ethylene flow nanotubes grew only from the big catalyst clusters (Figure 5.5a)). With 1'000 ppm ethylene there are in addition tubes growing from smaller catalyst particles and some small particles in the background (Figure 5.5b)). These particles might be amorphous carbon. On Figure 5.6a) (with 3'000 ppm ethylene) there are less tubes and more particles visible and on b) (with 9'000 ppm ethylene) there are only a few tubes and a lot of particles. The abundance of amorphous carbon increases with the amount of ethylene in the methane flow. The appearing of nanotubes in the background with an ethylene flow of 1'000 ppm can be explained either by a heightened reactivity of the ethylene or by a better contrast in SEM due to the covering of the sample with amorphous carbon. There are no tubes in the background with higher ethylene flows since the catalyst particles are covered from amorphous carbon and become inactive.

Methane plus hydrogen process

It was impossible to grow unbundled single-wall carbon nanotubes with all the processes presented till now. The growth protocol was changed due to personal contacts to H. van Zant and J. Kong. The addition of hydrogen allows the growth of unbundled single-wall carbon nanotubes, which was proven by Raman spectroscopy measurements by A. Hartschuh and electrical transport measurements (see Chapter 7 for details).

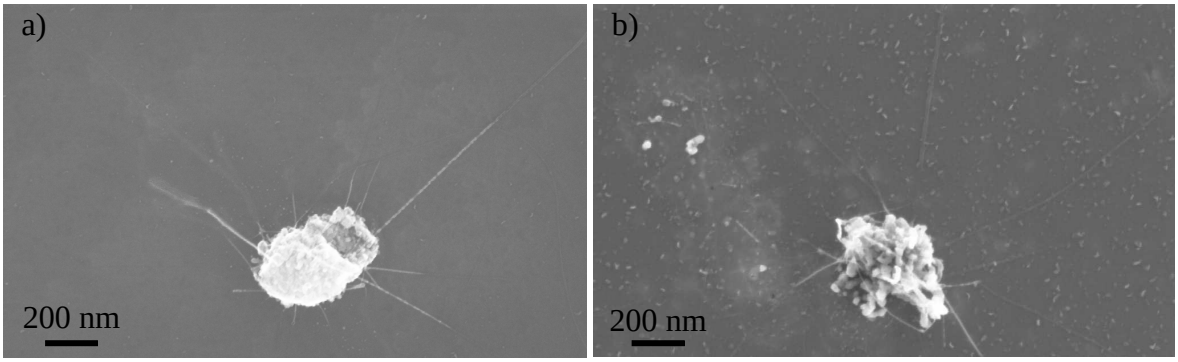

Figure 5.5: Changes due to an increasing flow of ethylene a) no ethylene b) 1'000 ppm ethylene.

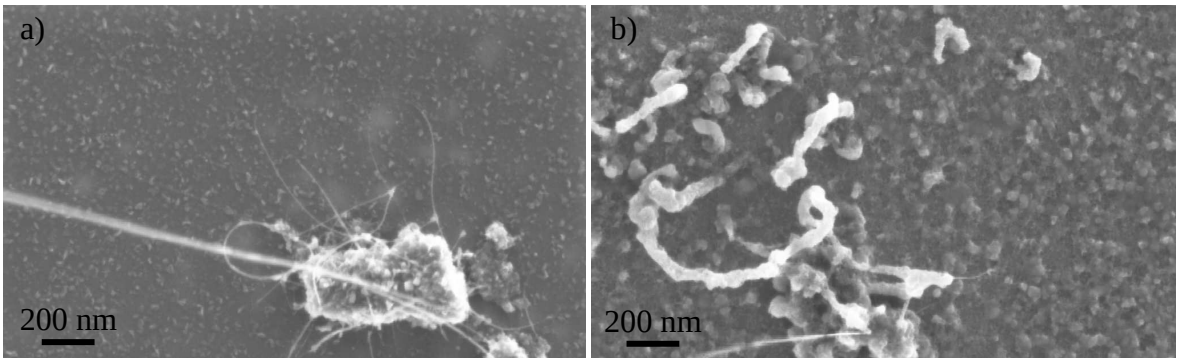

Figure 5.6: Changes due to an increasing flow of ethylene a) 3'000 ppm ethylene and b) 9'000 ppm ethylene.

Figures 5.7 and 5.8 show tubes grown with the iron molybdenum alumina catalyst dissolved in 2-propanol at different temperatures. With a growth temperature of 1'000 °C the abundance of tubes is clearly smaller than with 900 or 950 °C and the average tube diameter seems to be bigger. (The tubes were grown for 10 minutes with methane at 1'000 ml/min±3% and hydrogen at 500 ml/min±3%, the argon flow was 1'500 ml/min±3% during heating and cooling down, but not during growth, using gas system IV.)

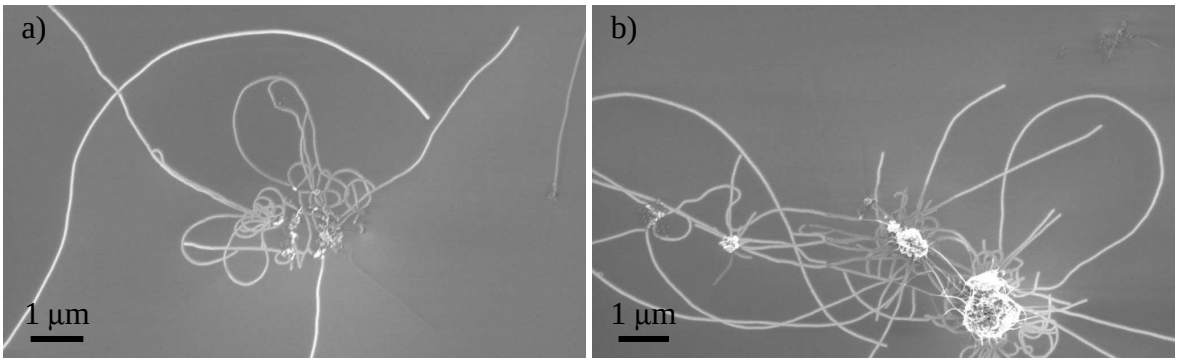

Figure 5.7: Nanotubes grown at a) 900 and b) 950 °C.

Figure 5.9a) shows that the use of an evaporated Fe layer as catalyst would not bring an advantage compared with the iron molybdenum alumina catalyst since the tubes have visible

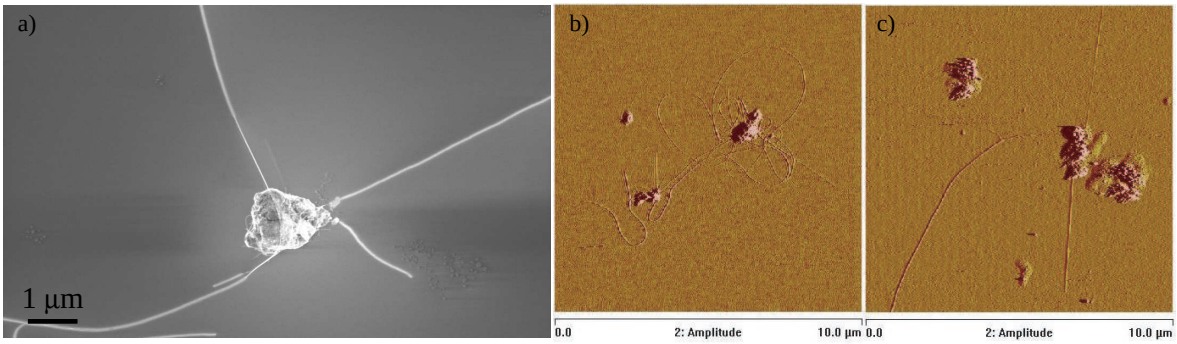

Figure 5.8: SEM picture of nanotubes grown at a) 1'000 °C and AFM pictures of nanotubes grown at b) 950 and c) 1'000 °C.

impurities. Compared with this the tubes grown with solution #30 look similar to the tubes grown with the iron molybdenum alumina catalyst (Figure 5.9b)). This solution has the advantages that no big catalyst clusters are formed and that it is spread homogeneously on the sample surface.

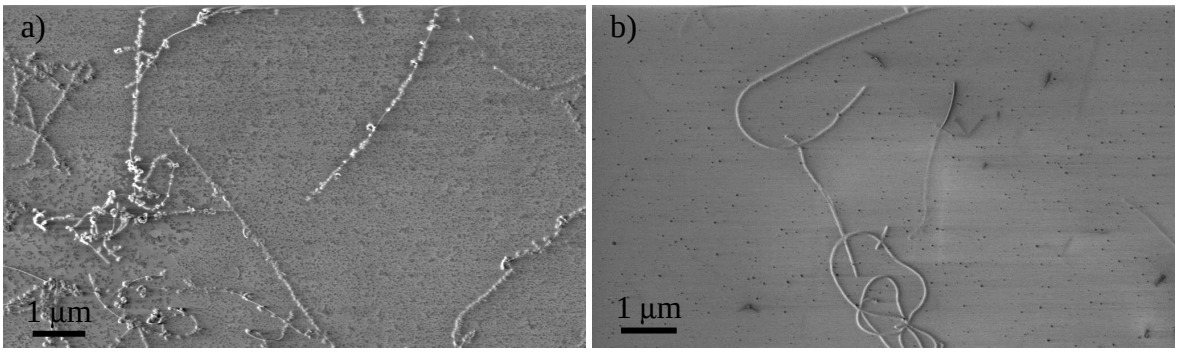

Figure 5.9: Nanotubes with a) a 1 nm thick Fe layer and b) solution #30, grown at 900 °C.

Conclusions

The results of the presented experiments can be summarized as follows: It is possible to grow nanotubes with all processes, but only the methane plus hydrogen process delivers separated single-wall carbon nanotubes. SEM and AFM are not suitable to distinguish bundled from separated nanotubes, therefore other methods as TEM (see Chapter 6), electrical transport measurements (see Section 7.7) or STM (see Section 5.3) have to be used to acquire this information. The Raman studies should be continued either on a quartz substrate or with nanotubes suspended over gaps in silicon nitride windows (see Section 6.2).
The dependence of the average diameter from the growth temperature should be investigated with AFM. So it would be possible to provide on request thinner or thicker nanotubes for the transport measurements.

5.2 Control of the growth process: amorphous carbon, oxidation and bulk carbon feedstock

Beside the utilized gasses and catalysts there are other parameters which have to be considered. The formation of amorphous carbon is a permanent and unwanted companion of the growth of carbon nanotubes with CVD. Its abundance increases when the growth temperature is too high or when the gas flow is stopped. Moreover the contrary effect occurs as well: the grown tubes can be oxidized when the samples are taken out of the oven at a to high temperature.

Amorphous carbon

Figure 5.10 shows amorphous carbon a typical result for growth at high temperatures. For growth at lower temperatures the abundance of amorphous carbon is less prominent.

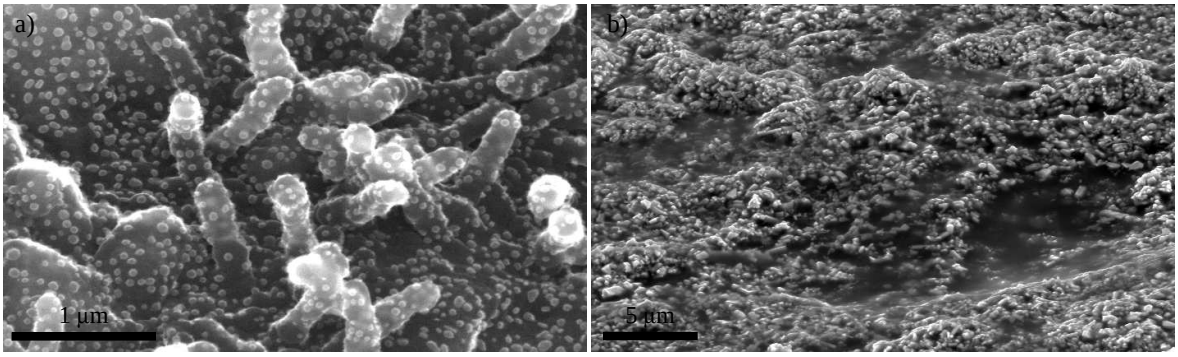

Figure 5.10: Amorphous carbon a typical result for growth at high temperatures. The catalyst was a 1 nm thick evaporated Fe layer (prepared by Z. Liu). a) Growth at 1'100 °C for 10 minutes with methane at 700 ml/min±3%, b) growth at 1'100 °C for 10 minute with methane at 4'180 ml/min±3%, the argon flow was 880 ml/min±3% during heating and cooling down, but not during growth, using gas system I.

Oxidation

It is possible to force oxidation by just leaving open the oven on one side. So the oxygen in the air has free access to the sample. For the first oxidation tests six samples with a 2 nm Fe layer were produced (at 950 °C for 10 minutes with ethylene at 1.2 ml/min±20% and hydrogen at 688 ml/min±20%, the argon flow was 1'058 ml/min±20% during the whole process, using gas system II). One sample was kept for 30 minutes at 600 °C, the number of tubes was evidently reduced. On a sample kept at 700 °C for 30 minutes most of the tubes disappeared. On a sample kept at 700 °C only for a moment many of the tubes disappeared, however the remaining tubes were very straight. For samples kept at 800, 900 and 1'000 °C only for a moment only a few and very long tubes survived.
This experiment was refined in such a way that the same sample was heated for 5 minutes to different temperatures. It was tried to find again the same position for all temperatures to be able to make a comparison of the results for different temperatures. Figure 5.11a) shows tubes grown at 950 °C for 10 minutes with ethylene at 12.4 ml/min±20% and hydrogen at 680 ml/min±20%, the argon flow was 1'058 ml/min±20% during the whole process, using gas system II. Figures 5.11b) and 5.12a) show the same sample at the same position after being kept at 550 and 575 °C for 5 minutes. Figures 5.12b) and 5.13 show the same sample

but at a different position after being kept at 600, 625 and 650 °C. At least for temperatures above 600 °C a clear reduction of the number of tubes is visible.
Considering the results of the oxidation tests the temperature at which the oven is opened to take out the samples was set to 350 °C.

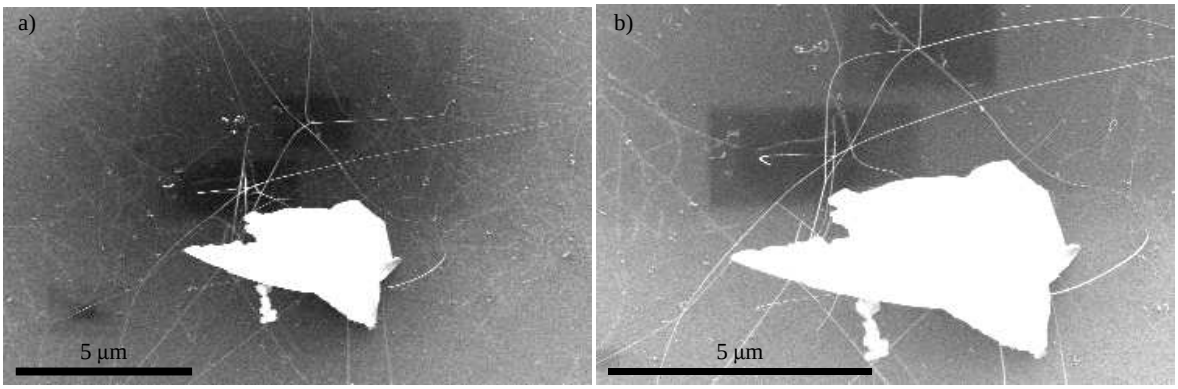

Figure 5.11: The same sample a) after growth and b) after oxidation at 550 °C.

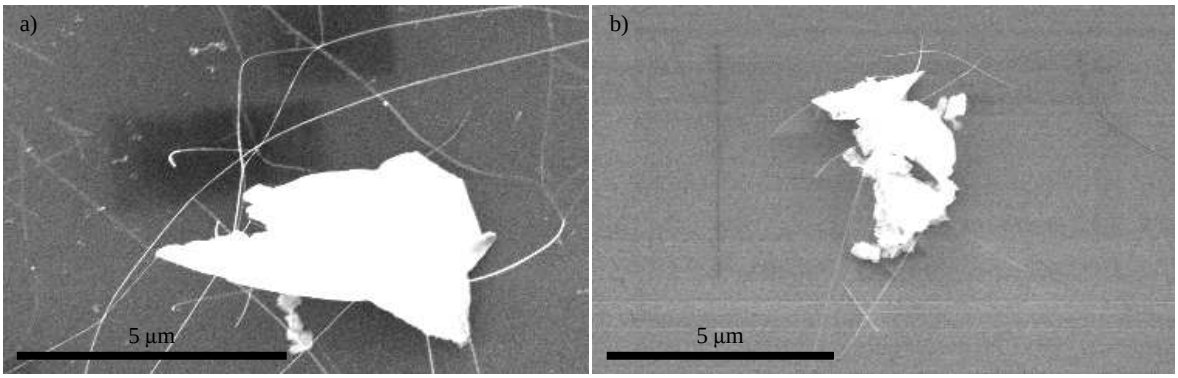

Figure 5.12: The same sample after oxidation at a) 575 and b) 600 °C.

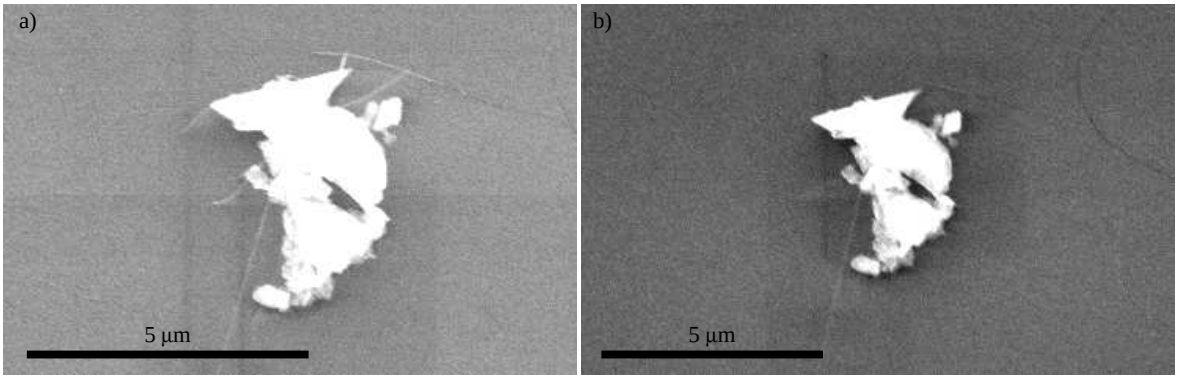

Figure 5.13: The same sample after oxidation at a) 625 and b) 650 °C.

Bulk carbon feedstock

Another parameter which can be changed is the phase of the carbon feedstock. In principle it should be possible to grow nanotubes from a bulk carbon feedstock. Additional experiments with PMMA (polymethyl-methacrylate, a carbon polymer), HOPG (Highly Ordered Pyrolytic Graphite, prepared by the pyrolysis of hydrocarbons at temperatures above 2'000 °C) and cast iron (containing graphite embeddings) did not show any growth at all. The experiments were done in a hydrogen atmosphere using the iron molybdenum alumina catalyst, solution #30 and evaporated Fe as catalyst.

Conclusions

The formation of amorphous carbon and the oxidation of the grown tubes are facts which must not be ignored.
Nanotubes and amorphous carbon can be etched with oxygen or hydrogen. A careful heat treatment in an oxidizing or reducing (hydrogen) atmosphere is very promising. It should be tested if it is possible to remove the amorphous carbon with such a treatment without damaging the tubes. This can be done by opening the quartz tube of the oven at a certain temperature for a certain time. Another approach is to alternate the flow of CH_4 plus H_2 with a flow of H_2 only over several cycles. It might be necessary to heighten the temperature during the H_2 flow to intensify the etching effect. SEM is not the optimal investigation method for such experiments. AFM is more suitable.

5.3 Preliminary experiments for the characterization of CNTs with scanning tunnelling microscopy

The characterization of the grown nanotubes with scanning tunnelling microscopy (STM) would allow the distinction of bundled and separated nanotubes. However the SiO_2 samples can not be measured with an STM since their surface is not conducting. This means that for STM measurements the grown tubes have to be transferred on a conducting substrate. The growth directly on a conducting substrate would be possible too. In that case it has to be proven that the results from this substrate are applicable for SiO_2 too.
Different approaches were tried to master this challenge. Nanotubes were grown on the backside (the SiO_2 side) of a silicon nitride window (see Section 6.2 and Figure 6.14 for more details). A 200 nm thick gold layer was evaporated and the Si_3N_4 SiO_2 bilayer was etched with 40% HF. These trials were not crowned with success.
A very simple approach is to evaporate a 100 nm thick gold film on a sample covered with grown nanotubes, to cover the sample with a two component glue (EPOTEK 377) and to separate the gold film with a razor blade from the sample [163]. Figure 5.14 shows that it is possible to transfer nanotubes with this method. However the yield is extremely low and the Au surface is very bumpy.
The most direct approach to prepare samples suitable for STM is to use the standard substrate and to etch away the SiO_2 with a buffered hydrofluoric acid solution (BHF: 28 ml 40% HF and 113 g NH_4F are dissolved in 107 ml H_2O, the etch rate for SiO_2 is 50 nm/min [44]).
Figure 5.15 shows experiments with samples which were etched as first step. The sample with solution #30 as catalyst shows rare growth, in addition the whole sample is covered from catalyst which did not react. The iron molybdenum alumina catalyst dissolved in 2-propanol on the other hand provides a good result. The tubes on the sample look the same as e.g. the tubes on Figure 5.7, the etching step seems not to affect the tubes. However the tubes have a tendency to bundle when the etching step is after the growth. Furthermore there is a remarkable phenomenon: there is no blurring of the tubes in SEM pictures, this means it is

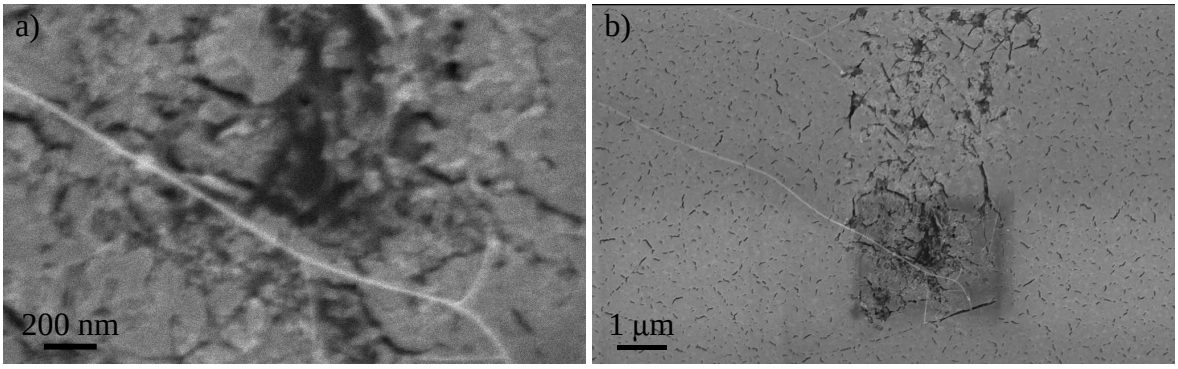

Figure 5.14: Nanotubes transferred with a gold layer on an EPOTEK film.

easier to estimate the diameters of the grown tubes on etched samples.
First tests with the STM show it is possible to make measurements with these samples (Figure 5.15c)). (Remark: pure silicon oxidizes very fast, however the BHF treatment leaves a hydrogenated surface which slows down the oxidation. This means the use of Si instead of SiO_2 would not have an advantage.)

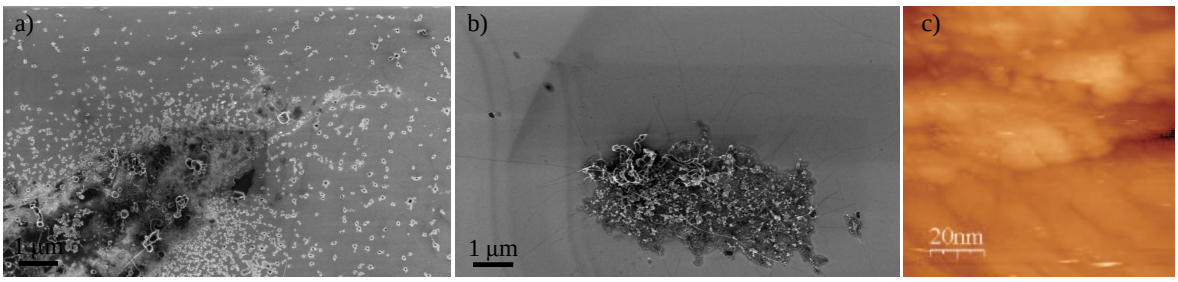

Figure 5.15: Nanotubes on SiO_2 etched with BHF: a) solution #30 and b) iron molybdenum alumina catalyst. c) STM picture of the etched SiO_2 surface.

Conclusions

Etching the SiO_2 layer is a promising approach.
On SEM pictures of tubes grown on SiO_2 there is always a blurring effect when the tubes lay on the surface which makes the pictures fuzzy. It is noteworthy that this is not the case for samples etched with BHF.

Chapter 6

Growth on TEM grids and silicon nitride windows

The information about the structure of the grown tubes has to be as precise as possible. TEM is a possibility to get insight into the internal structure of the tubes, whereas nanotubes grown on SiO_2 can not be investigated with TEM directly, since the samples are not transparent for electrons. SiO_2 or more precise a 100 or 400 nm thick thermal oxide layer on Si is our standard substrate utilized for electronic transport measurements. There are two possibilities to overcome this challenge: the carbon nanotubes can be transferred to a TEM-grid after they were grown on SiO_2, or they can be grown on a substrate which is transparent for electrons and that resists the growth temperature of 1'000 °C.
The common setup for electrical transport measurements consists of a nanotube contacted with several electrodes. This means the density of the tubes must not be too high to avoid shorts between the electrodes induced by a series of nanotubes in direct contact. The tubes stick on the substrate surface additionally. This makes a transfer very difficult.
The second approach of finding a suitable substrate promises to be more successful. However for a different substrate than SiO_2 it has to be proven that the growth of the nanotubes is not affected by the substrate.
A first idea was to grow the tubes directly on TEM grids made of different materials. The outcome of these experiments was that the results depend extremely from the chosen grid material. This fact is surely interesting however it makes any conclusions on the structure of nanotubes grown on SiO_2 impossible.
The next idea was to use little gaps in lithographically patterned silicon nitride windows. These are adequate candidates since they are transparent for electrons, stable at high temperatures and not too fragile. The grown nanotubes span gaps (down to 200 nm) in the silicon nitride windows. The silicon nitride windows can be used as a substrate for the production of devices for e.g. electrical transport measurements. This has the additional advantage that it is possible to make TEM pictures from a nanotube used for other types of measurements.

Details about the gas systems and the catalysts are described in Chapters 3 and 4, respectively.

6.1 Growth of carbon nanotubes on TEM grids

To use TEM grids as a substrate for the growth of carbon nanotubes is a very simple approach. TEM grids are thin metal foils with punched (quadratic) holes. The grids have a diameter of 3.05 mm and a thickness of 12 to 15 μm. Grids made of Au, Cu, Mo, Ni, stainless steel (SS) and Ti were tested. The melting point of all these metals is higher than 1'000 °C which

means that these grids should withstand the growth process. Quantifoils R2/2 were tested as well.
It was tried to grow nanotubes on the untreated grids and on grides covered with a thin evaporated metal layer (see Section 4.1 for more details about evaporation). The grids were mounted for the evaporation step on a self made sample holder. Figure 6.1b) shows a schematics.
The first test was to try if tubes grow on Mo, Ni or SS grids without the use of a catalyst. This was done since Fe and Ni are known to be catalysts for the growth of carbon nanotubes and Mo is used as a component in the iron molybdenum alumina catalyst. The result was negative, no tubes grew, the grids just became brittle. (The chosen temperatures were 850 °C and a 950 °C with an ethylene flow of 1.2 ml/min±20% and hydrogen flow of 688 ml/min±20% for 10 minutes, the argon flow was 1'058 ml/min±20% during the whole process, using gas system II.)
A simultaneous experiment with a Ti grid with an evaporated bilayer of 5 nm Al and 0.1 nm Fe was more successful. Figure 6.1a) shows tubes grown at 950 °C for 10 minutes with ethylene at 1.2 ml/min±20% and hydrogen at 688 ml/min±20%, the argon flow was 1'058 ml/min±20% during the whole process, using gas system II. However the Ti grid became as unstable that it crumbled. On an Au grid treated in the same way no grown tubes could be found.

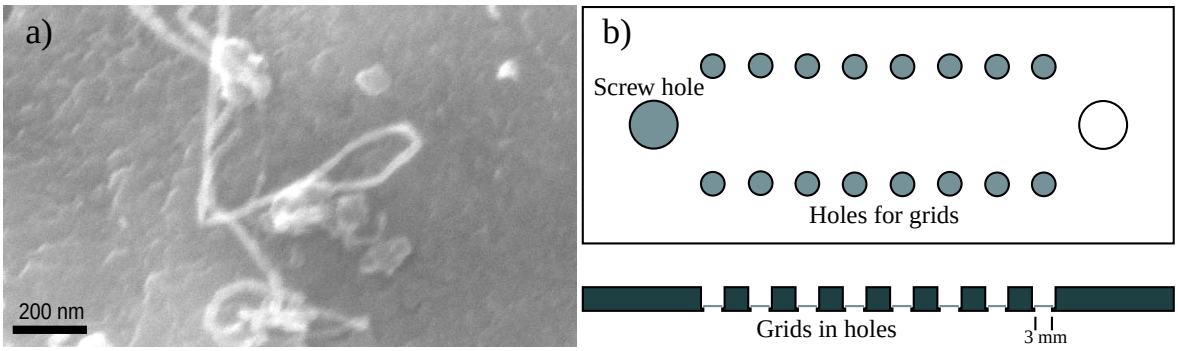

Figure 6.1: a) Nanotubes grown on a Ti TEM grid with an evaporated bilayer of 5 nm Al and 0.1 nm Fe. b) Schematics of the sample holder used for evaporation.

These first tests did show in addition strong changes of the grids due to the growth process, they changed their shape and surface. The next step was to check the changes of the surface which occur when the grids were heated to 600, 700, 800, 900, 1'000 and 1'100 °C in an argon atmosphere (1'058 ml/min±20% during the whole process, using gas system II).
The results of these experiments depend very strongly on the grid material. They can be summarized as follows:

- Au grid: The surface changes only a little, however the grids are extremely sensitive to deformations.
- Cu grid: The surface is uneven however stable (stable means that the shape of the surface did not change very much when heated). The grid is distorted at 1'100 °C.
- Mo grid: The surface is quite stable below 900 °C, however there is a recrystallization at higher temperatures.
- Ni grid: The surface is quite stable below 700 °C, however there is a recrystallization at higher temperatures.

- SS grid: The surface is stable below 700 °C however very uneven. The color changed to black at 600 °C.
- Ti grid: The surface is unstable. At 800 °C it becomes smoother but the grid becomes brittle. The color changed to brown at 600 °C.

Figure 6.2 shows an example demonstrating the changes of the surface when a Mo grid is heated to 600 and 1'100 °C in an argon atmosphere. The temperature dependence of the surface shape is really amazing.

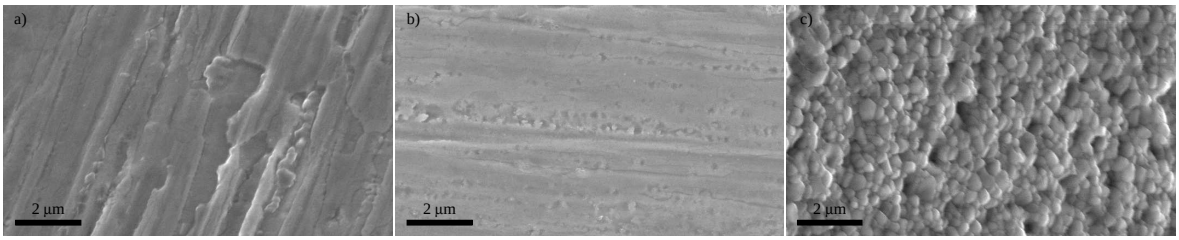

Figure 6.2: Changes of the surface of a Mo grid due to heating in an argon atmosphere: a) room temperature b) 600 and c) 1'100 °C.

For the following series of experiments the protocol was changed a little. In addition to a constant argon flow (1'058 ml/min±20%) during the whole process the samples were exposed to hydrogen (688 ml/min±20%) for 10 minutes. The results were quite similar to that of the first series of experiments however the surfaces lost their stability at lower temperatures. The Ni grid lost its brilliance at 900 °C.
These experiments can be summarized as follows: the shape and the surface of the grids change when they are heated. This is a challenge since it was shown in Section 4.1 that the evaporated Fe layer forms clusters when it is heated on SiO_2 samples. This process of cluster formation is obviously disturbed on TEM grids due to the changing substrate surface. This problem can be overcome in different ways. The catalyst can be added in preformed clusters, a diffusion barrier can be used to avoid the direct contact of the evaporated catalyst with the grid surface or the grids can be tempered.
For the following experiments the ethylene flow was heightened to 12±20% ml/min. The hydrogen flow was 688 ml/min±20% and the argon flow 1'058 ml/min±20% as before.
Tempering was tried with Au, Cu and Mo grids. The grids were heated to 950 °C in an argon flow of 1'058 ml/min±20%, thereafter a 5 nm thick Fe layer was evaporated. The growth was done at 800 and 900 °C, respectively. The outcome is as follows: there was growth of carbon nanotubes on the Cu and the Mo grids however not on the Au grids. The yield was higher at 900 °C.
The idea of applying preformed clusters was tried with the liquid catalyst #30. All six grid materials were tested. There are tubes identifiable on the Au, SS and Ti grids (growth at 800 and 900 °C). Figure 6.3a) shows carbon nanotubes grown on a SS grid.
This last experiment shows that the catalyst is not affected by Au, Ti and SS. It was tried to use a 10 nm thick Ti layer as a diffusion barrier between catalyst and grid. And indeed, this approach was successful. There were different catalysts tested: 0.3 and 5 nm Fe, 0.3 and 5 nm Ni and solution #30. Figures 6.3b), 6.4 and 6.5 show a selection of pictures grown with different catalysts. The differences are stupendous. There are long tubes and short ones, they are straight or curly, some are thick and others thin even when the same catalyst was used and the growth temperature was the same.
The results of the experiments with TEM grids can me summarized as follows:

- Au grids: Usually no growth, only on a Ti layer.

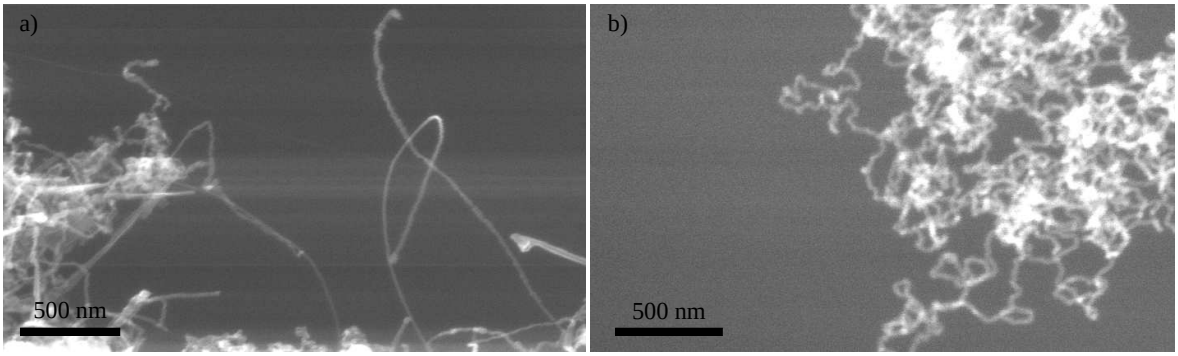

Figure 6.3: a) SS grid, 850 °C, #30 and b) Au grid, 850 °C, 10 nm Ti #30.

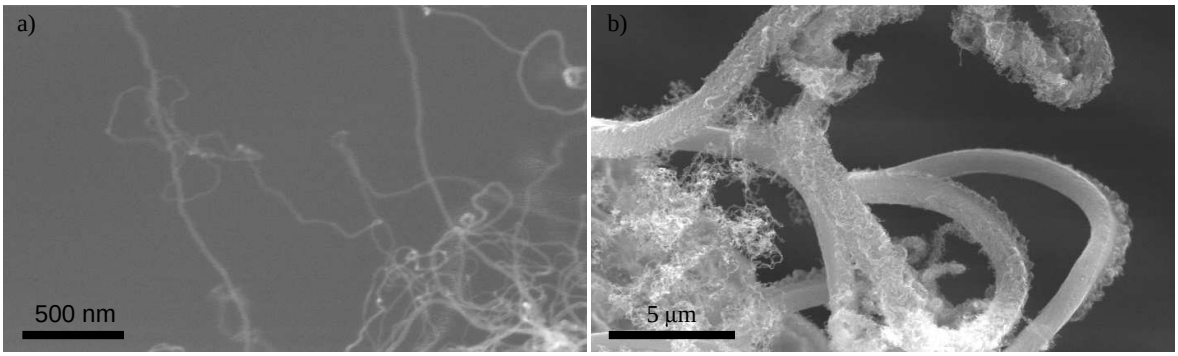

Figure 6.4: a) Cu grid, 850 °C, 10 nm Ti, 5 nm Fe and b) Mo grid, 850 °C, 10 nm Ti, 5 nm Fe.

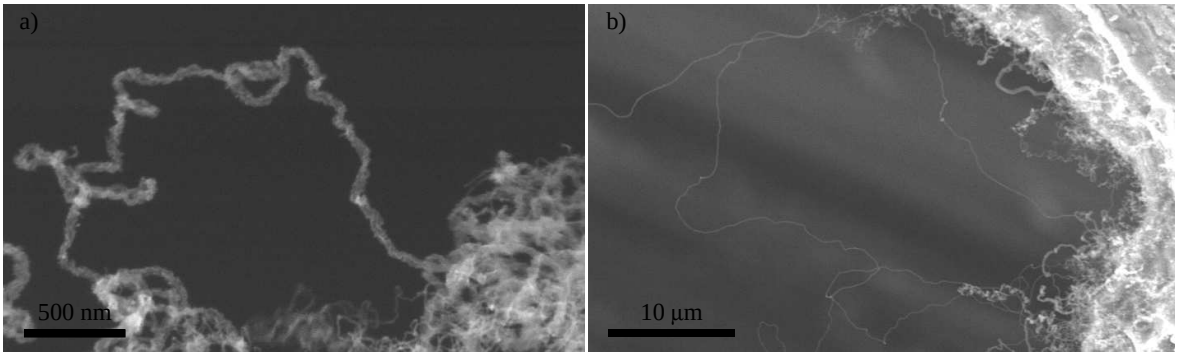

Figure 6.5: a) Ni grid, 850 °C, 10 nm Ti, 5 nm Ni and b) Ti grid, 850 °C, 10 nm Ti, 5 nm Fe.

- Cu grids: Usually no growth, only on a Ti layer.
- Mo grids: Usually growth, even twice without a Ti layer.
- Ni grids: Usually growth, even twice without a Ti layer.
- SS grids: Always growth.
- Ti grids: Nearly always growth.

Additional experiments with SiO_2 as substrate did show that the Ti influences the growth of the nanotubes, they become huge (see Section 5.1 for more details). This means that Ti is inappropriate as a diffusion barrier.

Quantifoils

Quantifoils R2/2 are Cu TEM grids covered with a thin carbon film of a thickness of 15 nm with a regular pattern of holes with a diameter of 2 μm. With quantifoils only a few tests were made, since the results are not convincing.
Figure 6.6a) shows that it is possible to grow nanotubes on quantifoils with solution #30 at 800 °C, however their quality is very bad. The result could be improved by evaporating a 200 nm thick SiO_2 layer (850 °C) (Figure 6.6b)). The growth process was the same as above.

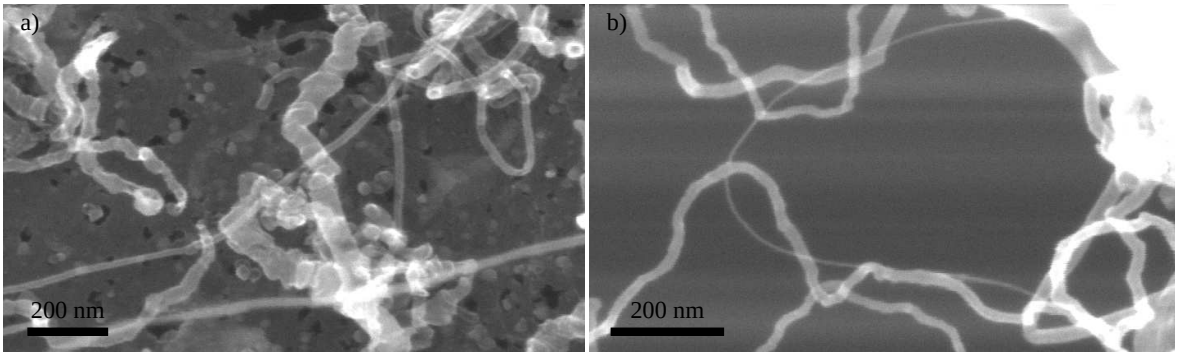

Figure 6.6: Nanotubes grown on quantifoils: a) with solution #30 and b) on a 0.5 nm thick Fe layer on 200 nm SiO_2.

Conclusions

It is possible to grow nanotubes on TEM grids however the surface changes dramatically when the grids are heated. In addition the results depend extremely on the used grid material.
The TEM characterization should be reliable and appropriate for the standard substrate SiO_2. This demand is surely not fulfilled for the use of TEM grids as growth substrate. A more adequate method is described in the next section.

6.2 Growth of carbon nanotubes over gaps in silicon nitride windows

TEM grids are not an appropriate substrate for the growth of carbon nanotubes as described in the last section. The idea behind the use of the Si_3N_4-windows was to have a substrate which can be used in TEM and that resists the heat in the CVD oven. The Si_3N_4 SiO_2 bilayer is to thick (150 and 100 nm, respectively) for a direct use as a substrate in TEM. However it is possible to etch holes in the windows which are spanned by the grown nanotubes.

Sample preparation

The substrate is a 525 μm thick Si wafer covered with 150 nm LPCVD Si_3N_4 on 100 nm thermal SiO_2. The Si is etched from the back side leaving a freestanding window of a Si_3N_4 SiO_2 bilayer of 0.5 mm x 0.5 mm. Etched predetermined breaking points allow the cleaving of the wafer in pieces of 4 mm x 4 mm with one window in the middle of every piece. The substrate was provided by the Université de Neuchâtel.
The samples are prepared as follows (Figure 6.7): The samples are cleaned only in the UV-ozone cleaner (for 10 minutes) since they are extremely brittle and do not survive sonication. The windows are covered with a 600 nm thick polymethyl methacrylate layer (E-beam resist

PMMA 950 K from Allresist GmbH). The resist is exposed with a JSM-IC848 Scanning Microscope from Jeol using Elphy (a program from Raith, parameters: area dose 750 $\mu As/cm^2$, step size 20 nm; the structures are quite big, so it is sufficient to focuss on a droplet of silver paint nearby the window at a current of 10^{-9} A). The samples are developed with 2-propanol:MIBK (3:1) for 50 seconds. The development is stopped with 2-propanol (60 seconds).

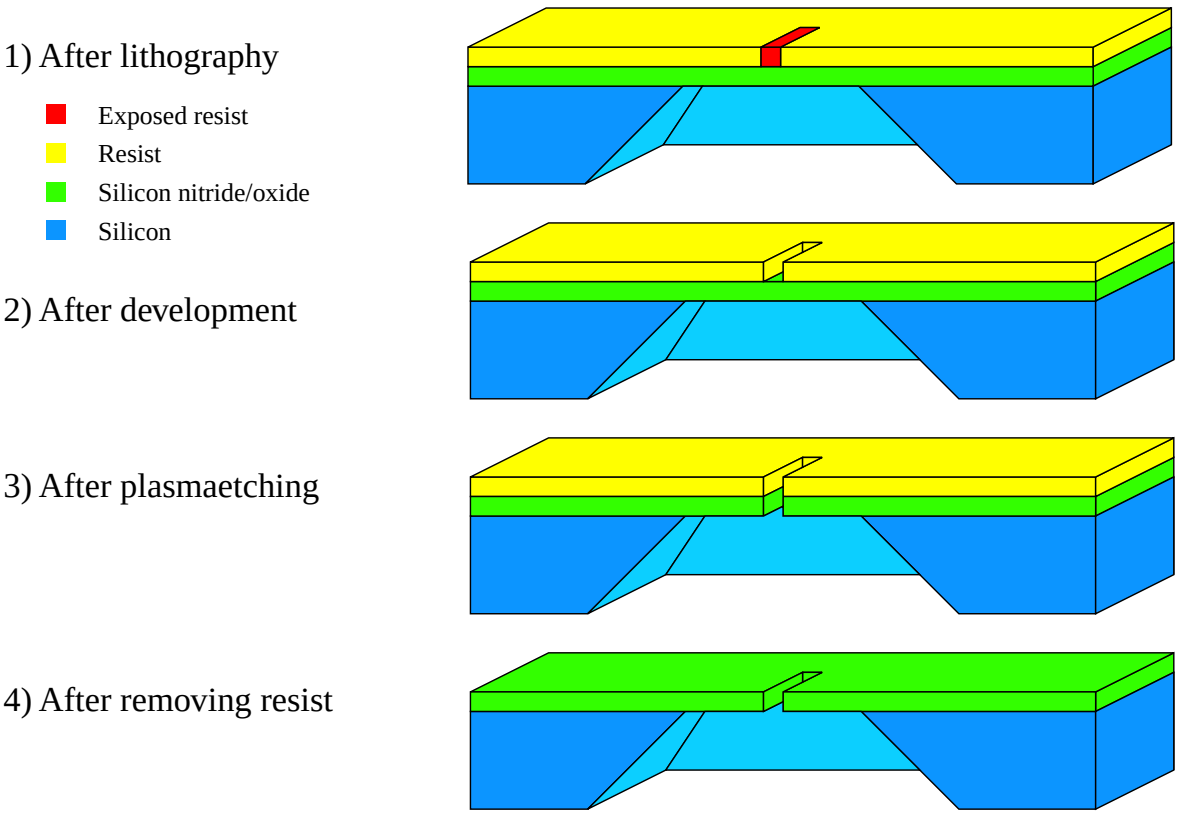

Figure 6.7: Schematics of the etching of gaps in silicon nitride windows.

The PMMA serves as an etching mask. Reactive ion etching (Plasmalab 80 plus from Oxford) is utilized to etch the Si_3N_4 SiO_2 bilayer (15 minutes, 34% CHF_3, 4% O_2, 70 W, 0.025 Torr) and to remove the remaining PMMA in a second step (3 minutes, 16% O_2, 100 W, 0.025 Torr). The PMMA can be removed with acetone as well however in that case the silver paint used for focussing spreads over the whole sample.
The end products are well defined gaps in the windows (Figure 6.8a)). It is clearly visible that the growth of the tubes is not homogenous (grown at 900 °C for 10 minutes with methane at 1'000 ml/min±3% and hydrogen at 500 ml/min±3%, the argon flow was 1'500 ml/min±3% during heating and cooling down, but not during growth, using gas system IV). There is another notable effect, plasma etching has the disadvantage that the surface of the samples becomes rough (Figure 6.8b)).
The liquid catalyst tends to accumulate and covers the gaps (Figure 6.9a)) (grown at 950 °C for 10 minute with a methane flow of 1'400 ml/min±3%, the argon flow was 890 ml/min±3% during heating and cooling down, using gas system III). This problem could be solved by spreading the catalyst before the PMMA (Figure 6.9b)). The remaining procedure is the same as described in sample preparation (grown at 900 °C for 10 minutes with methane at 1'000 ml/min±3% and hydrogen at 500 ml/min±3%, the argon flow was 1'500 ml/min±3% during heating and cooling down, but not during growth, using gas system IV).

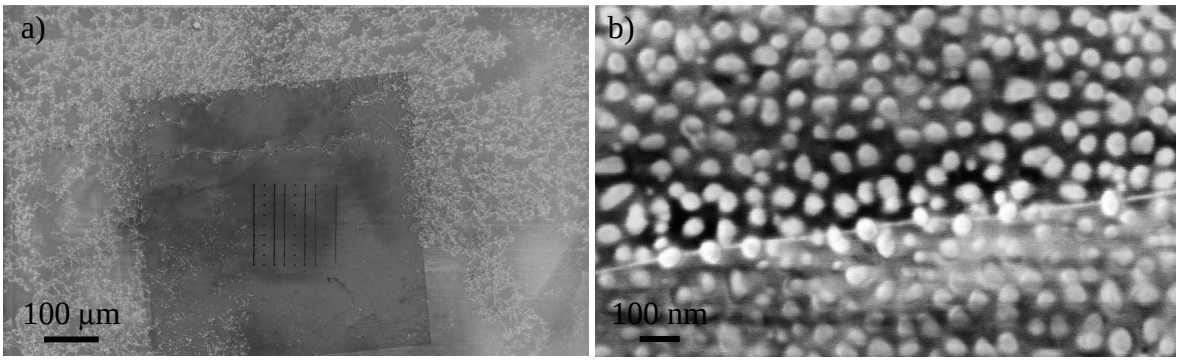

Figure 6.8: a) The silicon nitride window with the etched gaps is a little darker than the remaining sample. There are less tubes growing on the window. b) Roughening of the silicon nitride surface due to etching.

The catalyst can be evaporated directly on the etched samples as well.

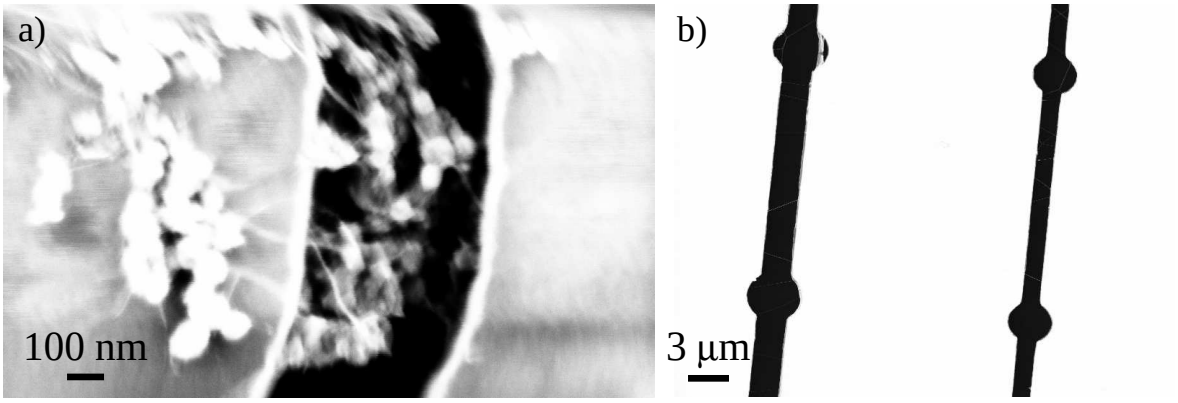

Figure 6.9: Carbon nanotubes grown with iron molybdenum alumina catalyst dissolved in 2-propanol. a) The catalyst covers the gap when it was spread as last step of the sample preparation. b) Catalyst was spread as first step.

Results

The TEM-pictures were made at the Biocenter Basel, in collaboration with members of A. Engel's group.
The TEM pictures of Figure 6.10 show that bundles of a) single-wall and b) double-wall nanotubes can be found, as well as multi-wall carbon nanotubes in Figure 6.11a). The TEM parameters are a challenge, since the tubes are affected by the electron beam, they change their shape. The tube in the middle of Figure 6.11b) looked like the other two tubes before it was investigated at higher resolution.
(If not other denoted the tubes were grown for 10 minutes with ethylene at 12 ml/min±20% and hydrogen at 680 ml/min±20%, the argon flow was 1'058 ml/min±20% during the whole process, using gas system II.)
Figures 6.10 and 6.12 show that the nanotubes have a tendency to form bundles [164], instead of spanning the gap one by one (Figure 6.13a)). This is due to the special sample geometry and depends on the growth parameters. It is possible to counteract this tendency by reducing the catalyst density.

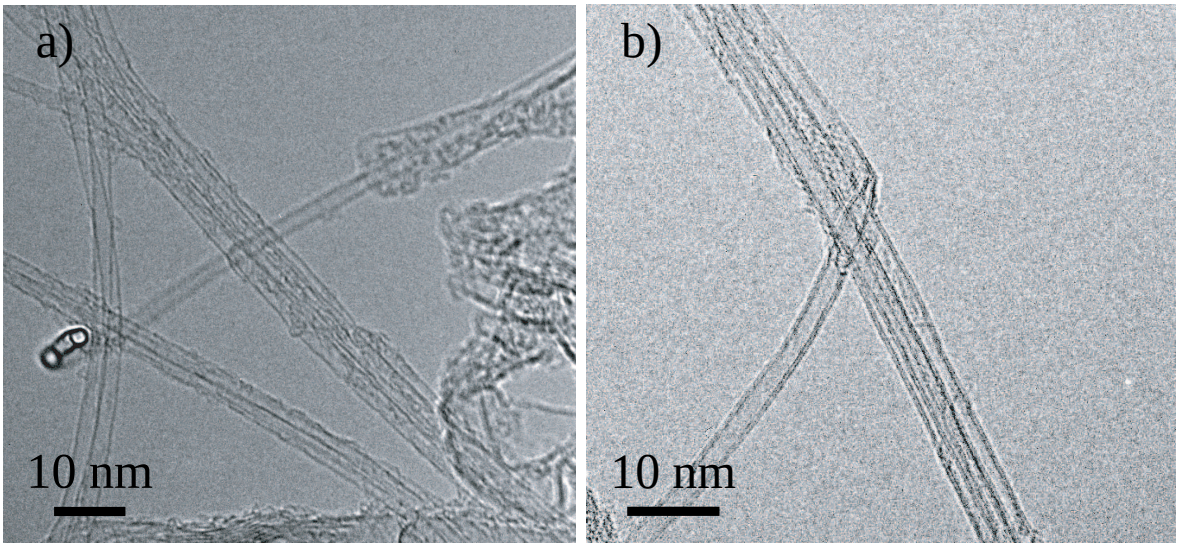

Figure 6.10: TEM pictures of bundles of a) single-wall (0.5 nm Fe on 10 nm Al, at 950 °C) and b) double-wall carbon nanotubes (0.2 nm Fe at 1'000 °C for 10 minutes with ethylene at 0.6 ml/min±20% and hydrogen at 400 ml/min±20%, the argon flow was 600 ml/min±20% during the whole process, using gas system II).

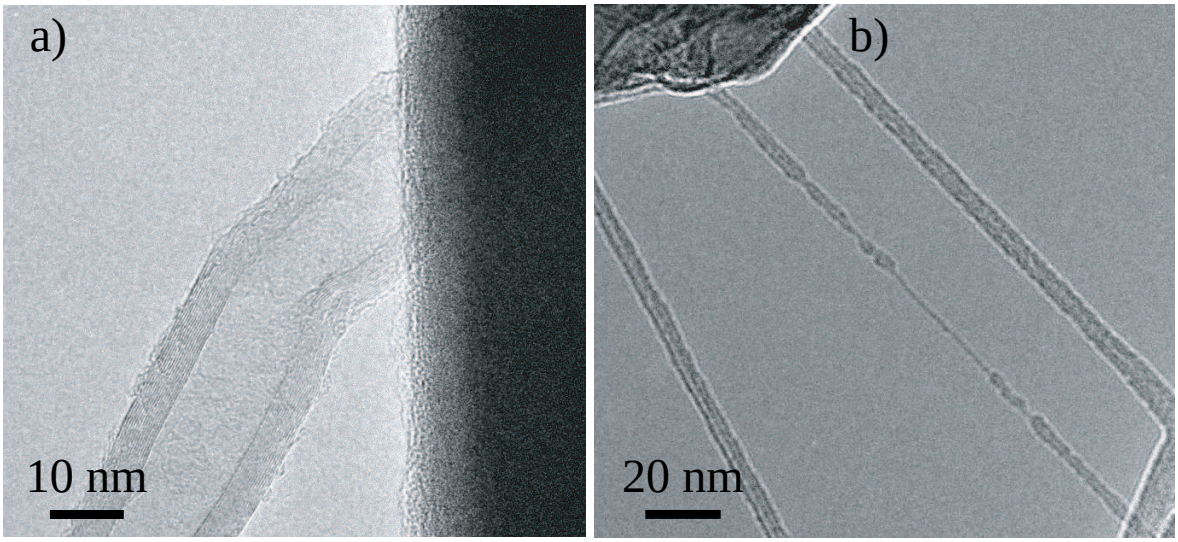

Figure 6.11: TEM pictures of a) a multi-wall carbon nanotube (0.5 nm Fe, at 850 °C) and b) a nanotube damaged by radiation.

Some tubes vibrate, as shown in Figure 6.13a) and b). This very interesting behavior is analyzed in more detail in Section 7.2 [48].

Nanotubes grown on the backside of a silicon nitride window

It was tried to use the silicon nitride windows for the preparation of samples suitable for STM (see Section 5.3). The idea was to grow nanotubes on the backside of the windows, to evaporate 200 nm gold and to etch the Si_3N_4 SiO_2 bilayer with 40% HF for 1 hour. Figure 6.14 shows that the yield of this process is very low. This approach was not progressed since it was not possible to stabilize the gold membrane. (The tubes were grown with the iron

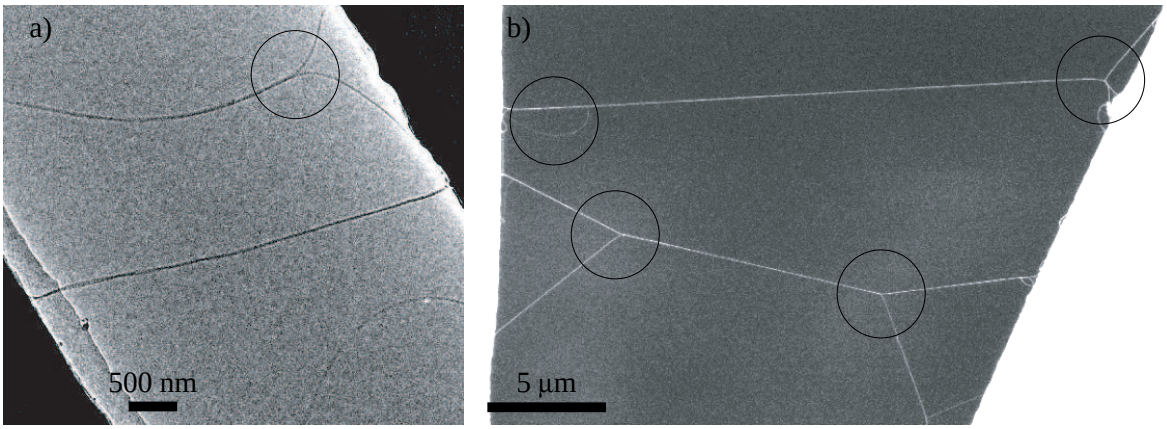

Figure 6.12: Nanotube framework on a) a TEM picture (0.3 nm Fe, at 900 °C) and b) a SEM picture (0.5 nm Fe on 10 nm Al, at 850 °C).

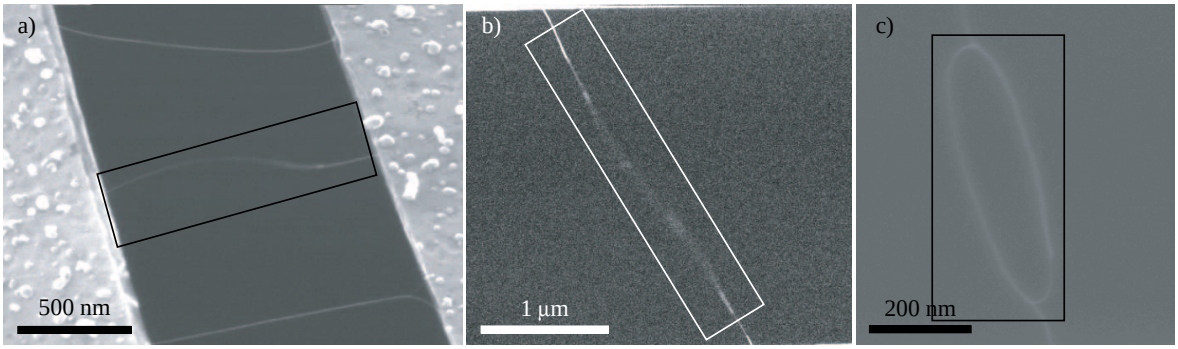

Figure 6.13: Vibrating nanotubes a) (1 nm Fe, at 850 °C) and b) (0.1 nm Fe, at 950 °C) spanning gaps in silicon nitride windows. c) A nano lasso (0.2 nm Fe, at 850 °C).

molybdenum alumina catalyst dissolved in 2-propanol at 900 °C for 10 minute with methane at 1'000 ml/min±3% and hydrogen at 500 ml/min±3%, the argon flow was 1'500 ml/min±3% during the whole process, using gas system IV.)

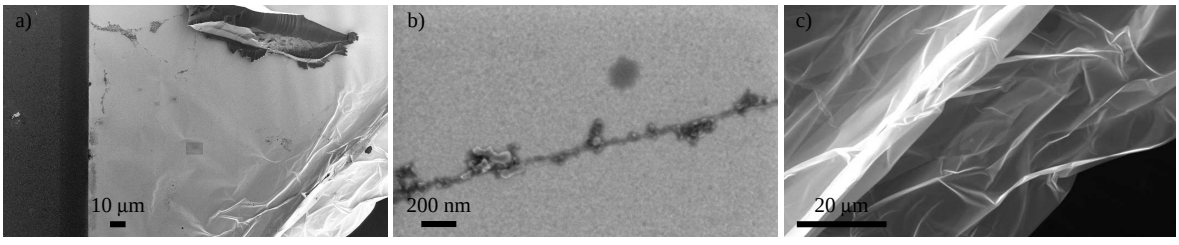

Figure 6.14: Nanotubes on an etched gold film. c) A 200 nm thick gold film.

6.3 Conclusions

The goal of the experiments presented in this chapter was to find a substrate suitable for investigations with TEM. It could be shown that it is possible to grow carbon nanotubes from different catalysts and with different growth protocols.

The process with the silicon nitride windows is surely more reliable and appropriate than the process with the TEM grids. However it is a fact that for both processes the substrates differ from SiO_2, and this has an influence on the growth of the nanotubes.
The setup with the silicon nitride windows increases obviously the tendency of the nanotubes to form bundles. Therefore it is not clear if the nanotube bundles arise only due to the special geometry of the samples or if the growth process has an influence as well. This means that both approaches are not optimal, although the silicon nitride windows are surely the better substrate.
If these experiments should be continued then the sample preparation should be changed. The top layer of the substrate should consist of SiO_2 to have the same initial conditions as with the standard substrate. There are different possibilities to fulfill this need. The backside of the silicon nitride windows consists of SiO_2 and it could be shown that it is possible to grow tubes on this side as well, this means the sample preparation is the same as described above with the only difference that the catalyst is spread on the backside. Another approach is the evaporation of a thick layer of SiO_2 on the silicon nitride windows or the TEM grids as a first step. However it has to be considered that evaporation is less accurate than thermal oxidation and that the evaporated layer consists of SiO_x with an unknown x. The third way is to buy silicon nitride windows with an oxide layer on the top (the silicon nitride layer is needed to stabilize the oxide layer which is very brittle).
Silicon nitride windows with grown suspended nanotubes can be used for Raman spectroscopy as well.

Chapter 7

Results from collaborations

There are several persons which are and were working with carbon nanotubes in our research group. Bakir Babić, Soufiane Ifadir, Dino Keller and Gunnar Gunnarsson used to use their own recipes for the growth of carbon nanotubes. However now all of them are working with the iron molybdenum alumina catalyst solved in 2-propanol. Matthias Gräber, Sangeeta Sahoo and Takis Kontos do not grow nanotubes by themselves, they have been provided with nanotubes for their running experiments grown with the methods presented in this thesis.
This chapter gives a short overview over the achieved results from these collaborations.

Details about the gas systems and the catalysts are described in Chapters 3 and 4, respectively.

7.1 Suitability of carbon nanotubes grown by chemical vapor deposition for electrical devices

Bakir Babić, Jürg Furer, and Christian Schönenberger

Published in "Electronic Properties of Synthetic Nanostructures", AIP Conf. Proc. Vol. 723, 574-582 (2004)

B. Babić *et al.* explored different strategies for the preparation of carbon nanotube devices suited for electrical and mechanical measurements. The target device is a single small diameter nanotube. Although, the tubes appear to be single, as judged from SEM and simple tapping-mode AFM in air, we find clear signs for the presence of more than one tube. Bundling is substantial for tubes grown over slits in silicon nitride windows (Figures 6.10 and 6.12). It has to be assumed that tubes grown on SiO_2 form bundles as well.
It is common practice to distinguish semiconducting and metallic nanotubes by the dependence of their electrical conductance (G) on the gate voltage (V_g), measured at room temperature ($T \approx 300\,\mathrm{K}$). This cannot prove that an individual single-wall tube has been contacted. Measurements performed on ropes of nanotubes show signatures which agree quite well with the behavior expected for a single-wall tube [165–167]. This has been attributed to a dominant electrode-CNT coupling to one nanotube only. Fano resonances were observed which are attributed to the interference of a single-wall tube which is strongly coupled to the electrodes with other more weakly coupled ones [50].
Assuming that all chiralities have equal probability to be formed in growth, 2/3 of the single-wall tubes are expected to be semiconducting and 1/3 metallic. From the measured response of the electrical conductance to the gate voltage (back-gate), $\approx 60\,\%$ of the devices display

metallic (the conductance does not depend on the gate voltage) and $\approx 40\,\%$ semiconducting behavior. Based on our assumption the larger fraction of metallic gate responses points to the presence of bundles or multi-shell tubes. If there are on average 2 or 3 tubes per bundle, which are coupled to the electrodes approximately equally, the probability to observe a semiconducting characteristic would amount to $(2/3)^2 = 44\,\%$ or $(2/3)^3 = 30\,\%$. Hence, it can be concluded that the number of tubes in a bundle or the number of shells in a multi-wall nanotube is very likely small and close to 2 on average.
Furthermore, is reported the fabrication of low-ohmic contacts to SWNTs. Au, Ti and Pd contacts are compared. Pd yields the best results.

For more details see [44, 48].

7.2 Intrinsic thermal vibrations of suspended doubly clamped single-wall carbon nanotubes

Bakir Babić, Jürg Furer, Sangeeta Sahoo, Shadyar Farhangfar, and Christian Schönenberger

Published in Nano Letters 3, 1577 (2003)

B. Babić *et al.* report the observation of thermally driven mechanical vibrations of suspended doubly clamped carbon nanotubes, grown by chemical vapor deposition. Several experimental procedures are used to suspend carbon nanotubes. The vibration is observed as a blurring in the images taken with a scanning electron microscope. The measured vibration amplitudes are compared with a model based on linear continuum mechanics.
Thermally driven excitations of multi-wall carbon nanotubes (MWNTs), clamped at one end only, were first investigated by Treacy *et al.* [168]. The mechanical oscillation appeared in the images, which were collected with a transmission electron microscope (TEM), as a blurring which increased towards the free end of the MWNTs.

For more details see [44, 47].

7.3 Electric field control of spin transport

Sangeeta Sahoo, Takis Kontos, Jürg Furer, Christian Hoffmann, and Christian Schönenberger

Published in Nature Physics 1, 99 (2005)

S. Sahoo *et al.* report on a pronounced gate-field controlled tunnel magneto-resistance (TMR) in devices made from carbon nanotubes with ferromagnetic contacts. In such devices, the electric resistance R depends on the orientation of the magnetization of the electrodes. The tunnel magneto-resistance $TMR = (R_{AP} - R_P)/R_P$ is defined as the relative difference between the resistances R_{AP} and R_P in the antiparallel (AP) and parallel (P) magnetization configuration. TMR can be observed in a spin-valve, which is for example formed if two ferromagnetic electrodes are separated by a thin tunnelling barrier, e.g. a nanotube. In multi-wall carbon nanotubes (MWNTs) with Co contacts it was found to be positive and amounted to $+4\,\%$ in agreement with Jullière's formula for tunnel junctions [169,170]. A negative TMR of about $-30\,\%$ was reported later for MWNTs contacted with similar Co contacts [162].
The reported TMR measurements used both multi-wall and single-wall carbon nanotubes which were contacted with ferromagnetic electrodes and capacitively coupled to a back-gate [32]. Both the amplitude and the sign of the TMR are tunable with the gate voltage in

a predictable manner. As a result of resonant tunnelling, it is observed a striking oscillatory amplitude and sign modulation of the TMR as a function of the gate voltage.

For more details see [30, 31].

7.4 Process dependence of the abundance of the nanotube type

If the process has no influence on the abundance and the distribution of the nanotubes should be 2/3 semiconducting and 1/3 metallic (see Section 2.1). However conductance measurements of S. Ifadir, D. Keller, M. Gräber and G. Gunnarson showed that almost all contacted tubes made with the methane process are metallic whereas most contacted tubes made with the methane/hydrogen process are semiconducting (Figure 7.1). This is a result comparable to [171]. The most simple explanation for this phenomenon is that the tubes grown with the methane process are bundled. This means that the tube with the best conductance (a metallic one) shortens all other tubes and determines the characteristic of the whole bundle. This fact can be exploited by using the methane process when a metallic nanotube (bundle) is desired, and the methane hydrogen process to get semiconducting nanotubes.

For more details see [8, 41, 46].

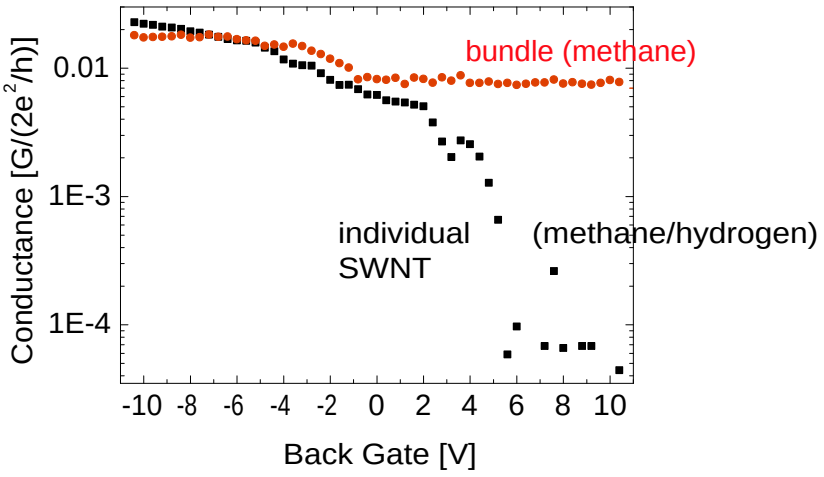

Figure 7.1: Conductance vs. applied voltage to back-gate for two different devices. In the curve of the (supposed) bundle the gating is obscured by the metallic contribution of the best conducting tube (methane process). The other sample shows semiconducting behavior (methane/hydrogen process). (Courtesy of S. Ifadir and D. Keller)

7.5 SEM/AFM comparison

SEM and AFM are both used for the characterization of the nanotubes. AFM gives a better resolution however the handling is much more difficult and time consuming than that of SEM. The localization of a convenient nanotube is a crucial step during the production of devices. It thus is important to make this as efficient as possible. Together with S. Ifadir and D. Keller a comparison was made between SEM and AFM with the aim to show that all nanotubes that are visible in AFM can also be imaged with SEM. Figure 7.2 shows that this is in fact correct, which means that SEM is a good mean for the localization of nanotubes.

For more details see [8, 45].

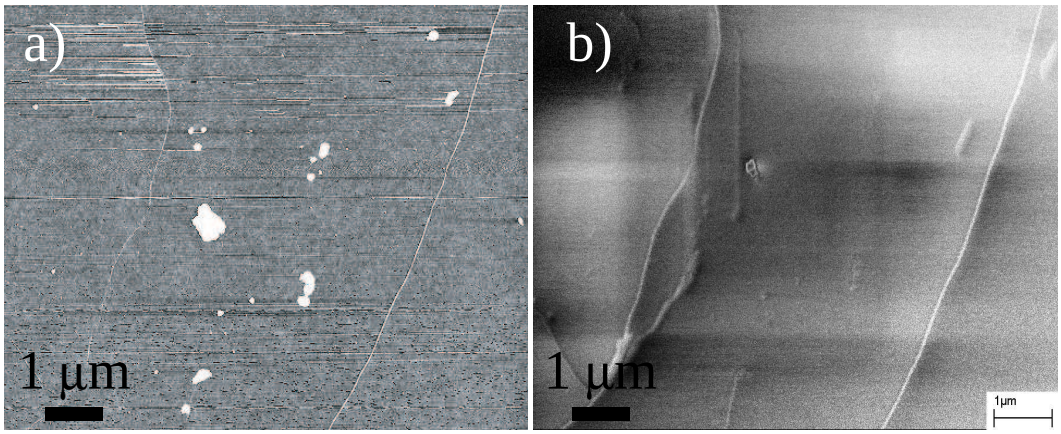

Figure 7.2: a) AFM picture of a sample. b) SEM picture of the same area. (Courtesy of S. Ifadir and D. Keller)

7.6 Carbon nanotubes in solution

S. Ifadir and D. Keller explored the electrical properties of carbon nanotubes in various solutions. The device was incubated with benzene derivatives (0.2M) solved in cyclohexane and then dried with N_2 (Figure 7.3). They found that the tubes are indeed responding to a changed environment. This sensitivity of the tubes makes them potential molecular sensors.

For more details see [8, 45].

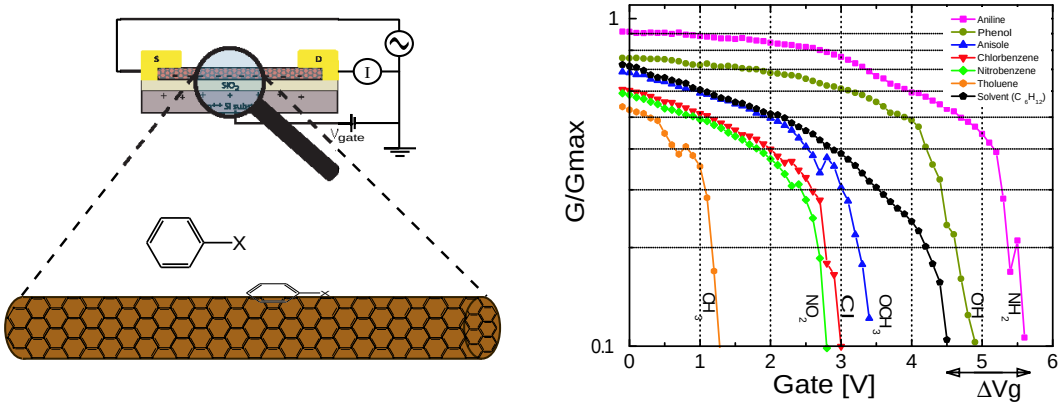

Figure 7.3: Normalized conductance vs. back gate voltage. The signal depends clearly on the benzene derivative. (Courtesy of S. Ifadir and D. Keller)

7.7 Transport measurements of carbon nanotubes

M. Gräber uses nanotubes for transport measurements at low temperature [172]. Figure 7.4a) shows a tube grown with the methane process at 900 °C. The length of the tube between

the two Pd electrodes is around 300 nm. The grey-scale plot in Figure 7.4b) was measured at 4.2 K. It shows both charging and finite size effects as seen in the different sizes of the coulomb diamonds [37].

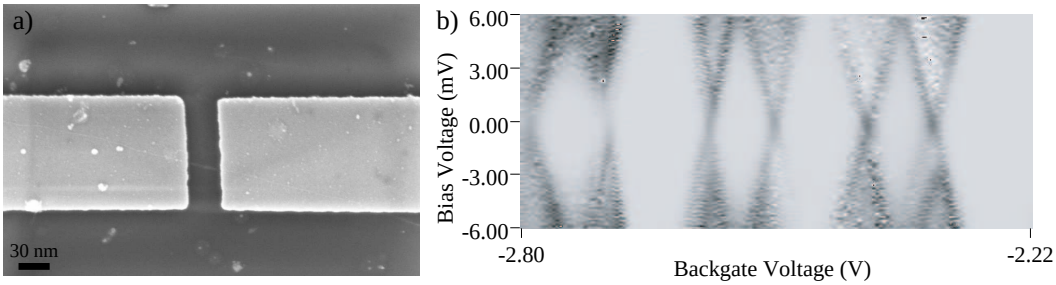

Figure 7.4: a) Carbon nanotube contacted with two Pd electrodes. b) Coulomb diamonds, white (dark) corresponds to 0 e^2/h (0.3 e^2/h). (Courtesy of M. Gräber)

Figure 7.5b) shows the honeycomb like charge-stability diagram of a double quantum dot formed in a nanotube with two topgates and a centergate measured at 300 mK (Figure 7.5a)). The regular honeycomb pattern indicates high-quality carbon nanotubes with only a few defects (if at all). The tube was grown at 900 °C with the methane/hydrogen process.

For more details see [41, 173].

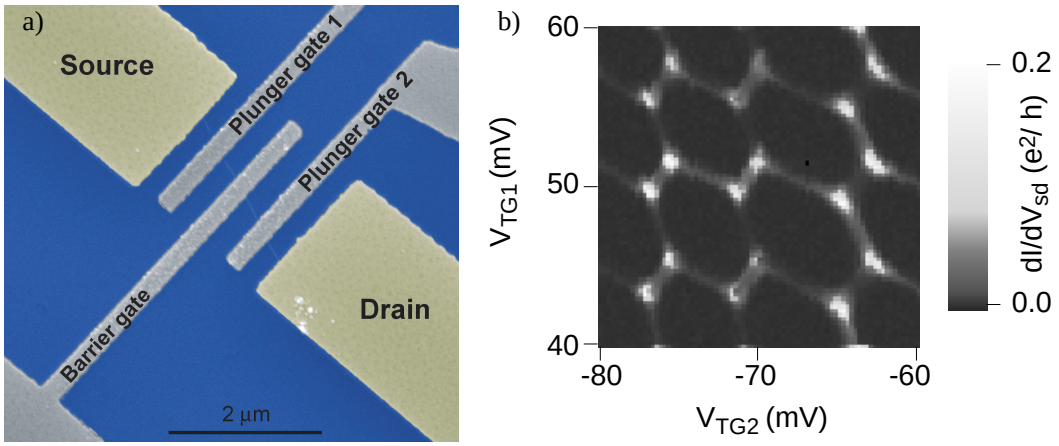

Figure 7.5: a) Carbon nanotube contacted with two topgates and a centergate (SiO_2 Ti Pd electrodes). b) Honeycomb structure of a double quantum dot. (Courtesy of M. Gräber)

Chapter 8

Conclusions and outlook

The aim of this thesis to overcome the problem of the bundling of the single-wall carbon nanotubes could be reached. Transport and Raman measurements prove the good quality of the carbon nanotubes (CNTs) grown with chemical vapor deposition.
The oven and the gas system were adjusted in several steps. Experiments on different substrates were performed (silicon dioxide, silicon nitride windows, TEM grids (Au, Cu, Mo, Ni, stainless steel, Ti) and quantifoils). Evaporated and liquid based catalysts were tested. CNTs were grown with different carbon feedstocks (ethylene/hydrogen, methane, methane/ethylene and methane/hydrogen). An iron molybdenum alumina catalyst solved in 2-propanol in combination with the methane/hydrogen process gives the best results.
The comparison between SEM and AFM revealed that SEM is a good tool for the localization of nanotubes dedicated for the preparation of samples for electrical transport measurements. As a result of the good quality of the nanotubes, they are used in several running projects. Experiments on quantum dots and spin valves promise very interesting results in the future.
A very noteworthy fact is that most of the tubes grown with the methane/hydrogen process are semiconducting and most of the tubes grown with the methane process are metallic. Therefore it is possible to preselect the characteristic of the CNT with high probability by using the appropriate process. However it has to be respected that the metallic tubes grown with the methane process are not separated but bundled.
Although the preparation of CNTs was optimized, there are still several possibilities of improving the growth process. It should be tested if the diameter of the nanotubes and their structure are depending on the growth temperature, the gas flows and the catalyst composition. It should be checked in more detail why the used process has such a strong influence on the characteristic of the grown tubes. The Raman studies are very promising and should be deepened. It should be tried to localize defects on the CNTs with STM.

Bibliography

[1] H. W. Kroto, J. R. Heath, S. C. O'Brien, R. F. Curl, and R. E. Smalley. C60: Buckminsterfullerene. *Nature*, 318:162, 1985.

[2] S. Iijima and T. Ichihashi. Helical microtubules of graphitic carbon. *Nature*, 354:56, 1991.

[3] M. Daenen, R. de Fouw, B. Hamers, P. Janssen, K. Schouteden, and M. Veld. *The Wondrous World of Carbon Nanotubes 'a review of current carbon nanotube technologies'*. Eindhoven University of Technology (WondrousWorldOfCNTs.pdf on CD), 2003.

[4] Hongjie Dai. Carbon nanotubes: opportunities and challenges. *Surface Science*, 500:218, 2002.

[5] M. Dresselhaus, G. Dresselhaus, and P. Avouris. *Carbon Nanotubes: Synthesis, Structure, Properties, and Applications*. Springer, 2001.

[6] H. Kajiura, S. Tsutsui, K. Kadono, M. Kakuta, M. Ata, and Y. Murakami. Hydrogen storage capacity of commercially available carbon materials at room temperature. *APPLIED PHYSICS LETTERS*, 82:1105, 2003.

[7] P. Mauron. *Growth Mechanism and Structure of Carbon Nanotubes*. PhD thesis, Universität Freiburg (Diss-Mauron.pdf on CD), 2003.

[8] D. Keller. *To be published*. PhD thesis, Universität Basel.

[9] Shankar Ghosh, A. K. Sood, and N. Kumar. Carbon Nanotube Flow Sensors. *Science*, 299:1042, 2003.

[10] Sylvain Latil, Stephan Roche, and Jean-Christophe Charlier. Electronic Transport in Carbon Nanotubes with Random Coverage of Physisorbed Molecules. *NANO LETTERS*, 5:2216, 2005.

[11] E. S. Snow, F. K. Perkins, E. J. Houser, S. C. Badescu, and T. L. Reinecke. Chemical Detection with a Single-Walled Carbon Nanotube Capacitor. *Science*, 307:1942, 2005.

[12] Q. Zhao, M. Buongiorno Nardelli, W. Lu, and J. Bernholc. Carbon Nanotube-Metal Cluster Composites: A New Road to Chemical Sensors? *NANO LETTERS*, 5:847, 2005.

[13] J. M. Kinaret, T. Nord, and S. Viefers. A carbon-nanotube-based nanorelay. *APPLIED PHYSICS LETTERS*, 82:1287, 2003.

[14] Byong M. Kim, Shizhi Qian, and Haim H. Bau. Filling Carbon Nanotubes with Particles. *NANO LETTERS*, 5:873, 2005.

[15] Neil R. Wilson and Julie V. Macpherson. Single-Walled Carbon Nanotubes as Templates for Nanowire Conducting Probes. *NANO LETTERS*, 3:1365, 2003.

[16] Jinquan Wei, Hongwei Zhu, and Dehai Wu. Carbon nanotube filaments in household light bulbs. *APPLIED PHYSICS LETTERS*, 84:4869, 2004.

[17] Mei Zhang, Ken R. Atkinson, and Ray H. Baughman. Multifunctional Carbon Nanotube Yarns by Downsizing an Ancient Technology. *Science*, 306:1358, 2004.

[18] Jean-Marc Bonard, Mirko Croci, Fabien Conus, Thomas Stöckli, and André Chatelain. Watching carbon nanotubes grow. *APPLIED PHYSICS LETTERS*, 81:2836, 2002.

[19] Jun Hee Choi, Andrei R. Zoulkarneev, Yong Wan Jin, Young Jun Park, Deuk Seok, Chung, Byung Kwon Song, In Taek Han, Hang Woo Lee, Sang Hyun Park, Ho Suk Kang, Ha Jong Kim, Jung Woo Kim, Jae Eun Jung, Jong Min Kimb, Hong Gu Baek, and Se Gi Yu. Carbon nanotube field emitter arrays having an electron beam focusing structure. *APPLIED PHYSICS LETTERS*, 84:1022, 2004.

[20] L. Gangloff, E. Minoux, K. B. K. Teo, P. Vincent, V. T. Semet, V. T. Binh, M. H. Yang, I. Y. Y. Bu, R. G. Lacerda, G. Pirio, J. P. Schnell, D. Pribat, D. G. Hasko, G. A. J. Amaratunga, W. I. Milne, and P. Legagneux. Self-Aligned, Gated Arrays of Individual Nanotube and Nanowire Emitters. *NANO LETTERS*, 4:1575, 2004.

[21] Niels de Jonge, Yann Lamy, Koen Schoots, and Tjerk H. Oosterkamp. High brightness electron beam from a multi-walled carbon nanotube. *Nature*, 420:393, 2002.

[22] Robert S. Service. Sorting Technique May Boost Nanotube Research. *Science*, 300:2018, 2003.

[23] B. Babić, M. Iqbal, and C. Schönenberger. Ambipolar field-effect transistor on as-grown single-wall carbon nanotubes. *Nanotechnology*, 14:327, 2003.

[24] R. Martel, T. Schmidt, H. R. Shea, T. Hertel, and Ph. Avourisa. Single- and multi-wall carbon nanotube field-effect transistors. *APPLIED PHYSICS LETTERS*, 73:2447, 1998.

[25] Ali Javey, Jing Guo, Qian Wang, Mark Lundstrom, and Hongjie Dai1. Ballistic carbon nanotube field-effect transistors. *Nature*, 424:654, 2003.

[26] E. Artukovic, M. Kaempgen, D. S. Hecht, S. Roth, and G. Grüner. Transparent and Flexible Carbon Nanotube Transistors. *NANO LETTERS*, 5:757, 2005.

[27] S. Auvray, J. Borghetti, M. F. Goffman, A. Filoramo, V. Derycke, and J. P. Bourgoin. Carbon nanotube transistor optimization by chemical control of the nanotube-metal interface. *APPLIED PHYSICS LETTERS*, 84:5106, 2004.

[28] M. R. Buitelaar, W. Belzig, T. Nussbaumer, B. Babic, C. Bruder, and C. Schönenberger. Multiple Andreev Reflection in a Carbon Nanotube Quantum Dot. *Physical Review Letters*, 91:057005, 2003.

[29] M. J. Biercuk, S. Garaj, N. Mason, J. M. Chow, and C. M. Marcus. Gate-Defined Quantum Dots on Carbon Nanotubes. *NANO LETTERS*, 5:1267, 2005.

[30] S. Sahoo. *An experimental investigation of spin transport through carbon nanotubes*. PhD thesis, Universität Basel, 2005.

[31] S. Sahoo, T. Kontos, J. Furer, C. Hoffmann, and C. Schönenberger. Electric field control of spin transport. *Nature Physics*, 1:99, 2005.

[32] S. Sahoo, T. Kontos, C. Schönenberger, and C. Sürgers. Electrical spin injection in multi-wall carbon nanotubes with transparent ferromagentic contacts. *Applied Physics Letters*, 86:112109, 2005.

[33] Ali Javey, Qian Wang, Ant Ural, Yiming Li, and Hongjie Dai. Carbon Nanotube Transistor Arrays for Multistage Complementary Logic and Ring Oscillators. *NANO LETTERS*, 2:929, 2002.

[34] Antonis N. Andriotis, Madhu Menon, Deepak Srivastava, and Leonid Chernozatonskii. Rectification Properties of Carbon Nanotube "Y-Junctions". *PHYSICAL REVIEW LETTERS*, 87:066802, 2001.

[35] S. Roth and C. Carroll. *One Dimensional Metals*. WILEY-VCH, 2004.

[36] A. Bachtold. *Electrical Properties of Single Multiwalled Carbon Nanotubes*. PhD thesis, Universität Basel, 1999.

[37] M. Buitelaar. *Electric Electron Transport in Multiwall Carbon Nanotubes*. PhD thesis, Universität Basel, 2002.

[38] M. Krüger. *Towards Single Molecule Electronics*. PhD thesis, Universität Basel, 2000.

[39] A. Bachtold, M. de Jonge, K. Grove-Rasmussen, P.L. McEuen M. Buitelaar, and C. Schönenberger. Suppression of tunneling into multi-wall carbon nanotubes. *Physical Review Letters*, 87:166801, 2001.

[40] M. R. Buitelaar, A. Bachtold, T. Nussbaumer, M. Iqbal, and C. Schönenberger. Multi-wall carbon nanotubes as quantum dots. *Physical Review Letters*, 88:156801, 2002.

[41] M. Gräber. *Accessing the quantum world through electronic transport in carbon nanotubes*. PhD thesis, Universität Basel.

[42] M. R. Gräber, T. Nussbaumer, W. Belzig, T. Kontos, and C. Schönenberger. Kondo resonance in a nanotube quantum dot coupled to a normal and a superconducting lead. *Proceedings of the XXXIXth Rencontres de Moriond on Quantum information and decoherence in nanosystems at La Thuile, Aosta Valley, Italy, Jan. 25 - Feb. 1st*, page 363, 2004.

[43] M. Gräber, T. Nussbaumer, W. Belzig, and C. Schönenberger. Quantum dot coupled to a normal and a superconducting lead. *Nanotechnology*, 15:479, 2004.

[44] B. Babić. *Electrical Characterization of Carbon Nanotubes grown by the Chemical Vapor Deposition Method*. PhD thesis, Universität Basel, 2003.

[45] S. Ifadir. *Liquid effect on the electronic properties of single contacted carbon nanotubes grown by chemical vapor deposition*. PhD thesis, Universität Basel, 2005.

[46] G. Gunnarsson. *To be published*. PhD thesis, Universität Basel.

[47] B. Babić, J. Furer, M. Iqbal, and C. Schönenberger. Suitability of carbon nanotubes grown by chemical vapor deposition for electrical devices. *"Electronic Properties of Synthetic Nanostructures", AIP Conf. Proc.*, 723:574, 2004.

[48] B. Babić, J. Furer, S. Sahoo, Sh. Farhangfar, and C. Schönenberger. Intrinsic Thermal Vibrations of Suspended Doubly Clamped Single-Wall Carbon Nanotubes. *NANO LETTERS*, 3(11):1577, 2003.

[49] B. Babić, T. Kontos, and C. Schönenberger. Kondo effect in carbon nanotubes at half filling. *Physical Review B*, 70:235419, 2004.

[50] B. Babić and C. Schönenberger. Observation of Fano-Resonances in Single-Wall Carbon Nanotubes. *Physical Review B*, 70:195408, 2004.

[51] Michael S. Arnold, Samuel I. Stupp, and Mark C. Hersam. Enrichment of Single-Walled Carbon Nanotubes by Diameter in Density Gradients. *NANO LETTERS*, 5:713, 2005.

[52] C. A. Furtado, U. J. Kim, H. R. Gutierrez, Ling Pan, E. C. Dickey, and Peter C. Eklund. Debundling and Dissolution of Single-Walled Carbon Nanotubes in Amide Solvents. *JACS*, 126:6095, 2004.

[53] Debjit Chattopadhyay, Izabela Galeska, and Fotios Papadimitrakopoulos. A Route for Bulk Separation of Semiconducting from Metallic Single-Wall Carbon Nanotubes. *JACS*, 125:3370, 2003.

[54] M. F. Islam, E. Rojas, D. M. Bergey, A. T. Johnson, and A. G. Yodh. High Weight Fraction Surfactant Solubilization of Single-Wall Carbon Nanotubes in Water. *NANO LETTERS*, 3:269, 2003.

[55] Valerie C. Moore, Michael S. Strano, Erik H. Haroz, Robert H. Hauge, Richard E. Smalley, Judith Schmidt, and Yeshayahu Talmon. Individually Suspended Single-Walled Carbon Nanotubes in Various Surfactants. *NANO LETTERS*, 3:1379, 2003.

[56] Ralph Krupke, Frank Hennrich, Hilbert v. Löhneysen, and Manfred M. Kappes. Separation of Metallic from Semiconducting Single-Walled Carbon Nanotubes. *Science*, 301:344, 2003.

[57] Ya-Qiong Xu, Haiqing Peng, Robert H. Hauge, and Richard E. Smalley. Controlled Multistep Purification of Single-Walled Carbon Nanotubes. *NANO LETTERS*, 5:163, 2005.

[58] http://cohesion.rice.edu/naturalsciences/smalley/emplibrary/allotropes.jpg.

[59] W. J. Moore. *Physikalische Chemie.* de Gruyter, 1983.

[60] K. Schwister. *Taschenbuch der Chemie.* Fachbuchverlag Leipzig GmbH, 1995.

[61] M. Merkel and K.-H. Thomas. *Taschenbuch der Werkstoffe.* Fachbuchverlag Leipzig GmbH, 4th edition, 1994.

[62] S. Reich, C. Thomsen, and J. Maultzsch. *Carbon Nanotubes.* WILEY-VCH, first reprint edition, 2004.

[63] X. Zhaon, Y. Liu, S. Inoue, T. Suzuki, R. O. Jones, and Y. Ando. Smallest Carbon Nanotube Is 3 Åin Diameter. *PHYSICAL REVIEW LETTERS*, 92:125502, 2004.

[64] L. X. Zheng, M. J. O'Connell, S. K. Doorn, X. Z. Liao, Y. H. Zhao, E. A. Akhadov, M. A. Hoffbauer, B. J. Roop, Q. X. Jia, R. C. Dye, D. E. Peterson, S. M. Huang, J. Liu, and Y. T. Zhu. Ultralong single-wall carbon nanotubes. *Nature materials*, 3:673, 2004.

[65] S. Rotkin and S. Subramoney. *Applied Physiks of Carbon Nanotubes.* Springer, 2005.

[66] E. L. Ivchenko and B. Spivak. Chirality effects in carbon nanotubes. *PHYSICAL REVIEW B*, 66:155404, 2002.

[67] P. J. F. Harris. *Carbon Nanotubes and Realted Structures.* Cambridge University Press, 1999.

[68] T. W. Ebbesen. *Carbon Nanotubes: Preparation and Properties.* CRC Press, 1997.

[69] Jing Kong, Alan M. Cassell, and Hongjie Dai. Chemical vapor deposition of methane for single-walled carbon nanotubes. *Chemical Physics Letters*, 292:567, 1998.

[70] Anna Moisala, Albert G. Nasibulin, and Esko I. Kauppinen. The role of metal nanoparticles in the catalytic production of single-walled carbon nanotubes-a review. *JOURNAL OF PHYSICS: CONDENSED MATTER*, 15:3011, 2003.

[71] T. Uchino, K. N. Bourdakos, C. H. de Groot, P. Ashburn, M. E. Kiziroglou, G. D. Dilliway, and D. C. Smith. Metal catalyst-free low-temperature carbon nanotube growth on SiGe islands. *APPLIED PHYSICS LETTERS*, 86:233110, 2005.

[72] R. G. Lacerda, A. S. Teh, M. H. Yang, K. B. K. Teo, N. L. Rupesinghe, S. H. Dalal, K. K. K. Koziol, D. Roy, G. A. J. Amaratunga, W. I. Milne, M. Chhowalla, D. G. Hasko, F. Wyczisk, and P. Legagneux. Growth of high-quality single-wall carbon nanotubes without amorphous carbon formation. *APPLIED PHYSICS LETTERS*, 84:269, 2004.

[73] J. Kong, H. T Soh, A. M. Cassel, C. F. Quate, and H. Dai. Synthesis of individual singlewalled carbon nanotubes on patterned siliconwafers. *Nature*, 395:878, 1998.

[74] Iuliana Radu, Yael Hanein, and David H. Cobden. Oriented growth of single-wall carbon nanotubes using alumina patterns. *Nanotechnology*, 15:473, 2004.

[75] H. Cui, G. Eres, J. Y. Howe band A. Puretkzy, M. Varela, D. B. Geohegan, and D. H. Lowndes. Growth behavior of carbon nanotubes on multilayered metal catalyst film in chemical vapor deposition. *Chemical Physics Letters*, 374:222, 2003.

[76] S. Iijima. Carbon nanotubes: past, present, and future. *Physica B*, 323:1, 2002.

[77] J. B. Nagy, G. Bister, A. Fonseca, D. Méhn, Z. Kónya, I. Kiricsi, Z. E. Horváth, and L. P. Biró. On the Growth Mechanism of Single-Walled Carbon Nanotubes by Catalytic Carbon Vapor Deposition on Supported Metal Catalysts. *Journal of Nanoscience and Nanotechnology*, 4:326, 2004.

[78] http://www.nanotechweb.org/articles/news/2/8/5/1/070803.

[79] Deli Wang, Fang Qian, Chen Yang, Zhaohui Zhong, and Charles M. Lieber. Rational Growth of Branched and Hyperbranched Nanowire Structures. *NANO LETTERS*, 4:871, 2004.

[80] Yuegang Zhang, Aileen Chang, Jien Cao, Qian Wang, Woong Kim, Yiming Li, Nathan Morris, Erhan Yenilmez, Jing Kong, and Hongjie Dai. Electric-field-directed growth of aligned single-walled carbon nanotubes. *APPLIED PHYSICS LETTERS*, 79:3155, 2001.

[81] Ernesto Joselevich and Charles M. Lieber. Vectorial Growth of Metallic and Semiconducting Single-Wall Carbon Nanotubes. *NANO LETTERS*, 2:1137, 2002.

[82] Ant Ural, Yiming Li, and Hongjie Dai. Electric-field-aligned growth of single-walled carbon nanotubes on surfaces. *APPLIED PHYSICS LETTERS*, 81:3464, 2002.

[83] Ki-Hong Lee, Jeong-Min Cho, and Wolfgang Sigmunda. Control of growth orientation for carbon nanotubes. *APPLIED PHYSICS LETTERS*, 82:448, 2003.

[84] Huijun Xin and Adam T. Woolley. Directional Orientation of Carbon Nanotubes on Surfaces Using a Gas Flow Cell. *NANO LETTERS*, 4:1481, 2004.

[85] Nathan R. Franklin and Hongjie Dai. An Enhanced CVD Approach to Extensive Nanotube Networks with Directionality. *ADVANCED MATERIALS*, 12:890, 2000.

[86] Yoshikazu Homma, Yoshihiro Kobayashi, Toshio Ogino, and Takayuki Yamashitab. Growth of suspended carbon nanotube networks on 100-nm-scale silicon pillars. *APPLIED PHYSICS LETTERS*, 81:2261, 2002.

[87] Georg S. Duesberg, Andrew P. Graham, Maik Liebau, Robert Seidel, Eugen Unger, Franz Kreupl, and Wolfgang Hoenlein. Growth of Isolated Carbon Nanotubes with Lithographically Defined Diameter and Location. *NANO LETTERS*, 3:257, 2003.

[88] L. B. Direktor, V. M. Zaichenko, I. L. Maikov, G. F. Sokol, Yu. L. Shekhter, and E. E. Shpil'rain. Investigation of Pyrolysis of Methane under Conditions of Filtering through a Heated Porous Medium. *High Temperature*, 39:85, 2001.

[89] M. J. Perkins. *Radical Chemistry: The Fundamentals.* Oxford University Press, 2000.

[90] A. F. Parsons. *An introduction to free radical chemistry.* Blackwell Science Ldt., 2000.

[91] C. Wentrup. *Reakive Zwischenstufen I.* Thieme, 1979.

[92] P. W. Atkins. *Physical Chemistry.* Oxford University Press, second edition, 1999.

[93] R. D. Levine and R. B. Berstein. *Molekulare Reaktionsdynamik.* Teubner Studienbücher, 1991.

[94] B. Giese. *Radicals in Organic Synthesis.* Pergamon Press, 1986.

[95] M. Meyyappan, Lance Delzeit, Alan Cassell1, and David Hash. Carbon nanotube growth by PECVD: a review. *Plasma Sources Sci. Technol.*, 12:205, 2003.

[96] R. I. Masel. *Chemical Kinetics and Catalysis.* John Wiley & Sons, Inc., 2001.

[97] Nathan R. Franklin, Yiming Li, Robert J. Chen, Ali Javey, and Hongjie Dai. Patterned growth of single-walled carbon nanotubes on full 4-inch wafers. *APPLIED PHYSICS LETTERS*, 79:4571, 2001.

[98] I. Chorkendorff and J. W. Niemantsverdriet. *Concepts of Modern Catalysis and Kinetics.* Wiley-VCH, 2003.

[99] J. E. Leffler. *Am Introduction to Free Radicals.* John Wiley & Sons, Inc., 1993.

[100] Yu. A. Mankelevich, N. V. Suetin, M. N. R. Ashfold, W. E. Boxford, A. J. Orr-Ewing, J. A. Smith, and J. B. Wills. Chemical kinetics in carbon depositing d.c.-arc jet CVD reactors. *Diamond and Related Materials*, 12:383, 2003.

[101] Tao Wu, Hans-Joachim Werner, and Uwe Manthe. First-Principles Theory for the H + CH_4 $\longrightarrow$ H_2 + CH_3 Reaction. *Science*, 306:2227, 2004.

[102] I. E. Baranov, S. A. Demkin, V. K. Zhivotov, I. I. Nikolaev, V. D. Rusanov, and N. G. Fedotov. Methane Pyrolysis Stimulated by Admixture of Atomic Hydrogen: 1. An Experimental Study. *High Energy Chemistry*, 38:191, 2004.

[103] I. E. Baranov, S. A. Demkin, V. K. Zhivotov, I. I. Nikolaev, V. D. Rusanov, and N. G. Fedotov. Methane Pyrolysis Stimulated by Admixture of Atomic Hydrogen: 2. Mechanism Analysis. *High Energy Chemistry*, 39:268, 2005.

[104] http://www.infosteel.net/images/fe3c.gif.

[105] L. Scheer. *Was ist Stahl*. Springer-Verlag, 14th edition, 1974.

[106] W. Pepperhoff and M. Acet. *Constitution and Magnetism if Iron and its Alloys*. Springer, 2001.

[107] E. Hornbogen and H. Warlimont. *Metallkunde*. Springer-Verlag, second edition, 1991.

[108] Avetik R. Harutyunyan, Bhabendra K. Pradhan, U. J. Kim, Gugang Chen, and P. C. Eklund. CVD Synthesis of Single Wall Carbon Nanotubes under "Soft" Conditions. *NANO LETTERS*, 2:525, 2002.

[109] Richard W. Borry III and Enrique Iglesia. Non-Oxidative Conversion of Methane with Continuous Hydrogen Removal. *FETC Publications Conference Proceedings*, 4:709, 1997.

[110] http://www.netl.doe.gov/publications/proceedings/97/97ng/ng97_pdf/NGP14.PDF (RBa97 on CD).

[111] F. J. Bargel and G. Schulze. *Werkstoffkunde*. Springer, 7th edition, 2000.

[112] http://www.seilnacht.com/Chemie/ch_fe2o3.htm.

[113] G. Gottstein. *Physical Foundations of Material Science*. Springer, 2004.

[114] Teresa de los Arcos, M. Gunnar Garnier, Peter Oelhafen, Daniel Mathys, Jin Won Seo, Concepción Domingo, José Vicente García-Ramos, and Santiago Sánchez-Cortés. Strong influence of buffer layer type on carbon nanotube characteristics. *Carbon*, 42:187, 2004.

[115] T. de los Arcos, Z. M. Wu, and P. Oelhafen. Is aluminum a suitable buffer layer for carbon nanotube growth? *Chemical Physics Letters*, 380:419, 2003.

[116] Henning Kanzow and Adalbert Ding. Formation mechanism of single-wall carbon nanotubes on liquid-metal particles. *PHYSICAL REVIEW B*, 60:11180, 1999.

[117] Vincenzo Vinciguerra, Francesco Buonocore, Giuseppe Panzera, and Luigi Occhipinti. Growth mechanisms in chemical vapour deposited carbon nanotubes. *Nanotechnology*, 14:655, 2003.

[118] Woong Kim, Hee Cheul Choi, Moonsub Shim, Yiming Li, Dunwei Wang, and Hongjie Dai. Synthesis of Ultralong and High Percentage of Semiconducting Single-walled Carbon Nanotubes. *NANO LETTERS*, 2:703, 2002.

[119] Caterina Ducati, Ioannis Alexandrou, Manish Chhowalla, Gehan A. J. Amaratunga, and John Robertson. Temperature selective growth of carbon nanotubes by chemical vapor deposition. *JOURNAL OF APPLIED PHYSICS*, 92:3299, 2002.

[120] Yoshinori Ando, Xinluo Zhao, Toshiki Sugai, and Mukul Kumar. Growing carbon nanotubes. *Materials today*, 7:22, 2004.

[121] Y. Zhang, Y. Li, W. Kim, D. Wang, and H. Dai. Imaging as-grown single-walled carbon nanotubes originated from isolated catalytic nanoparticles. *Applied Physics A*, 74:325, 2002.

[122] Christian Klinke, Jean-Marc Bonard, and Klaus Kern. Thermodynamic calculations on the catalytic growth of multiwall carbon nanotubes. *PHYSICAL REVIEW B*, 71:035403, 2005.

[123] Caterina Ducati, Ioannis Alexandrou, Manish Chhowalla, Gehan A. J. Amaratunga, and John Robertson. The role of the catalytic particle in the growth of carbon nanotubes by plasma enhanced chemical vapor deposition. *JOURNAL OF APPLIED PHYSICS*, 95:6387, 2004.

[124] E. Hornbogen. *Werkstoffe*. Springer-Verlag, 1991.

[125] Weizhi Rong, Andrew E. Pelling, Andrew Ryan, James K. Gimzewski, and Sheldon K. Friedlander. Complementary TEM and AFM Force Spectroscopy to Characterize the Nanomechanical Properties of Nanoparticle Chain Aggregates. *NANO LETTERS*, 4:2287, 2004.

[126] Jinseong Heo and Marc Bockrath. Local Electronic Structure of Single-Walled Carbon Nanotubes from Electrostatic Force Microscopy. *NANO LETTERS*, 5:853, 2005.

[127] Toru Kuzumaki, Shintaro Kitakata, Kazuki Enomoto, Tatsuyuki Yasuhara, Naoto Ohtake, and Yoshitaka Mitsuda. Separation of Metallic from Semiconducting Single-Walled Carbon Nanotubes. *Carbon*, 42:2329, 2004.

[128] A. M. Rao, E. Richter, Shunji Bandow, Bruce Chase, P. C. Eklund, K. A. Williams, S. Fang, K. R. Subbaswamy, M. Menon, A. Thess, R. E. Smalley, G. Dresselhaus, and M. S. Dresselhaus. Diameter-Selective Raman Scattering from Vibrational Modes in Carbon Nanotubes. *Science*, 275:187, 1997.

[129] S. Bandow, M. Takizawaa, K. Hiraharaa, M. Yudasakac, and S. Iijimaa. Raman scattering study of double-wall carbon nanotubes derived from the chains of fullerenes in single-wall carbon nanotubes. *CHEMICAL PHYSICS LETTERS*, 337:48, 2001.

[130] J. Maultzsch, S. Reich, and C. Thomsen. Raman scattering in carbon nanotubes revisited. *PHYSICAL REVIEW B*, 65:233402, 2002.

[131] http://www-g.eng.cam.ac.uk/edm/research/nanotubes/cnt_raman.html.

[132] A. Hassaniena, M. Tokumotoa, T. Shimizua, and H. Tokumotoa. STM on suspended single wall carbon nanotubes. *Thin Solid Films*, 464:338, 2004.

[133] P. Lambin, G. I. Mark, V. Meunier, and L. P. Biro. Computation of STM Images of Carbon Nanotubes. *International Journal of Quantum Chemistry*, 95:493, 2003.

[134] Miron Hazani, Ron Naaman, Frank Hennrich, and Manfred M. Kappes. Confocal Fluorescence Imaging of DNA-Functionalized Carbon Nanotubes. *NANO LETTERS*, 3:153, 2003.

[135] Sumit Chaudhary, Joong Hyun Kim, Krishna V. Singh, and Mihrimah Ozkan. Fluorescence Microscopy Visualization of Single-Walled Carbon Nanotubes Using Semiconductor Nanocrystals. *NANO LETTERS*, 4:2415, 2004.

[136] Jay Gaillard, Malcolm Skove, and Apparao M. Raoa. Mechanical properties of chemical vapor deposition-grown multiwalled carbon nanotubes. *APPLIED PHYSICS LETTERS*, 86:233109, 2005.

[137] S. B. Legoas, V. R. Coluci, S. F. Braga, P. Z. Coura, S. O. Dantas, and D. S. Galvao. Molecular-Dynamics Simulations of Carbon Nanotubes as Gigahertz Oscillators. *PHYSICAL REVIEW LETTERS*, 90:055504, 2003.

[138] José L. Rivera, Clare McCabe, and Peter T. Cummings. Oscillatory Behavior of Double-Walled Nanotubes under Extension: A Simple Nanoscale Damped Spring. *NANO LETTERS*, 3:1001, 2003.

[139] Vera Sazonova, Yuval Yaish, Hande Üstünel, David Roundy, Tomas A. Arias, and Paul L. McEuen. A tunable carbon nanotube electromechanical oscillator. *Nature*, 431:284, 2004.

[140] J. Y. Huang, S. Chen, Z. Q. Wang, K. Kempa, Y. M. Wang, S. H. Jo, G. Chen, M. S. Dresselhaus, and Z. F. Ren. Superplastic carbon nanotubes. *Nature*, 439:281, 2006.

[141] P. A. Williams, S. J. Papadakisa, A. M. Patel, M. R. Falvo, S. Washburn, and R. Superfine. Fabrication of nanometer-scale mechanical devices incorporating individual multiwalled carbon nanotubes as torsional springs. *APPLIED PHYSICS LETTERS*, 82:805, 2003.

[142] M. A. L. Marques, H. E. Troiani, M. Miki-Yoshida, M. Jose-Yacaman, and A. Rubio. On the Breaking of Carbon Nanotubes under Tension. *NANO LETTERS*, 4:811, 2004.

[143] Ki-Ho Lee, Pawel Keblinski, and Susan B. Sinnott. Deflection of Nanotubes in Response to External Atomic Collisions. *NANO LETTERS*, 5:263, 2005.

[144] Mitsumasa Nishio, Shintaro Sawaya, Seiji Akitaa, and Yoshikazu Nakayama. Carbon nanotube oscillators toward zeptogram detection. *APPLIED PHYSICS LETTERS*, 86:133111, 2005.

[145] Sang Wook Lee, Dong Su Lee, Raluca E. Morjan, Sung Ho Jhang, Martin Sveningsson, O. A. Nerushev, Yung Woo Park, and Eleanor E. B. Campbell. A Three-Terminal Carbon Nanorelay. *NANO LETTERS*, 4:2027, 2004.

[146] Bertrand Bourlon, D. Christian Glattli, Csilla Miko, Laszlo Forró, and Adrian Bachtold. Carbon Nanotube Based Bearing for Rotational Motions. *NANO LETTERS*, 4:709, 2004.

[147] Sulin Zhang, Wing Kim Liu, and Rodney S. Ruoff. Atomistic Simulations of Double-Walled Carbon Nanotubes (DWCNTs) as Rotational Bearings. *NANO LETTERS*, 4:293, 2004.

[148] Antonio J. R. da Silva, A. Fazzio, and Alex Antonelli. Bundling up Carbon Nanotubes through Wigner Defects. *NANO LETTERS*, 5:1045, 2005.

[149] Madhu Menon, Antonis N. Andriotis, Deepak Srivastava, Inna Ponomarevax, and Leonid A. Chernozatonskiik. Carbon Nanotube "T Junctions": Formation Pathways and Conductivity. *PHYSICAL REVIEW LETTERS*, 91:145501, 2003.

[150] Mina Yoon, Seungwu Han, Gunn Kim, Sang Bong Lee, Savas Berber, Eiji Osawa, Jisoon Ihm, Mauricio Terrones, Florian Banhart, Jean-Christophe Charlier, Nicole Grobert, Humberto Terrones, Pulickel M. Ajayan, and David Tomanek. Zipper Mechanism of Nanotube Fusion: Theory and Experiment. *NANO LETTERS*, 92:075504, 2004.

[151] Manual. *MTF Tube furnaces: Installation, Operation and Maintenance Instructions*. Carbolite (MTF-Carbolite.pdf on CD).

[152] M. Altendorf. *Flow Handbook*. Endress-Hauser, 2004.

[153] Manual. *Kleinstmengen-Durchflussmesser/-wächter. KDF für Flüssigkeiten, KDG für Gase*. Kobold.

[154] Manual. *Control and Read Out Unit, Models 0152/0154*. Brooks, 1999.

[155] Manual. *Model 5850E Mass Flow Controller*. Brooks (5850-E-BROOKS.pdf on CD), 1997.

[156] Author not mentioned. *Physik der Schwebekörperdurchflussmessgeräte*. Kirchner (KirchnerSchwebekoerpertheorie.pdf on CD).

[157] G. Rollmann. *Die Berechnung von Korrekturfaktoren für Schwebekörperdurchflussmessgeräte bei geänderten Betriebsbedingungen*. Kirchner (KirchnerKorrekturfaktorenberechnung.pdf on CD).

[158] Manual. *Installation and Operation Manual: Model 5850S*. Brooks, 2000.

[159] J. Furer. *Semesterarbeit: Herstellung mesoskopischer Ueberlappungszonen mit einer Vakuumbedampfungsanlage*. 1996.

[160] J. Furer. *Diplomarbeit: Lithographische Herstellung von Goldmikroelektroden für die Leitfähigkeitsuntersuchung elektrochemisch synthetisierter leitender Polymere*. 1997.

[161] D. R. Lide. *Handbook of Chemistry and Physiks*. CRC Press, 75th edition, 2004.

[162] B. Zhao, I. Mönch, H. Vinzelberg, T. Mühl, and C. M. Schneider. Spincoherent transport in ferromagnetically contacted carbon nanotubes. *Applied Physics Letters*, 80:3144, 2002.

[163] M. Hegner, P. Wagner, and G. Semenza. Ultralarge atomically flat template-stripped Au surfaces for scanning probe microscopy. *Surface Science*, 291:39, 1993.

[164] H. R. Gutiérrez, U. J. Kim, and J. P. Kimand P. C. Eklund. Thermal Conversion of Bundled Carbon Nanotubes into Graphitic Ribbons. *NANO LETTERS*, 5:2195, 2005.

[165] S. J. Tans, M. H. Devoret, R. J. A. Groeneveld, and C. Dekker. Electron-electron correlations in carbon nanotubes. *Nature*, 394:761, 1998.

[166] M. Bockrath, D. H. Cobden, P. L. McEuen, N. G. Chopra, A. Zettl, A. Thess, and R. E. Smalley. Single-Electron Transport in Ropes of Carbon Nanotubes. *Science*, 275:1922, 1997.

[167] J. Nygård, D. Cobden, and P. E. Lindelof. Kondo physics in carbon nanotubes. *Nature*, 408:342, 2000.

[168] M. M. J. Treacy, T. W. Ebbesen, and J. M. Gibson. Exceptionally high Young's modulus observed for individual carbon nanotubes. *Nature*, 381:678, 1996.

[169] M. Jullière. Tunneling between ferromagnetic films. *Physics Letters A*, 54:225, 1975.

[170] P. M. Tedrow and R. Meservey. Spin Polarization of Electrons Tunneling from Films of Fe, Co, Ni, and Gd. *Physical Review B*, 7:318, 1973.

[171] Yiming Li, David Mann, Marco Rolandi, Woong Kim, Ant Ural, Steven Hung, Ali Javey, Jien Cao, Dunwei Wang, Erhan Yenilmez, Qian Wang, James F. Gibbons, Yoshio Nishi, , and Hongjie Dai. Preferential Growth of Semiconducting Single-Walled Carbon Nanotubes by a Plasma Enhanced CVD Method. *NANO LETTERS*, 4:317, 2004.

[172] S. Datta. *Electronic Transport in Mesoscopic Systems*. Cambridge University Press, first edition, 1995.

[173] M. R. Gräber, W. A. Coish, C. Hoffmann, M. Weiss, J. Furer, S. Oberholzer, D. Loss, and C. Schönenberger. Molecular States in Carbon Nanotube Double Quantum Dots. *To be published*.

Appendix A

Materials and Methods

A.1 Equipment

- AFM: Nanoscope IV, Digital Instruments
- Annealing oven: AZ 500, MB Komponenten GmbH
- CVD oven: MTF 12/38/250, Carbolite
- E-beam lithography: JSM-IC848 Scanning Microscope, Jeol; with Elphy and Proxy software from Raith
- Evaporator: PLS 500 Labor System, Balzers-Pfeiffer
- Fittings: Swagelok
- Flowmeters (variable area flowmeter): KDG1213 (1.6 - 16 sccm), KDG1228 (10 - 100 sccm) and KDG1137 (50 - 500 sccm), Kobold
- Flowmeters (thermal profile): 5850S and 5850E, Brooks Instrument
- Flowmeter controller: 0154, Brooks Instrument
- Magnetic stirrer: RCTbasic, KIKA Labortechnik
- Manometers: Swagelok
- Microscope (optical): SM-LUX HL, Leitz
- Needle valve: EVN116, Pfeiffer Vacuum
- Oven: UT 5042 EK, Heraeus
- Reactive ion etcher (RIE): Plasmalab 80 plus, Oxford
- SEM: XL 30 FEG, Philips
- SEM: SUPRA 35, LEO
- Sonicator (standard): Ultrasonik300, Ney
- Sonicator (high power): Digital Sonifier, Branson
- Spinning table: Lanz Reinraumtechnik
- Surface profiler: Alpha-step 500, TENCOR
- TEM: H8000, Hitachi
- TEM: CM 200 FEG, Philips
- Tubes: Swagelok
- UV-ozone Cleaner: UVO Model 42-220, Jelight company
- Vacuum annealing oven: self development
- Water deionizer: Wilhelm Werner GmbH, Reinstwassertechnik

A.2 Materials

- Acetone EP: Schweizerhall Chemie AG, item 80932-106
- Alumina: Al_2O_3, Aluminum oxide purum p.a., MW: 101.96, Fluka, 06285
- Alumina 4: Al_2O_3, Aluminum oxide nanopowder 4 nm, MW: 101.96, Aldrich, 55,164-3

- Alumina 40: Al_2O_3, Aluminum oxide nanopowder 40 nm, MW: 101.96, Aldrich, 544833
- Ammonium fluoride: > 95%, NH_4F, MW: 37.04, Merck, 1162
- Gold: Au for evaporation, ingots from different banks
- Calcium carbonate: $CaCO_3$
- Chlorbenzene, purum: > 98%, Fluka, 23580
- EPOTEK 377: Epoxy Technology Inc.
- Ethanol 96% EP: Schweizerhall Chemie AG, item 82352-102
- HMDS: Hexamethyldisilazane, puriss p.a., Fluka 52619
- Hydrochloric acid 36-38%: (HCl, MW: 36.46, J. T. Baxter, 6081)
- Hydrofluoric acid 40%: HF, MW: 20.01, Fluka, 47590
- Hydrogen peroxide 30% EP 4: H_2O_2, MW: 38.01, Schweizerhall Chemie AG, item 82570-102
- Iron: Fe, 99.9%, Starter-Slug for evaporation, unaxis, M00-0947/1
- Iron nitrate: $Fe(NO_3)_3$-$9H_2O$, MW: 404.00, Sigma, F-1143
- 2-propanol, pro analysis: > 99,8%, Isopropylic alcohol, IPA, Merck, 1.09634.1000
- Methanol: pro analysis, MW: 32.04, Merck 1.06009.1000
- MIBK, purum: > 99,0%, Methyl-isobutyl-ketone, 4-Methyl-2-pentanone, Fluka, 58600
- Nickel: Ni 99.98%, wire for evaporation, Balzers Materials, BD481143T
- Molybdenum dioxide dichloride: MoO_2Cl_2, MW: 198.85, Aldrich, 37,371-0
- Molybdenum(IV)dioxide: MoO_2 99%, Aldrich, 23,476-1
- PMMA: Polymethyl methacrylate, E-beam resist PMMA 950 K, Allresist GmbH, AR-P 671.09
- Quantifoils R2/2: Cu TEM grids covered from a thin carbon film of a thickness of 15 nm with a regular pattern of holes with a diameter of 2 μm, Planno
- SiO_2: Silicon dioxide 99.9%, 1.6 - 5 mm granules for evaporation, Balzers Materials, BD481689-T
- SiO_2 (high doped): silicon oxide, 100 nm oxide on 500 μm Si (100), positively doped with boron, Paul Scherrer Institut
- SiO_2 (low doped): silicon oxide, 100 nm thermal oxide on 500 μm Si (100), negatively doped with phosphorous, 4 - 6 Ωcm
- Si_3N_4 windows: The substrate is a 525 μm thick Si wafer covered with 150 nm LPCVD Si_3N_4 on 100 nm thermal SiO_2, 4 Ωcm. The Si is etched from the back side leaving a freestanding Si_3N_4 SiO_2 bilayer of 0.5 mm x 0.5 mm. Etched predetermined breaking point allow the cleaving of the wafer in pieces of 0.5 mm x 0.5 mm. Université de Neuchâtel.
- Solution #30: 10 mM $Fe(NO_3)_3$-$9H_2O$ in H_2O was kept for 1 day at 85 °C
- TEM grids: Au, Cu, Mo, Ni, stainless steel (SS) and Ti, Planno

A.3 Gasses

- Acetylene 26 (C_2H_2, > 99,6%, Carbagas):
  N_2 < 4000 ppm, PH_3 < 10 ppm.
- Argon 48 (Ar, > 99,998%, Carbagas):
  O_2 < 2 ppm, H_2O < 3 ppm, N_2 < 10 ppm, H_2 < 1 ppm, CH_4 < 1 ppm, CO_2 < 1 ppm.
- Argon 60 (Ar, > 99,9999%, Carbagas):
  O_2 < 0,2 ppm, H_2O < 0,6 ppm, N_2 < 0,3 ppm, H_2 < 0,01 ppm, CH_4 < 0,05 ppm, CO+CO_2 < 0,05 ppm.
- Ethylene 35 (C_2H_4, > 99,95%, Carbagas):
  O_2 < 10 ppm, H_2O < 5 ppm N_2, < 35 ppm, CO_2 < 5 ppm, CH_4 < 25 ppm, C_nH_m < 420 ppm.
- Hydrogen 60 (H_2, > 99,9999%, Carbagas):
  O_2 < 0,2 ppm, H_2O < 0,8 ppm, N_2 < 0,3ppm, CO_2 < 0,05 ppm, CO < 0,05 ppm, CH_4 < 0,05 ppm, D_2 + HD ≈ 150 ppm.
- Methane 55 (CH_4, > 99,9995%, Carbagas):
  O_2 < 0,5 ppm, H_2O < 2 ppm, N_2 < 2 ppm, H_2 < 0,1 ppm, C_2H_6 < 0,1 ppm, CO_2 < 0,1 ppm, C_nH_m < 0,05 ppm.
- Nitrogen technical (N_2, > 99.5%, Carbagas and Sauerstoffwerk Lenzburg)
- Oxygen 55 (O_2, > 99,9995%, Carbagas):
  H_2O < 1 ppm, N_2 < 4 ppm, CO_2 < 0,1 ppm, CO < 0,1 ppm, H_2 < 0,1 ppm, CH_4 < 0,2 ppm, NO_x < 15 ppb.
- Trifluoro methane (CHF_3, Multigas)

Appendix B

Recipes

B.1 Growth protocols

This Section presents the step by step protocols. For more details about the setup of gas systems see Section 3.2. More information about how corrections have to be done can be found in Section 3.3. The effect of a room temperature deviating from the calibration temperature 20 °C is negligible ($< 2\%$).

B.1.1 Gas system I - Methane protocol

The gas system was operated with two gas lines for argon and methane, respectively. The pressure at the reducing valve of the gas bottles was set to 2 bar and the pressure after the flowmeter was 0.1 bar.

1. Open Ar up to 880 ml/min±3% (The reading at the variable area flow meter was 100 l/h, this corresponds to a corrected flow of: $\frac{100'000ml}{60min}\sqrt{\frac{1.293}{1.784}}\sqrt{\frac{0.2+1}{2.0-0.1+1}} = 882ml/min$).)
2. Heat oven
3. Open CH_4 up to 700 or 4'180 ml/min±3% (The reading at the variable area flowmeter was either 50 or 300 l/h, this corresponds to a corrected flow of: $\frac{50'000ml}{60min}\sqrt{\frac{1.293}{0.717}}\sqrt{\frac{0.2+1}{2.0-0.1+1}} = 696ml/min$).)
4. Close Ar
5. Leave CH_4 flowing for 10 minutes
6. Open Ar
7. Close CH_4
8. Let oven cool down below 350 °C
9. Close Ar

B.1.2 Gas system II - Ethylene/hydrogen protocol

The gas system was operated with three gas lines for argon, hydrogen and ethylene, respectively. Ethylene was replaced by either methane or acetylene for some experiments.

1. Open Ar up to 1'058 ml/min±20% (reading at the controller)
2. Heat oven
3. Open H_2 up to 600 - 688 ml/min±20% (reading at the controller)
4. Open C_2H_4 (or CH_4 or C_2H_2) up to either 1.2 (or 1.5 or 1.2) ml/min±20% or 12.4 (or 15.3 or 12.3) ml/min±20% (The reading at the controller was 2 or 20 ml/min, the flowmeter is calibrated with N_2, this corresponds to a correction for the other kind of gas of: $2ml/min\frac{0.619}{1.000} = 1.24ml/min$.)
5. Leave the gasses flowing for 10 minutes

6. Close C_2H_4 (...)
7. Close H_2
8. Let oven cool down below 350 °C
9. Close Ar

B.1.3 Gas system II - Methane/ethylene protocol

The gas system was operated with three gas lines for argon, methane and ethylene, respectively.

1. Open Ar up to 1'058 ml/min±20% (reading at the controller)
2. Heat oven
3. Open CH_4 up to 530 ml/min±20% (The reading at the controller was 700 ml/min, the flowmeter is calibrated with H_2, this corresponds to a correction for the other kind of gas of: $700ml/min\frac{0.763}{1.008} = 530ml/min$.)
4. Open C_2H_4 up to either 0.6 (or 1.9 or 9) ml/min±20% (The reading at the controller was 1, 3 or 9 ml/min, the flowmeter is calibrated with N_2, this corresponds to a correction for the other kind of gas of: $1ml/min\frac{0.619}{1.000} = 0.62ml/min$.)
5. Close Ar
6. Leave the gasses flowing for 10 minutes
7. Open Ar
8. Close C_2H_4
9. Close H_2
10. Let oven cool down below 350 °C
11. Close Ar

B.1.4 Gas system III - Methane protocol

The gas system was operated with two gas lines for argon and methane as well as a switch with two inlets (argon and methane) and two outlets (oven and out). The pressure at the manometers before the flowmeters was set to 0.2 bar for both gasses using the reduction valves of the gas bottles, the downstream pressure was 0.1 bar with an accuracy of 10%. This corresponds to a pressure drop of 0.1 bar over the flowmeters. The switch has two positions: In position 1 methane is connected to the oven and argon to out. In position 2 argon is connected to the oven and methane to out.

1. Open Ar up to 890 ml/min±3%, connected to oven (The reading at the variable area flow meter was 60 l/h, this corresponds to a corrected flow of: $\frac{60'000ml}{60min}\sqrt{\frac{1.293}{1.784}}\sqrt{\frac{1.2}{1.1}} = 888ml/min$).)
2. Heat oven until 1'000 °C (first experiments 950 °C)
3. Open CH_4 up 1'400 ml/min±3%, connected to out (The reading at the variable area flowmeter was 60 l/h, this corresponds to a corrected flow of: $\frac{60'000ml}{60min}\sqrt{\frac{1.293}{0.717}}\sqrt{\frac{1.2}{1.1}} = 1'402ml/min$).)
4. Flush CH_4 line for 5 minutes
5. Switch Ar and CH_4 flow (for details see: Cleaning of the gas lines)
6. Leave the gasses flowing for 10 minutes
7. Switch Ar and CH_4 flow
8. Close CH_4 line
9. Let oven cool down below 350 °C
10. Close Ar

B.1.5 Gas system IV - Methane/hydrogen protocol

The gas system is operated with three gas lines for argon, hydrogen and methane, respectively. The pressure drop over the flowmeters is set to 0,2 bar, using the reduction valves of the gas bottles. This makes a pressure correction unnecessary.

1. Mount sample, close tube
2. Open all gas valves (Ar (check if there are bubbles), CH_4, H_2)
3. Flush the lines for 2 minutes
4. Close H_2 and CH_4 valves
5. Keep Ar flowing at 1'500 ml/min±3% (The reading at the variable area flow meter is 105 l/h, this corresponds to a corrected flow of: $\frac{105'000ml}{60min}\sqrt{\frac{1.293}{1.784}} = 1'489ml/min$).)
6. Heat oven to 900 °C
7. Open H_2 flow up to 500 ml/min±3% (The reading at the variable area flowmeter is 8 l/h, this corresponds to a corrected flow of: $\frac{8'000ml}{60min}\sqrt{\frac{1.293}{0.090}} = 505ml/min$).)
8. Close Ar
9. Open CH_4 up to 1000 ml/min±3% (The reading at the variable area flowmeter is 45 l/h, this corresponds to a corrected flow of: $\frac{45'000ml}{60min}\sqrt{\frac{1.293}{0.717}} = 1'007ml/min$).)
10. Leave the gasses flowing for 10 minutes
11. Open up Ar up to 1.5 l/min (leave H_2 open)
12. Close CH_4
13. Let oven cool down to 550 °C
14. Close H_2
15. Unmount sample when temperature ¡ 350 °C
16. Close Ar

B.2 Correction table for variable area flowmeters

The reading of a variable area flowmeter depends on the kind of gas flowing, its pressure and its temperature. The used variable area flowmeters are gauged with air (at 0.2 bar relative and 20 °C), however used for measuring the flow of argon, methane and hydrogen, respectively. This makes a correction necessary ($\Phi_{V1} = \Phi_{V0}\sqrt{\frac{\varrho_0}{\varrho_1}}\sqrt{\frac{P_0}{P_1}}\sqrt{\frac{T_1}{T_0}}$, see Section 3.3 for more details). The correction factors ($\sqrt{\frac{\text{density air}}{\text{density new gas}}}$) are listed in Table B.1 together with the corresponding gas densities.

The correction table is used as follows: The 'Desired flow' of 1'000 ml/min methane corresponds to a 'Reading on flowmeter' of 45 l/h when the pressure drop over the flowmeter is set to 0.2 bar. The room temperature fluctuates between 13 and 31 °C over the year. This deviation from the calibration temperature 20 °C is negligible ($<$ 2%).

	Air	Ar	CH_4	H_2
Density (kg/m^3)	1.293	1.784	0.717	0.090
Correction factor	1.00	0.85	1.34	3.79
Desired flow	Reading	on	flow-	meter
(ml/min)	(l/h)	(l/h)	(l/h)	(l/h)
50	3.00	3.52	2.23	0.79
100	6.00	7.05	4.47	1.58
150	9.00	10.57	6.70	2.37
200	12.00	14.10	8.94	3.17
250	15.00	17.62	11.17	3.96
300	18.00	21.14	13.40	4.75
350	21.00	24.67	15.64	5.54
400	24.00	28.19	17.87	6.33
450	27.00	31.71	20.11	7.12
500	30.00	35.24	22.34	7.91
550	33.00	38.76	24.57	8.71
600	36.00	42.29	26.81	9.50
650	39.00	45.81	29.04	10.29
700	42.00	49.33	31.28	11.08
750	45.00	52.86	33.51	11.87
800	48.00	56.38	35.74	12.66
850	51.00	59.91	37.98	13.46
900	54.00	63.43	40.21	14.25
950	57.00	66.95	42.45	15.04
1000	60.00	70.48	44.68	15.83
1050	63.00	74.00	46.91	16.62
1100	66.00	77.53	49.15	17.41
1150	69.00	81.05	51.38	18.20
1200	72.00	84.57	53.62	19.00
1250	75.00	88.10	55.85	19.79
1300	78.00	91.62	58.08	20.58
1350	81.00	95.14	60.32	21.37
1400	84.00	98.67	62.55	22.16
1450	87.00	102.19	64.79	22.95
1500	90.00	105.72	67.02	23.74
1550	93.00	109.24	69.25	24.54
1600	96.00	112.76	71.49	25.33
1650	99.00	116.29	73.72	26.12
1700	102.00	119.81	75.96	26.91
1750	105.00	123.34	78.19	27.70
1800	108.00	126.86	80.42	28.49
1850	111.00	130.38	82.66	29.28
1900	114.00	133.91	84.89	30.08
1950	117.00	137.43	87.13	30.87
2000	120.00	140.95	89.36	31.66

Table B.1: Correction table for variable area flowmeters.

Appendix C

Publication list

Publications in journals and proceedings

- *Suitability of carbon nanotubes grown by chemical vapor deposition for electrical devices*, Bakir Babić, Jürg Furer and Christian Schönenberger, Published in "Electronic Properties of Synthetic Nanostructures", AIP Conf. Proc. Vol. 723, 574-582 (2004)
- *Intrinsic thermal vibrations of suspended doubly clamped single-wall carbon nanotubes*, Bakir Babic, Jürg Furer, Sangeeta Sahoo, Shadyar Farhangfar and Christian Schönenberger, Nano Letters 3, 1577 (2003)
- *Electric field control of spin transport*, Sangeeta Sahoo, Takis Kontos, Jürg Furer, Christian Hoffmann and Christian Schönenberger, Nature Physics 1, 99 (2005)
- *Molecular States in Carbon Nanotube Double Quantum Dots*, M. R. Gräber, W. A. Coish, C. Hoffmann, M. Weiss, J. Furer, S. Oberholzer, D. Loss and C. Schönenberger, to be published

Poster contributions

- *Growth of Carbon Nanotubes*, Jürg Furer, Michel Calame, Mahdi Iqbal, Thomas Nussbaumer, Zuqin Liu, Bakir Babic, Soufiane Ifadir, Vreni Thommen, Andreas Engel, Henning Stahlberg, Marco Gregorini, Christian Schönenberger, Twannberg workshop on nanoscience (Switzerland), Twannberg, 30.9-4.10.2002
- *Vibrating Carbon Nanotubes*, B. Babić, Sh. Farhangfar, J. Furer, T. Nussbaumer, S. Sahoo, G. Gantenbein and C. Schönenberger, NCCR review panel, Basel (Switzerland), May 2003
- *Growth of Carbon Nanotubes*, J. Furer, B. Babic, M. Calame, A. Engel, S. Farhangfar, G. Gantenbein, S. Ifadir, M. Iqbal, Z. Liu, T. Nussbaumer, H. Stahlberg, V. Thommen and C. Schönenberger, SFB 513 Workshop 2003 & Krupp-Symposium in Konstanz (Germany), Konstanz, 6-9.7.2003
- *Exploring Carbon Nanotubes for Biosensing Purpose.* D. Keller, S. Ifadir, J. Furer, M. Calame and C. Schönenberger, Kirchberg Conference IWEPNM 05, Kirchberg (Austria), 15.3.2005
- *Carbon Nanotube Double Quantum Dots.* M. Gräber, W.A. Coish, J. Furer, C. Hoffmann, M. Weiss, S. Oberholzer, A. Eichler, D. Loss and C. Schönenberger, Gwatt (Switzerland), May 2005

- *Electric Field Control of Spin Transport in Carbon Nanotubes*. Sangeeta Sahoo, Takis Kontos, Jürg Furer, Christian Hoffmann and Christian Schönenberger, Spintronics'05, Poznan (Poland), 25-30.9.2005

Danksagung

Während meiner Doktorarbeit habe ich Hilfe von verschiedener Seite erfahren. Mein ganz besonderer Dank gilt Prof. Dr. Christian Schönenberger für seine Unterstützung und seinen ansteckenden Enthusiasmus. Prof. Lásló Forró von der Ecole Polytechnique Fédérale de Lausanne und Prof. Hans-Werner Fink von der Universität Zürich danke ich sehr für die Uebernahme des Korreferats.
Bei Mahdi Iqbal, Zuqin Liu, Thomas Nussbaumer, Verena Thommen und ganz besonders bei Bakir Babić möchte ich mich für die Unterstützung bei meinen ersten Experimenten mit dem CVD-Ofen bedanken. Ein grosses Dankeschön geht an Bakir Babić, Dino Keller, Soufiane Ifadir und Gunnar Gunnarson für Ihre Mithilfe bei der Entwicklung des optimalen Wachstumsprozesses. Merci auch Matthias Gräber, Sangeeta Sahoo und Takis Kontos für die Messungen an den Nanotubes.
Sehr wertvoll war die Unterstützung durch die anderen Mitglieder der Gruppe Schönenberger: Laetitia Bernard, Erasmus Bieri, Mark Buitelaar, Michel Calame, Bong-Ryoul Choi, François Dewarrat, Shadyar Farhangfar, Teresa González, Lucia Grüter, Adam Hansen, Christian Hoffmann, Roman Huber, Derek Kelly, Andreas Kleine, Jianhui Liao, Stefan Oberholzer, Markus Weiss, Songmei Wu und Zheng Ming Wu.
Merci Sangeeta für die moralische Unterstützung, während wir zur gleichen Zeit an unseren Dissertationen schrieben.
Ganz besonders geschätzt habe ich die Zusammenarbeit mit Senta Karotke, Stephan Messmer, Zeng Ming Wu und Christian Wattinger. Während der Vorbereitung der Experimente für die Vorlesungen war der grosse Hörsaal regelmässig von Lachen erfüllt.
Ein grosses Dankeschön geht an die Mitarbeiter der mechanischen Werkstatt Heinz Breitenstein, Silvester Jakob, Jeanpierre Ramseyer, P. Cattin, S. Martin, D. Michel, W. Roth und P. Wunderlin, und der Elektronik-Werkstatt Michael Steinacher, Werner Erni, Bernd Heimann, Sheeba Madathilparambil und H.-R. Hidber die mir bei technischen Problemen gerne weiterhalfen.
Andreas Engel, Henning Stahlberg, Marco Gregorini und Grazyna Gantenbein danke ich für die Zusammenarbeit und die Bereitschaft mir die Benutzung Ihrer TEMs zu erlauben.
Herre van Zant und Jing Kong danke ich für Ihre wertvollen Hinweise für eine optimale Prozessführung. Bei A. Hartschuh möchte ich mich für die Raman- und bei Gilles Buchs für die STM-Messungen bedanken. U. Wüst danke ich herzlich für die Beantwortung meiner Fragen zur Funktionsweise der Schwebekörperdurchflussmesser.
Mein Dank gilt auch den Dozenten bei denen ich während meines Physikstudiums Vorlesungen besucht habe: C. Bandle, W. Breymann, C. Bruder, R. Buser, H. Burkhart, F.-J. Elmer, J. Fünfschilling, A. Gautschy, H.-J. Güntherodt, T. Gyalog, M. Hegner, J. Jourdan, E. Meyer, P. Oelhafen, H. Rudin, Scarpellini, C. Schönenberger, I. Sick, G. Tammann, L. Tauscher, F.-K. Thielemann, H. Thomas, D. Trautmann, U. Ullrich and I. Zschocke.